BIOGEOCHEMISTRY AND HYDROLOGY OF THREE ALPINE PROGLACIAL ENVIRONMENTS RESULTING FROM GLACIER RETREAT

By Monica Zanzola Bruckner

A thesis submitted in partial fulfillment
of the requirements for the degree

of

Master of Science

in

Earth Sciences

MONTANA STATE UNIVERSITY
Bozeman, Montana

December 2008

©COPYRIGHT

by

Monica Zanzola Bruckner

2008

All Rights Reserved

APPROVAL

of a thesis submitted by

Monica Zanzola Bruckner

This thesis has been read by each member of the thesis committee and has been found to be satisfactory regarding content, English usage, format, citation, bibliographic style, and consistency, and is ready for submission to the Division of Graduate Education.

Dr. Mark L. Skidmore

Approved for the Department of Earth Sciences

Dr. Stephen G. Custer

Approved for the Division of Graduate Education

Dr. Carl A. Fox

STATEMENT OF PERMISSION TO USE

In presenting this thesis in partial fulfillment of the requirements for a master's degree at Montana State University, I agree that the Library shall make it available to borrowers under rules of the Library.

If I have indicated my intention to copyright this thesis by including a copyright notice page, copying is allowable only for scholarly purposes, consistent with "fair use" as prescribed in the U.S. Copyright Law. Requests for permission for extended quotation from or reproduction of this thesis in whole or in parts may be granted only by the copyright holder.

Monica Zanzola Bruckner

December 2008

ACKNOWLEDGMENTS

I would like to thank my thesis advisor, Dr. Mark Skidmore, and my committee members, Dr. Brian McGlynn and Dr. Cathy Whitlock for their support and advice. Thank you to Jeff Bond, and the Yukon Geological Survey, the American Alpine Club, the MSU Department of Earth Sciences (especially the family of Barry C. Bishop), Dave Mogk and Carleton College, and the Big Sky Institute's GK-12 Program for funding my research and education. Thank you also to Karl Birkeland, Al vonFinster, George Aiken, and Julia Foght for their loan of field equipment and laboratory space. I would like to express my gratitude toward my field assistants, Galena Ackerman and Shawn McGlynn, who played endless games of Scrabble and cards with me in the field (and helped to collect data too, of course). And finally, I would like to thank my friends and family who provided me abundant laughter and fun, stimulating conversations, helpful advice, and unyielding encouragement throughout my years of education.

TABLE OF CONTENTS

1. INTRODUCTION 1

Site and Study Description 1
Background 5
Field Site Regional Physiography 10
References Cited 15

2. QUATERNARY GLACIAL HISTORY OF SOUTHERN YUKON 19

Glacial History of Southern Yukon, Canada 19
Onset of Glaciation 21
Glacial Maximum 22
Deglaciation 23
The Early Holocene and Current Interglacial 23
References Cited 24

3. FIELD SAMPLING METHODS AND LABORATORY ANALYSES 26

Field Site Description 26
Sampling Scheme and Catchment Characteristics: Glacial Retreat, Lake Profile, and Weather 27
Glacial Retreat 30
Lake Physical Characteristics 31
Weather 33
Hydrology Methods 34
Stream Gauging 34
Lake Water Residence Time and Groundwater Connectivity Among the Subcatchments (Salt and Rhodamine Tracers) 36
Water Chemistry Sampling 38
Primary Productivity and Cell Biomass 40
Water Chemistry Laboratory Analyses 43
Ion Chemistry 43
Charge Balance 44
Particulate Organic Carbon (POC) 44
Dissolved Organic Carbon (DOC) 45
Primary Productivity 46
Cell Enumeration 47
References Cited 49

4. RESULTS 51

TABLE OF CONTENTS – CONTINUED

Meteorological Conditions and Hydrology....51
Stream Discharge....52
Water Temperature....58
Suspended Sediment and Lake Sediment Deposition....59
Rhodamine Tracer: Surface Water Flow Path and Residence Time....63
Water Chemistry....65
pH and Electrical Conductivity....65
Ion Chemistry....67
Salt Tracer and Ion Chemistry....75
Carbon Chemistry: Dissolved Organic Carbon....79
Carbon Chemistry: Particulate Organic Carbon....80
Cell Enumeration....81
Primary Productivity....81
References Cited....83

5. DISCUSSION....86

Thermal Regime of the Wheaton Glacier....87
Meltwater Solute and Biogeochemical Weathering....91
The Effect of Water Storage Time on Meltwater Biogeochemistry....93
The Effect of Water Storage on Organic Carbon and Biota....97
Primary Productivity at the Wheaton Glacier Proglacial Lake....101
References Cited....104

6. SUMMARY AND CONCLUSIONS....108

APPENDIX A: Supplementary Materials....112

LIST OF TABLES

Table Page

1.1: Average climate from 1951-2000. Haines Junction is ~155 km west of Whitehorse and Burwash Landing is ~280 km west-northwest of Whitehorse. Table modified from Ogden, (2006).....12

3.1: Sampling frequency chart. Continuous data collection depicted by solid lines. Discrete sampling is indicated by "x." Sampling location abbreviations are as follows: ELS- East Lobe Stream; UWLS- Upper West Lobe Stream; LOS- Lake Outlet Stream; L1- Lake 0.5 m depth; L2- Lake 1.5 m depth; L3- Lake 5.0 m depth 29

4.1: Albedo (%) for various glacial surfaces (modified from Paterson, 1994).....56

4.2: Best fit lag times between air temperature and discharge for each stream based on correlation coefficients 57

4.3: Median ion concentrations ($\mu eq\ L^{-1}$) for the ELS, LOS, UWLS, and snow. Range of each dissolved ion is shown in parentheses. $n = 15$ for all ions except Cl^- and Na^+ ($n = 12$) which exclude data after the salt slug addition; $n = 2$ for snow.....68

4.4: Solute matrix showing r (upper right) and p-values (lower left) among major dissolved ions and suspended sediment concentrations (SSC). Correlations with a significant p-value ($p \leq 0.1$) are bolded and in larger font 68

4.5: Fluctuations in major dissolved ions in each stream from June-August 2006 74

4.6: Percent contribution of total discharge that comes from groundwater for each stream based on the salt slug travel from the lake to the UWLS and ELS assuming dilution efficiency of 100%, 20%, and 10%.....79

4.7: Particulate organic carbon as determined by mass loss on ignition 80

5.1: C-ratios for the ELS, UWLS, and LOS. 91

5.2: Rates of primary productivity (PP) for lakes located in mid- and high-alpine sites north of Sweden, Swiss Alps, the high Arctic, the Antarctic peninsula, and this study. Z_m represents maximum lake depth, Z represents mean lake depth, and PP represents rates of primary productivity.....103

LIST OF TABLES – CONTINUED

Table Page

A1: Ion concentrations (blank subtracted) and charge balance errors (CBE) for all samples. 113

A.2: pH values measured in the field on filtered samples from L1 (lake surface), L2 (1.5 m lake depth), L3 (5 m lake depth). LOS, ELS, and UWLS. pH values listed are averages of two measurements.. 115

A.3: Electrical conductivity (EC) ($\mu S\ cm^{-1}$) measured in the laboratory from filtered field samples from L1 (lake surface), L2 (1.5 m lake depth), L3 (5 m lake depth), LOS, ELS, and UWLS. 115

A.4: Suspended sediment ($mg\ L^{-1}$) for the lake surface (L1), 1.5 m lake depth (L2), 5 m lake depth (L3), LOS, ELS, and UWLS. 116

A.5: Regression relationships between discharge and ions in the ELS and LOS determined by LINEST function in Excel. Se-y refers to the standard error on the y-variable (ion concentration). 116

LIST OF FIGURES

Figure Page

1.1: Photograph of study site and flow chart of the Wheaton Glacier subcatchments. The entire catchment is approximately 4 km^2. Arrows on the photo represent the location of the East Lobe Stream (ELS), Upper West Lobe Stream (UWLS), and Lake Outlet Stream (LOS). The dashed line in the flow chart indicates the medial moraine and all streams flow north from the glacier to the Wheaton River 3

2.1: Map of glacial limits and distribution of glacial deposits in the Yukon. Red box indicates approximate location of the Wheaton Glacier. Figure modified from Bond, 2004 (after Duk-Rodkin, 1999) 20

2.2: Map of major physiographic regions referred to in this section; yellow box in inset defines area of larger image. Cassiar Mountains are to the east of this map section and Wheaton Glacier study area is indicated by the white star WSW of Bennett Lake. White arrows and stars represent locations of major bodies of water and cities, respectively. Figure modified from Bond, 2004.....22

3.1: (A) Wheaton Glacier location map (modified from Bond, personal comm.); contour interval is 100 ft. Photographs of (B) east lobe on 18 July 2006 and (C) west lobe on 1 August 2006 26

3.2: (A) September 1995 aerial photograph (# A28240-88) of the Wheaton Glacier catchment (National Air Photo Library, 1995) with drainage areas delineated and streams outlined in green, purple, and orange. Stream gauging and EC monitoring stations (dots) for the (B) East Lobe Stream (ELS), (C) Upper West Lobe Stream (UWLS), and (D) Lake Outlet Stream (LOS) are shown. The (E) temperature monitoring station was set up ~10 m N of the LOS monitoring station. Rebar pole height was ~1.5 m (B, C, D, E). 28

3.3: Glacier termini locations in September 1995 (green), June 2004 (yellow), and August 2006 (red) based on cairns (dots) constructed from a 1995 aerial photograph (# A28240-88, National Air Photo Library, 1995), June 2004 field season and 2006 field season, respectively. Lake location is indicated in blue on the west lobe 30

LIST OF FIGURES – CONTINUED

Figure Page

3.4: (A) The proglacial lake, with lake depths, major inflow and outflow locations, sites of tracer injections, short axis of the lake (T1), and the long axis of the lake (T2). (B) A coarse bathymetric map of the lake based on water depths from (A). The site of chemistry sampling and primary productivity assays is indicated by the white box. Pink "X"s represent sediment trap locations, pink numbers indicate Secchi disk depths measured at 10am and 3pm on 1 July and purple numbers indicate Secchi disk depths measured at 11am on 3 August. The sediment trap on the upper left corner of the figure moved via current along the dotted line between deployment and collection....32

3.5: (A) A 500 mL rhodamine slug was injected at the delta at 9am. (B) The rhodamine dispersion at 10 am and (C) 12 pm....37

4.1: Climograph for Whitehorse showing average precipitation (blue bars) and average temperature from 1971-2000 (red line) and average temperature for the 2006 field season (blue line). Error bars indicate 1 standard deviation. Data accessed online from records courtesy of Environment Canada (http://climate.weatheroffice.ec.gc.ca/) (2006) 51

4.2: Moving average (period = 24 hrs) of (A) air temperature (blue), ELS discharge (green), LOS discharge (orange), and UWLS discharge (purple) for June-August, 2006. Precipitation events are depicted by relative magnitude by blue arrows; the snow to ice transition on the glacier surface at the west lobe and lower third of the east lobe is depicted by a red line just above the x-axis (23 July-29 July); clear (blue) and overcast (gray) days are indicated by the line at the top of the graph. (B) Moving average of (period = 24 hrs) air temperature and area-normalized discharge 53

4.3: Rapid snowline retreat on the west (lake) and east (stream) lobes. Photos were taken at ~7am. The rapid snowline retreat began on 21 July (stream) and 23 July (lake), but note the dramatic change in ice exposure between 23 and 24 July....56

4.4: ELS (green), UWLS (purple), and LOS (orange): (A) 24-hr moving average of water and air (blue) temperature. (B) 12-hr moving average of diurnal fluctuations in water and air (blue) temperature 1-7 August....60

LIST OF FIGURES – CONTINUED

Figure Page

4.5: UWLS is the most turbid of the three streams.....61

4.6: Total suspended sediment (mg L^{-1}) in the lake (L1 = 0.5 m, L2 = 1.5 m, and L3 = 5 m depth), LOS, ELS, and UWLS. Note that the UWLS is plotted on a logarithmic secondary axis 61

4.7: Scatterplot of SSC and discharge. Note the secondary axis for the UWLS SSC, which was 1-2 orders of magnitude higher than in the LOS and ELS. 62

4.8: Sediment trap locations and depth of sediment collected (cm) from each trap 5 July-13 August, 2006. The yellow arrow indicates the movement of one sediment trap due a lake current. Note that the scale bar only pertains to the long axis of the lake. 63

4.9: Rhodamine export from the lake. The area under the dashed pink line (A) is based on discrete samples taken every 30-45 minutes (pink dots). The gold dashed line represents a hypothetical curve based on an exponential decay equation derived from discrete samples taken from 14 August 4:45pm through 16 August 9:30am 64

4.10: Time-series plot of electrical conductivity (EC) in μS cm^{-1} for the lake and streams.....66

4.11: Concentration of ions in the ELS, LOS and UWLS over the melt season as determined using a Metrohm Peak ion chromatograph and [HCO_3^-] via acid titration. Area normalized discharge from figure 4.2B for comparison. Concentration data were based on quadruplicate samples; error bars indicate 1 standard deviation from the mean of quadruplicate samples. 69

4.12: Anion concentrations (μeqL^{-1}) for the lake water samples. L1 indicates surficial lake waters, L2 is 1.5 m water depth, L3 is 5 m water depth, and LOS is Lake Outlet Stream. Bicarbonate was measured once in the field. Error bars on SO_4^{2-}, F^-, Cl^-, and NO_3^- denote 1 standard deviation from the mean of quadruplicate samples. Note the different y-axis scales.....70

LIST OF FIGURES – CONTINUED

Figure Page

4.13: Anion concentrations (μeqL^{-1}) for LOS, ELS, and UWLS. Single measurements of bicarbonate concentration were made on each sample. Error bars on SO_4^{2-}, F^-, Cl^-, and NO_3^- denote 1 standard deviation from the mean of quadruplicate samples. Note the difference in y-axis scales 71

4.14: Cation concentrations (μeqL^{-1}) for the lake. L1 indicates surficial lake waters, L2 is 1.5 m water depth, L3 is 5 m water depth, and LOS is Lake Outlet Stream. Error bars denote 1 standard deviation from the mean of quadruplicate samples. Variability in Mg^{2+} is likely due to sample concentrations near the detection limit of the ion chromatograph. Note the difference in y-axis scales 72

4.15: Cation concentrations (μeqL^{-1}) for LOS, ELS, and UWLS. Error bars represent 1 standard deviation from the mean of quadruplicate samples. Variability in Mg^{2+} is likely due to sample concentrations near the detection limit of the ion chromatograph. Note the difference in y-axis scales.....73

4.16**:** Possible salt injection groundwater flow path (arrow); green dot is the ELS sampling site, purple dot is the UWLS sampling site, and the tan dot indicates site of salt tracer injection (aerial photograph # A28240-88, National Air Photo Library, 1995). Inset and estimated contour lines (based on field observations) show that the lake is at a slightly higher elevation than the ELS sampling site. CI = 10 m, assume ELS is the 0 m reference point. 77

4.17: DOC concentrations.....80

4.18: Bacterial cell enumerations through the field season. Note L1 data point for 8 July is underneath L2 and L3 data points (numbers are similar to L2 and L3) and there is no data for L1 on 26 July due to loss of sample.....81

4.19: Rates of primary productivity in the lake at surface (L1), 1.5 m (L2), and 5 m (L3) water depths after 24-hour incubations in each environment following inoculation with ^{14}C bicarbonate 82

5.1: Surface flow path for UWLS water (red arrow) along the medial moraine, which provided a stable source for sediment acquisition for the UWLS water 90

LIST OF FIGURES – CONTINUED

Figure Page

5.2: Synthesis of organic carbon and biological time series data for the ELS, UWLS, and LOS and within the lake: 0.5 m lake depth (L1), 1.5 m lake (L2), and 5 m lake depth (L3) from 25 June-13 August, 2006 98

A.1: Proglacial stream ratings curves derived using the velocity-area method 116

A.2: Primary productivity data for 0.5 m lake depth (L1), 1.5 m lake depth (L2), 5 m lake depth (L3), and ELS. 117

A.3: Regression relationship between total dissolved solids (TDS) and electrical conductivity (EC) for LOS, ELS, and UWLS 117

A.4: Regression relationships for LOS, ELS, and UWLS. Dashed lines represent regression line for a bimodal distribution of suspended sediment in the UWLS, which may be dependent on water flowpath or sediment availability from the moraine. Mode 1 data points include data collected on 23 July and 4, 7, and 10 August. Mode 2 data points include data collected on 26 and 29 July and 1 and 4 August 118

A.2: Ion vs. discharge simple linear regression lines, equations, and R^2 values for the LOS and ELS. 119

A.3: Regression between dissolved Ca^{2+} and F^- and Na^+ and F^- for the ELS indicates weathering of fluorite or cryolite may be potential sources for high fluoride concentrations in the ELS 120

ABSTRACT

Proglacial environments, formed by glacier retreat, exhibit distinct characteristics in discharge, water temperature, water residence time, and dissolved ion, carbon, and suspended sediment concentrations. The unnamed alpine glacier at the headwaters of the Wheaton River, Yukon, Canada, provides an ideal setting to compare deglaciation processes that result in three different proglacial environments. The glacier has evolved from occupying one large catchment (~4 km^2) to two smaller catchments (each ~2 km^2) via glacier thinning and net mass loss, forming two lobes separated by a medial moraine. Field observations revealed neither crevasses nor evidence of subglacial drainage outlets and suggested this glacier had a non-temperate thermal regime with meltwater predominantly flowing from supraglacial and ice marginal sources. Climate and bedrock geology were similar for the subcatchments, providing a natural laboratory to compare deglaciation processes. This study compared the hydrology and biogeochemistry of three outlet streams from this glacier: one stream drained a proglacial lake which is fed by meltwater from the lower west lobe, a second stream drained the upper west lobe, and a third stream was the major drainage outlet for the east lobe. Hydrologic monitoring over the 2006 melt season (June-August) and analyses of water samples for dissolved ion content and carbon indicated that the meltwaters are dominated by Ca^{2+} and HCO_3^-, which are derived from biogeochemical weathering of crustal materials. The study demonstrated that the presence of the proglacial lake, which acted as a meltwater reservoir, measurably modified meltwater residence time, water temperature, water chemistry, and bacterial biomass relative to the proglacial streams. Rock:water interaction between meltwater and medial morainal sediment and fine-grained, reactive glacial flour suspended in the streams and the lake water column also enhanced biogeochemical weathering within the catchment. Thus, this study provided a small-scale example for how differences in proglacial environments and water flow paths affect headwater hydrology and biogeochemistry. This study was the first of its kind in the Coast Mountains, Yukon, Canada, and results presented here aid in the understanding of how proglacial environments created by climate-induced glacier retreat affect hydrochemistry, hydrology, and carbon dynamics in remote high elevation environments.

CHAPTER 1

INTRODUCTION

Information regarding headwater environments is important in understanding the effect of climate change on downstream environments. Headwater environments and processes occurring within them are the first in a chain of variables that affect downstream aquatic chemistry and biology. However, the effects of the development of new proglacial environments, such as proglacial lake formation, due to recent glacier retreat on downstream hydrology and ecology are not well understood. A proglacial lake created by glacial retreat modifies the hydrologic system, which affects headwater primary productivity and nutrient budgets and thus potentially changes the overall ecology of the system. A change in nutrient supply will affect food webs both in the headwaters and downstream. Hence, an understanding of processes related to different styles of deglaciation in headwater catchments is vital in assessing their downstream effects. The objective of this study was to evaluate how differing proglacial headwater environments (lake vs. stream) affected discharge, dissolved ion concentrations, and carbon dynamics in a 4 km^2 glaciated catchment, at the headwaters of the Wheaton River in the Canadian Coast Range, Yukon Territory.

Site and Study Description

The glacier complex at the headwaters of the Wheaton River, YK, Canada provided an ideal physical setting to contrast deglaciation processes. The unnamed glacier (hereafter referred to as the Wheaton Glacier) has evolved from occupying one

large catchment (4 km^2) to two smaller catchments (each 2 km^2) due to glacier thinning and net mass loss, forming two lobes separated by a medial moraine (Figure 1.1). The terminal moraine ~730 m down valley from the 2006 terminus of the Wheaton Glacier is considered to have formed during the Little Ice Age and there is also evidence of a prominent terminal moraine also likely from the little Ice Age in the neighboring glaciated valley to the East (J. Bond personal communication). Prominent trim-lines on the valley walls that trace to this terminal moraine indicate the glacier was xx meters deeper when the moraine was formed. The Wheaton Glacier has been retreating and thinning considerably since that time, depositing till on the valley floor during retreat, but specific rates of retreat, e.g. on a decadal basis, are undocumented (J. Bond personal communication).

The west lobe of the glacier terminated into a young (< 10 years old) proglacial lake, while the east lobe was drained via a single main outlet stream. Studies on proglacial lakes with a glacier terminating into them are uncommon in the literature since ice front calving typically makes access problematic. Calving did not occur at this glacier.

These “paired” catchments had comparable bedrock and climate and were essentially a natural laboratory where the effects of different headwater environments, the proglacial lake vs. the proglacial streams, on meltwater chemistry could be compared. The catchments primarily received atmospheric, solar, and bedrock nutrient and energy sources with minor macrobiotically-derived carbon inputs from sparse vegetation and minimal animal activity.

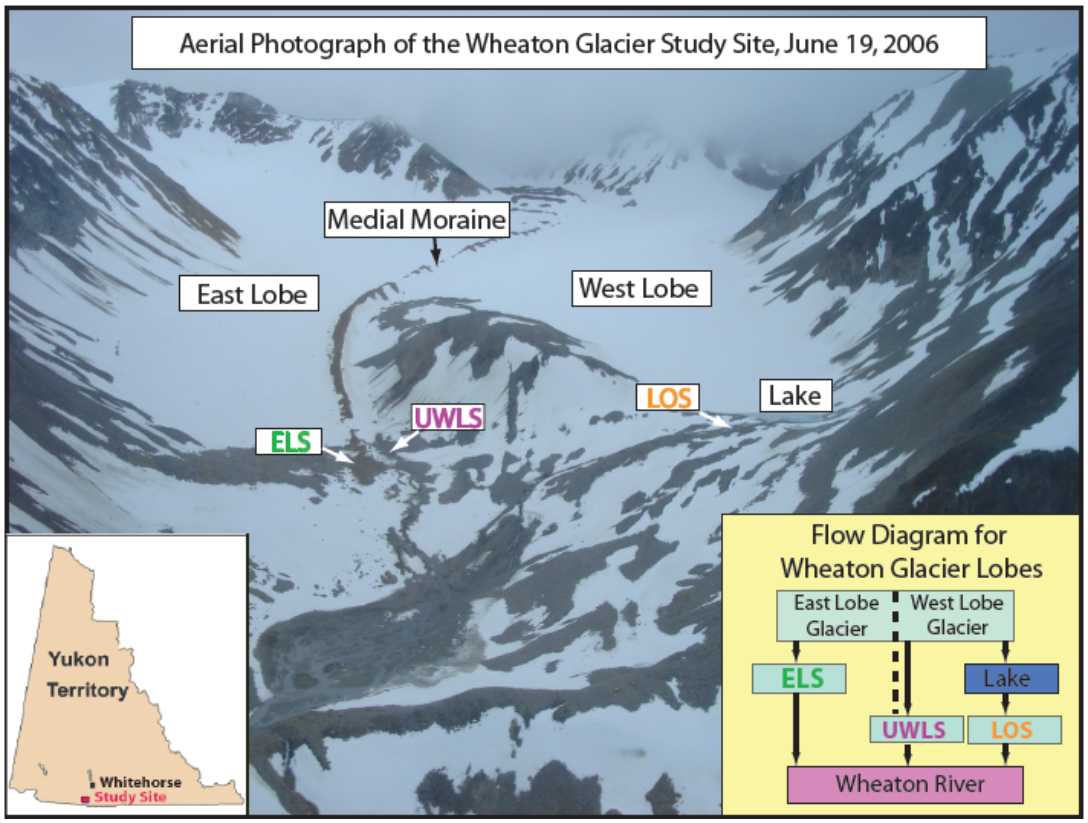


Figure 1.1: Photograph of study site and flow chart of the Wheaton Glacier subcatchments. The entire catchment is approximately 4 km^2. Arrows on the photo represent the location of the East Lobe Stream (ELS), Upper West Lobe Stream (UWLS), and Lake Outlet Stream (LOS). The dashed line in the flow chart indicates the medial moraine and all streams flow north from the glacier to the Wheaton River.

The Wheaton Glacier appeared to be non-temperate based on field observations and aerial photographs. Non-temperate glaciers can be either (1) cold-based with no liquid water flowing at the base, or (2) polythermal, with pockets of water at the base (Benn and Evans, 1998). Hodgkins (1997) documented a critical ice thickness of > 90 m for basal ice to reach its pressure-melting point (based on polythermal conditions at this depth at a 10 km^2 glacier at Austre Brøggerbreen, Svalbard) as necessary for polythermal conditions to exist. The small size (4 km^2), lack of crevassing on the glacier surface, and no evidence for subglacial drainage outlets at the terminus suggested that the Wheaton

Glacier was non-temperate. This study compared the hydrology and solute and carbon dynamics from three distinct proglacial streams: one stream was fed by meltwater that flowed directly from the east lobe of the glacier (ELS, Figure 1.1), a second stream was fed by meltwater from the upper west lobe and flowed along the medial moraine (UWLS, Figure 1.1), and a third stream drained a proglacial lake located directly in front of the west lobe (LOS, Figure 1.1).

This study tested the following hypotheses to address the overarching theme of the thesis to evaluate how differing proglacial environments affect discharge, dissolved ion concentrations, and carbon dynamics in a glaciated sub Arctic catchment:

(H1) The Wheaton Glacier is non-temperate.

Biogeochemical and hydrological analysis of proglacial stream water chemistry was used to assess whether there was a significant subglacial component to the outflowing streams at the Wheaton Glacier and thus whether the glacier is non-temperate with little to no water flowing at its base.

(H2) Water storage time differences between the proglacial streams vs. lake produce more consistent discharge and dissolved ion concentration in the LOS, and lower SSC in the LOS relative to the ELS and UWLS.

Lake water residence times were measured using salt and rhodamine tracers and discharge, dissolved ion concentrations, and SSCs were compared among the ELS, LOS, and UWLS.

(H3) Primary productivity, microbial biomass and thus organic carbon is higher in the lake, and LOS relative to the ELS and UWLS

Bacterial enumerations in the ELS, LOS, and in the lake compare the amount of biomass among the proglacial streams and lake. Discrete samples for organic carbon concentration were compared between the ELS, LOS, UWLS and lake to evaluate differences in concentrations of DOC and POC among the streams and lake.

Background

Rapid retreat of alpine glaciers has been observed around the world and is thought to be a result of warmer temperatures related to global climate change (Lemke et al., 2007). Alpine glaciers across the U.S. and Canadian Rocky Mountains and Coast Ranges are currently retreating and approximately 25% of ice cover in the Canadian Rocky mountains has disappeared since the Little Ice Age 130-150 years ago (Barry and Seimon, 2000). Glacier retreat affects the timing and magnitude of water, sediment, and nutrient supply downstream, which influences the biogeochemical and sediment fluxes to fluvial systems (Hauer et al., 1997).

High alpine lakes and streams, some of which are fed by glacial meltwater, have been found to be highly sensitive to climate change with respect to their solute content as measured by electrical conductivity, water temperature (McGowan et al., 2007), pH, biodiversity (e.g. Sommaruga-Wograth et al., 1997; Koinig et al., 1998; Hodson et al., 2000; Battin et al., 2004), and levels of UV radiation (Vinebrooke and Leavitt, 1996; Reche et al., 2001). The remote nature of high alpine lakes makes them unique systems in that they are sensitive to regional climate change with little direct anthropogenic influence (Koinig et al., 1998).

Seasonal melt can affect sediment load and water availability (via snowmelt) in snow-dominated or glaciated regions (Battin et al., 2004). Seasonal glacier dynamics can affect supraglacial, subglacial, and proglacial flowpaths (Fountain and Walder, 1998) and dissolved solutes in a catchment (Hodgkins et al., 1998), which can impact fluvial geomorphology and nutrient budgets in downstream lotic environments (e.g. Smith et al., 2001; Battin et al., 2004). Most studies to date have focused on hydrology and solute dynamics of temperate glacier systems where the subglacial drainage system is well-developed (e.g. Sharp et al., 1995; Hodson et al., 2000; Tranter et al., 2002; Hodson et al., 2005). Studies on solute dynamics in these temperate glacial environments have examined inorganic carbon and silica due to their geochemical feedbacks in the coupled cryosphere-atmosphere system and the importance of biogeochemical weathering at the glacier bed (Sharp et al., 1995; Hodson et al., 2000; Tranter et al., 2002).

Hodson et al. (2005) compared nutrient budgets for proglacial streams over two meltseasons in two adjacent, sparsely vegetated glaciated catchments in Svalbard; one glacier in the Austre Brøggerbreen basin was polythermal and almost entirely cold-based with no subglacial flow, whereas the other glacier in Midre Lovénbreen basin was classified as polythermal, and had a greater occurrence of subglacial flow. Hodson et al. (2005) found that the existence of subglacial drainage and subglacial water storage influenced meltwater chemistry by enhancing biogeochemical weathering. Enhanced weathering occurred as a result of increased contact between meltwater and fine-grained rock at the base of the glacier as well as by nutrient cycling by microbial populations at the wet glacier bed.

Preliminary air-photo analysis of the Wheaton glacier indicates that it is likely non-temperate, thus follows a brief review of non-temperate glacier hydrology and aqueous geochemistry. Non-temperate glaciers can be either (1) cold-based with no liquid water flowing at the base, or (2) polythermal, with water at the base in certain regions (Benn and Evans 1998). Non-temperate, cold-based glaciers are common at high latitudes and, unlike temperate and polythermal glaciers, they lack a developed subglacial drainage system (Hodgkins, 1997).

Meltwater from cold-based, non-temperate glaciers is sourced primarily via direct supraglacial melt. Studies involving hydrology and solute dynamics of proglacial streams fed by non-temperate glaciers in Svalbard indicate that the lack of a developed subglacial drainage system beneath a cold-based glacier results in major differences in the associated hydrology, sediment dynamics, and aqueous geochemistry relative to that of a polythermal glacial with a more developed subglacial drainage system. These differences result from a large portion of biogeochemical weathering that occurs at the bed of polythermal glaciers which is due meltwater flow to the bed that facilitates long rock-water interaction duration and to the presence of reactive fine-grained glacial flour at the bed; in contrast, cold-based non-temperate glaciers have limited, if any, subglacial water flow and storage and thus are limited in subglacial geochemical weathering processes (Hodgkins, 1997; Hodgkins et al., 1998; Wadham et al., 1998). Studies on the smaller cold-based glaciers in the Dry Valleys region in Antarctica note that these glaciers lack a substantial subglacial drainage component (e.g. Lyons et al., 2003; Fortner et al., 2005.), with the exception of Taylor Glacier which is an outlet glacier for the West

Antarctic Ice Sheet and has polythermal characteristics (e.g. Hubbard et al. 2004/5?) These studies reveal the importance of aeolian-derived sediment and dust to the glacier surface since this supraglacial sediment and dust provides weatherable material to the meltwater system (Lyons et al., 2003; Fortner et al., 2005. Literature for hydrological and biogeochemical studies involving cold-based glaciers outside of Svalbard and the Antarctic Dry Valleys is sparse.

Few studies have focused on the hydrology, solute, and carbon dynamics of proglacial lakes at non-temperate glaciers. There is a large volume of literature for the Antarctic Dry Valley lakes, but these lakes generally have a permanent ice cover, with the exception of the hypersaline Don Juan Pond (Chinn, 1993). Additionally, these Dry Valley lakes receive little to no input from precipitation, are often saline, and are stratified for 10+ years (e.g. Chinn, 1993); thus they are not analogous to the Wheaton Glacier study. Most of the literature that exists regarding high alpine proglacial lakes has been related to contemporary measurements of hydrological and biogeochemical effects of climate change on long-term measurements of lake water pH (Sommaruga-Wograth et al., 1997; Koinig et al., 1998), influxes of atmospheric dust, especially as they relate to decreasing duration of lake ice cover due to warming climates (Sommaruga-Wograth et al., 1997; Koinig et al., 1998; Psenner, 1999), and diatom biodiversity (Sommaruga-Wograth et al., 1997; Koinig et al., 1997). Other studies use paleoclimate proxies, such as diatoms (e.g. Koinig et al. 1998; McGowan et. al, 2007), as indicators for effects of climate-induced temperature change on pH and diatom diversity, which are related to the duration of ice cover and atmospheric dust deposition.

Studies involving alpine lakes in non-glaciated catchments have revealed the importance of catchment characteristics on lake water chemistry. Bedrock mineralogy, vegetation, and slope (Kamenik et al., 2001) as well as altitude (Anderson et al., 2001) have been used to explain variability in water chemistry in 44 alpine lakes in the Eastern Alps across an elevation gradient of 1502-2309 m asl (Kamenik et al., 2001) and at 69 lakes in West Greenland (Anderson et al., 2001). Bedrock mineralogy was important as a source of weathering material, vegetation affected sources and sinks for nutrients and carbon, and slope affected overland flow (run-off) which was found to affect nitrogen retention on 40-60° slopes (Kamenik et al., 2001). Altitude was important when considering weathering rates, vegetation cover, and soil development, which all tend to decline at higher altitudes (Anderson et al., 2001). Aspect was found not to be significantly related to water chemistry (Kamenik et al., 2001), but it is likely important in biological processes and the effects of UV radiation on primary productivity in alpine lakes (Vinebrooke and Leavitt, 1996; Reche et al. 2001).

Concentrations of dissolved organic material in alpine catchments are low compared with non-alpine lakes due to a lack of vegetation in the catchment that provides allochthonous organic material (Reche et. al, 2001). Low concentration of dissolved organic material in high alpine lakes makes them among the most UV transparent aquatic systems in the world (Sommaruga, 2001) and thus renders them sensitive to UV radiation, especially as it relates to increased depths of UV transmission (Reche et al., 2001) and photoinhibition of primary producers due to high solar irradiance (Vinebrooke and Leavitt, 1996). Therefore, primary productivity in oligotrophic alpine lakes is

sensitive to climate change because organisms living within these lakes are affected by increases in UV radiation caused by decreased duration of lake ice cover (Laurion et al., 2000; Sommaruga, 2001).

Lake and stream processes differ on many levels. Streams are generally more dynamic, high energy systems with short water residence times, while lakes tend to be lower energy environments with longer residence times (Wetzel, 2001). Residence time affects water temperature, sediment dynamics, weathering processes, nutrient cycling, and biologic community structure (Wetzel, 2001).

This study compared sediment, dissolved ion, and organic carbon dynamics among three proglacial stream subcatchments to demonstrate the influence of processes occurring in a proglacial lake relative to processes occurring in proglacial streams on headwater hydrology and biogeochemistry. The study also investigated primary productivity dynamics for a young (< 10 years old), small proglacial lake in the Canadian Coast Mountains fed by supraglacial waters thus providing insight into aspects of the limnology of young proglacial lakes.

Field Site Regional Physiography

The Wheaton Glacier (informal name) field site is located in the Coast Mountains of southwest Yukon Territory, Canada (latitude 60° 04.016' N, longitude 135° 33.848' W, elevation from glacier head to terminus spans ~1705-2225 m asl). The field site is approximately 80 km south-southwest of the Yukon's capital city of Whitehorse. The Wheaton Glacier field site is located within the Canadian Subarctic region of the Moist

Continental Climate (*Dfc*) Highlands in the Köppen climate classification system (Strahler and Strahler, 2006). Climate data averaged from records spanning from 1951-2000 at three sites (Haines Junction, Burwash Landing, and Whitehorse) indicated that mean annual temperatures in southwest Yukon have ranged from -4.4 to -0.7°C and have increased through the 50 year period (Table 1.1; Ogden, 2006). Annual precipitation, which ranged from 261.2 to 305.7 mm, has generally increased from the 1951-1980 normals at Whitehorse and decreased at Burwash Landing during the 50-year climate record (Table 1.1; Ogden, 2006).

The Wheaton Glacier field site is part of the Boreal Cordillera Ecozone and the Yukon Stikine Highlands ecoregion, which bounds the northernmost Coast Mountains and extends south into British Columbia (Smith et al., 2004). This ecoregion is characterized by Pacific maritime weather systems, with relatively moderate temperatures and precipitation (Brabets et al., 2000). Mean annual temperature for the ecoregion is approximately -2.5°C, with temperatures ranging between ~ -18°C at high elevations (> 2000 m asl) in January to ~5°C in July, which are typically the coldest and warmest months, respectively (Smith et al., 2004). Mean annual precipitation is 300-500 mm, with the lowest precipitation occurring from February-May, and precipitation occurring mainly as snow from October-May (Smith et al., 2004).

Table 1.1: Average climate from 1951-2000. Haines Junction is ~155 km west of Whitehorse and Burwash Landing is ~280 km west-northwest of Whitehorse. Table modified from Ogden, (2006).

Station	1951-1980	1961-1990	1971-2000	Δ1951-1980 & 1971-2000
Annual Mean Temperatures (ºC)				
Haines Junction	-3.2	-2.9	n/a	n/a
Burwash Landing	-4.4	-4.0	-3.8	0.6
Whitehorse	-1.2	-1.0	-0.7	0.5
Mean Daily Temperatures for January (ºC)				
Haines Junction	-22.9	-21.5	n/a	n/a
Burwash Landing	-24.4	-22.3	-22.0	2.4
Whitehorse	-20.7	-18.7	-17.7	3.0
Mean Daily Temperatures for July (ºC)				
Haines Junction	12.5	12.6	n/a	n/a
Burwash Landing	12.3	12.5	12.8	0.5
Whitehorse	14.1	14.0	14.1	no change
Annual Mean Total Precipitation (mm)				
Haines Junction	292.5	305.7	n/a	n/a
Burwash Landing	301.0	290.0	279.7	-21.3
Whitehorse	261.2	268.8	267.4	6.2

The ecoregion hydrologic system drains to both the Alsek and Yukon Rivers, the latter being the drainage catchment for this study. Within this ecoregion, the Yukon River drainage basin includes the upper Takhini, Primrose, Watson, and Wheaton (the tributary in this study) rivers (Smith et al., 2004). Glacier coverage in this ecoregion comprises 1.42% of the total area, yet glacier melt contributions dominate the hydrologic system in the Yukon portion of the ecoregion. The lowest discharge occurs in March and is followed by a rapid increase in discharge during snowmelt in early May. Discharge peaks in July-August as a result of high elevation snowfield and ice melt (Smith et al., 2004). Permafrost is discontinuous and sporadic within this region and soils generally fall into the Brunisol classification (mildly weathered mineral soil) (Brabets et al., 2000).

Treeline in the Yukon Stikine ecoregion occurs at approximately 1200 m asl, thus most of the region lies above treeline (Smith et al., 2004). The three main vegetation zones in the ecoregion are alpine tundra, dominated by dwarf birch (*Betula*), willow

(*Salix*), grass and lichen; subalpine forest of alpine fir (*Abies lasiocarpa*) and white spruce (*Picea glauca*); and closed boreal forest with black and white spruce (*Picea mariana* and *Picea glauca*) (Brabets et al., 2000).

The Yukon Stikine Highlands encompass four exotic terranes, which are from east to west, the Yukon-Tanana, Stikinia, Wrangellia, and Alexander Terranes; the Coast Plutonic Complex and other undivided metamorphic rocks (Gordey and Makepeace, 2001). Granitic intrusions, mainly from the Coast Plutonic Complex, outcrop in ~60% of the region (Smith et al., 2004). Other common rock types include andesite and dacite flows and breccia, biotite granodiorite, quartz-mica schist, micaceous quartzite, and weakly metamorphosed volcanic and sedimentary rocks (e.g. basalt, andesite, sandstone, and conglomerate) from the Wrangellia Terrane (Smith et al., 2004). This region contains gold, silver, and antimony-bearing quartz veins at Mount Stukum and Montana Mountain as well as copper, zinc, and lead-bearing quartz veins and placer deposits in addition to picrolite asbestos in Wrangellian volcanics (Smith et al. 2004). Bedrock geology at the Wheaton Glacier field site is composed of late Proterozoic and Paleozoic biotite-muscovite-quartz-feldspar schist, granulite-quartzite, and chlorite-biotite orthogneiss at the lower quarter of the catchment, with early Tertiary granite/alaskite/quartz monzonite/granodiorite in the upper three-quarters of the catchment (Bond, J., personal comm.).

Late Pleistocene glaciers emanated from the St. Elias Mountains, eastern Coast Ranges, and the Cassiar lobe of the Cordilleran Ice Sheet during the McConnell Glaciation (23 ka) and created most of the surficial geology and landforms of this region

(Smith et al., 2004). The glacial history of the region will be discussed in further detail in Chapter 2.

References Cited

Anderson, N.J., Harriman, R., Ryves, D.B., and Patrick, S.T., 2001. Dominant factors controlling variability in the ionic composition of West Greenland lakes. *Arctic, Antarctic, and Alpine Research*, v. 33, n. 4, pp. 418-425.

Barry, R.G., and Seimon, A., 2000. Research for Mountain Area Development: Climatic Fluctuations in the Mountains of the Americas and Their Significance. *Ambio*, v. 29, n. 7, pp. 364-370.

Battin, T.J., Wille, A., Psenner, R., and Richter, A., 2004. Large-scale environmental controls on microbial biofilms in high-alpine streams. Biogeosciences, v. 1, pp. 159-171.

Benn, D.I. and Evans, D.J.A., 1998. Glaciers and Glaciation. New York: Arnold Publishing Co., 734 p.

Brabets, T.P., Wang, B., and Meade, R.H., 2000. Environmental and Hydrologic Overview of the Yukon River Basin, Alaska and Canada. USGS Water-Resources Investigations Report 99.4204. 106 p.

Chinn, T.J., 1993. Physical hydrology of the Dry Valley Lakes. *Antarctic Research Series ANTSA4*, Vol. 59, pp. 1-51.

Fortner, S.K., Tranter, M., Fountain, A., Lyons, W.B., and Welch, K.A., 2005. The geochemistry of supraglacial streams of Canada Glacier, Taylor Valley (Antarctica) and their evolution into proglacial waters. *Aquatic Geochemistry*, v. 11, pp. 391-412.

Fountain, A.G. and Walder, J.S., 1998. Water flow through temperate glaciers. *Reviews of Geophysics*, v. 36, n. 3, pp. 299-328.

Gordey, S.P. and Makepeace, A.J. (eds.), 2001. Bedrock geology, Yukon Territory. Exploration and Geological Sciences Division, Yukon Region, Indian and Northern Affairs Canada, Open File 2000-12.

Hauer, R.F., Baron, J.S., Campbell, D.H., Fausch, K.D., Hostetler, S.W., Leavensley, G.H., Leavitt, P.R., McKnight, D.M., and Stanford, J.A., 1997. Assessment of climate change and freshwater ecosystems of the Rocky Mountains, USA and Canada. *Hydrological Processes*, v. 11, pp. 903-924.

Hodgkins, R., 1997. Glacier hydrology in Svalbard, Norwegian high Arctic. *Quaternary Science Reviews*, v. 16, pp. 957-973.

Hodgkins, R., Tranter, M., and Dowdeswell, J.A., 1998. The hydrochemistry of runoff from a 'cold-based' glacier in the High Arctic (Scott Turnerbreen, Svalbard). *Hydrological Processes*, v. 12, pp. 87-103.

Hodson, A.J., Tranter, M., and Vante, G., 2000. Contemporary rates of chemical denudation and atmospheric CO_2 sequestration in glacier basins: an Arctic perspective. *Earth Surface Processes and Landforms*, v. 25, pp. 1447-1471.

Hodson, A.J., Mumford, P.N., Kohler, J., and Wynn, P.M., 2005. The High Arctic glacial ecosystem: new insights from nutrient budgets. *Biogeochemistry*, v. 72, pp. 233-256.

Kamenik, C., Schmidt, R., Kum, G., and Psenner, R. 2001. The influence of catchment characteristics on the water chemistry of mountain lakes. *Arctic, Antarctic, and Alpine Research*, v. 33, n. 4, pp. 404-409.

Koinig, K.A., Schmidt, R., Sommaruga-Wograth, S., Tessardri, R., and Psenner, R., 1998. Climate change as the primary cause for pH shifts in a high alpine lake. *Water, Air and Soil Pollution*, v. 104, pp. 167-180.

Laurion, I., Ventura, M., Catalan, J., Psenner, R., and Sommaruga, R., 2000. Attenuation of ultraviolet radiation in mountain lakes: Factors controlling the among- and within-lake variability. *Limnology and Oceanography*, v. 45, n. 6, pp 1274-1288.

Lemke, P., J. Ren, R.B. Alley, I. Allison, J. Carrasco, G. Flato, Y. Fujii, G. Kaser, P. Mote, R.H. Thomas and T. Zhang, 2007. Observations: Changes in Snow, Ice and Frozen Ground. In: *Climate Change 2007: The Physical Science Basis. Contribution of Working Group I Fourth Assessment Report of the Intergovernmental Panel on Climate Change* [Solomon, S., D. Qin, M. Manning, Z. Chen, M. Marquis, K.B. Averyt, M. Tignor and H.L. Miller (eds.)]. Cambridge University Press, Cambridge, United Kingdom and New York, NY, USA. 48pp.

Lyons, W.B., Welch, K.A., Fountain, A.G., Dana, G.L., Vaughn, B.H., and McKnight, D.M., 2003. Surface glaciochemistry of Taylor Valley, southern Victoria Land, Antarctica and its relationship to stream chemistry. *Hydrological Processes*, v. 17, pp. 115-130.

McGowan, S., Juhler, R.K., and Anderson, N.J., 2007. Autotrophic response to lake age, conductivity, and temperature in two West Greenland lakes. *Journal of Paleolimnology*, v. 39, pp. 301-317.

Ogden, A., 2006. Backgrounder: Climate, Climate Variability and Climate Change in the Southwest Yukon. Environment Canada Northern Climate ExChange, 24 p.

Psenner, R., 1999. Living in a dusty world: airborne dust as a key factor for alpine lakes, *Water, Air, and Soul Pollution*, v. 112, pp. 217-227

Reche, I., Pulido-Villena, E., Conde-Porcuna, J.M., and Carrillo, P., 2001. Photoreactivity of dissolved organic matter from high-mountain lakes of Sierra Nevada, Spain. *Arctic, Antarctic, and Alpine Research*, v. 33, n. 4, pp. 426-434.

Sharp, M., Tranter, M., Brown, G.H., and Skidmore, M., 1995. Rates of chemical denudation and CO_2 drawdown in a glacier-covered alpine catchment. *Geology*, v. 23, pp. 61-64.

Smith, B.P.G., Hannah, D.M., Gurnell, A.M., and Petts, G.E., 2001. A hydrogeomorphological context for ecological research on alpine glacial rivers. *Freshwater Biology*, v. 46, pp. 1579-1596.

Smith, C.A.S., Meikle, J.C., and Roots, C.F. (eds), 2004. Ecoregions of the Yukon Territory: Biophysical properties of Yukon landscapes. Agriculture and Agri-Food Canada, PARC Technical Bulletin No. 04-01, Summerland, British Columbia, 313 p.

Sommaruga, R. 2001. The role of solar UV radiation in the ecology of alpine lakes. *Journal of Photochemistry and Photobiology B: Biology*, v. 62, pp. 35-42.

Sommaruga-Wograth, S., Koinig, K. A., Schmidt, R., Sommaruga, R., Tessadri, R., and Psenner, R., 1997. Temperature effects on the acidity of remote alpine lakes. *Nature*, v. 387, pp. 64-67.

Strahler, A. and Strahler, A., 2006. Introducing Physical Geography. 4th ed. Hoboken: John Wiley and Sons, Inc., 728 p.

Tranter, M., Sharp, M.J., Lamb, H., Brown, G.H., Hubbard, B.P., and Willis, I.C., 2002. Geochemical weathering at the bed of Haut Glacier d' Arolla, Switzerland- a new model. *Hydrological Processes*, v. 16, pp. 959-993.

Vinebrooke, R. D. and Leavitt, P.R., 1996. Effects of ultraviolet radiation on periphyton in an alpine lake. *Limnology and Oceanography*, v. 41, pp. 1035-1040.

Wadham, J.L., Hodson, A.J., Tranter, M., and Dowdeswell, J.A., 1998. The hydrochemistry of meltwaters draining a polythermal-based, high Arctic glacier, south Svalbard: I. The ablation season. *Hydrological Processes*, v. 12, pp. 1825-1849.

Wetzel, R.G., 2001. Limnology: Lake and River Ecosystems. 3rd ed. San Francisco: Academic Press. 1006 p.

CHAPTER 2

QUATERNARY HISTORY OF SOUTHERN YUKON, CANADA

Glacial History of Southern Yukon, Canada

The glacial history of the Yukon is complex, with a series of glacial and interglacial periods that were partially controlled by relative uplift of coastal mountain ranges over a 2 million year time frame, since these mountains acted as precipitation barriers (Schweger, 1997). The three major glaciations in the Yukon area were the McConnell Glaciation (23.9 ka-10.7 ka) (Bond, 2004), Reid Glaciation (300 ka-200 ka) (Huscroft et al., 2004), and Pre-Reid Glaciation (> 311 ka) (Huscroft et al., 2006). Figure 2.1 illustrates the glacial limits and distribution of glacial deposits for each glaciation in the Yukon. Little evidence remains of early glaciations (e.g. Reid and pre-Reid) in the Whitehorse area due to erosion or burial by the more extensive McConnell advances; however, a history of glacial and interglacial periods can be constructed from well-preserved stratigraphic records from the arid and hence minimally-glaciated central Yukon region (Bond, 2004). Due to limited information regarding early glaciations, the following description will focus on the McConnell Glaciation.

The McConnell Glaciation is divided into four stages: onset of glaciation, glacial maximum, deglaciation, and early Holocene (Bond, 2004). During the McConnell Glaciation, the Cassiar and Coast Mountain lobes of the Cordilleran ice sheet advanced northeastward and westward into southern and central Yukon (Jackson et al., 1991; Bond, 2004; Smith et al., 2004). Montane glaciers in the Yukon Stikine Highlands (e.g. those

from the St. Elias Mountains and eastern Coast Range) augmented this ice cover during interglacial periods, resulting in the preservation of ice during the interglacials (Smith et al., 2004).

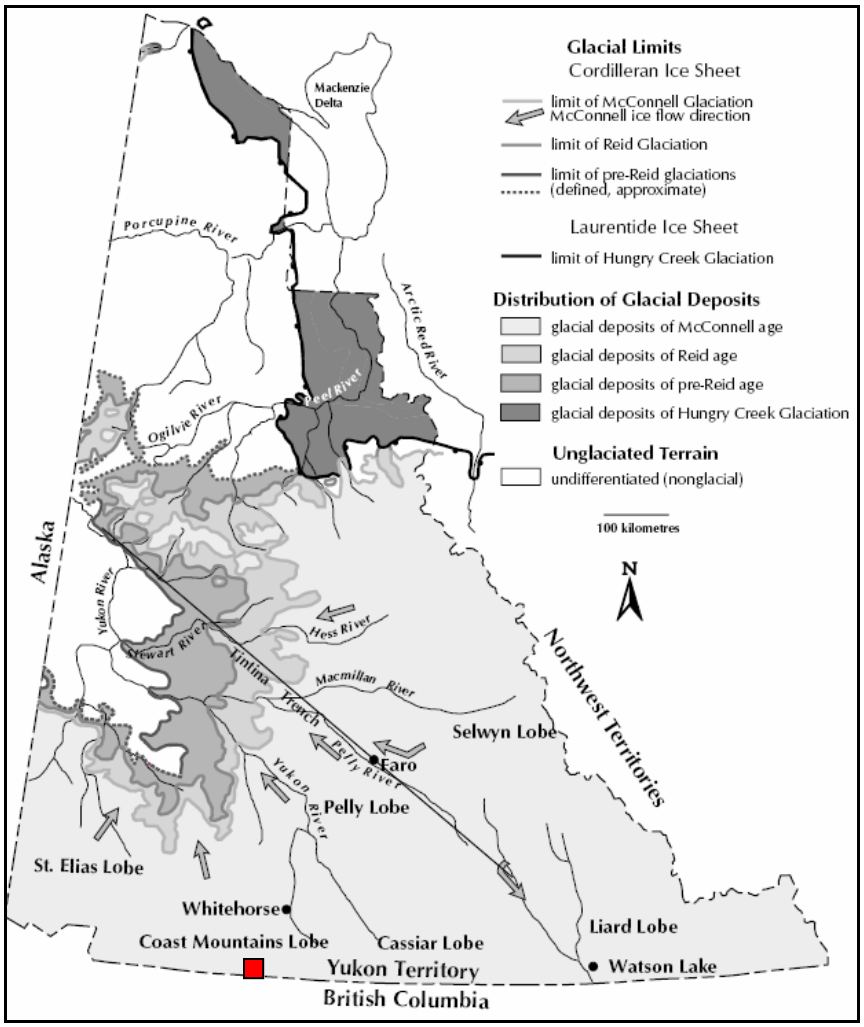


Figure 2.1: Map of glacial limits and distribution of glacial deposits in the Yukon. Red box indicates approximate location of the Wheaton Glacier. Figure modified from Bond, 2004 (after Duk-Rodkin, 1999).

Deglaciation in the southern Yukon is characterized by punctuated periods of stillstands and readvances during an overall frontal retreat (Bond, 2004). Differential retreat of the Cassiar and Coast Mountain ice lobes enabled the readvance of the Cassier

lobe up-gradient into Coast Mountain valleys and produced a pattern of deglaciation that resulted in changes in drainage patterns due to ice damming and the formation of proglacial lakes (Bond, 2004; Smith et al., 2004). The stages of the McConnell Glaciation will be discussed in further detail below.

Onset of Glaciation

Evidence for the onset of glaciation (~29 ka) in south-central Yukon is scarce since it was removed or buried by subsequent ice readvances. The timing of the onset of glaciation is inferred from pollen records from sediments at sites north and west of Whitehorse. The oldest evidence for the onset of glaciation is a tree stump with radiocarbon age of approximately 38 ka (Matthews et al., 1990), which was found in the Selwyn Mountains near Mayo (northwestern Yukon). The stump was rooted in sediments much like those that exist in the contemporary riverine environment (Jackson et al., 1991). Pollen analysis from this sediment suggests an extensive forest cover in the area at 38 ka (Matthews et al., 1990) and a disappearance of the forest by ~30 ka with the establishment of a periglacial climate (Matthews et al., 1990; Jackson et al., 1991).

Ice first accumulated in cirques in the Coast Mountains and then coalesced to form valley glaciers in the Wheaton River, Bennett Lake, and Watson River valleys (Figure 2.2). Eventually these formed a Coast Mountain ice cap with glaciers radiating outward to fill major valleys such as the upper Takhini, Primrose, Wheaton, and Watson river valleys (Bond, 2004). Ice accumulation in the Cassiar Mountains of south-central Yukon and the Atlin District of northern British Columbia also began at this time, leading to ice cap formation and advance northwestward into the Whitehorse area (Bond, 2004).

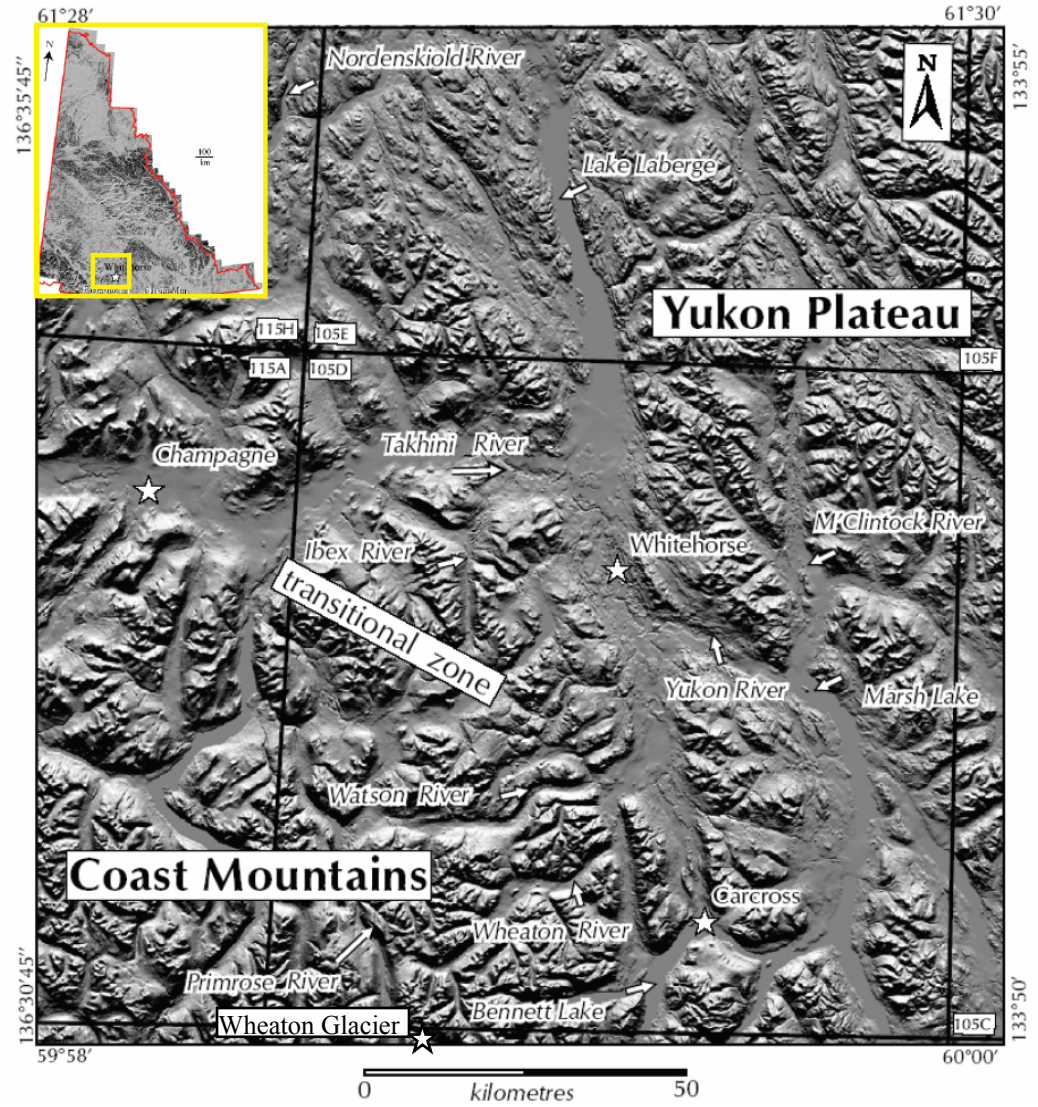


Figure 2.2: Map of major physiographic regions referred to in this section; yellow box in inset defines area of larger image. Cassiar Mountains are to the east of this map section and Wheaton Glacier study area is indicated by the white star WSW of Bennett Lake. White arrows and stars represent locations of major bodies of water and cities, respectively. Figure modified from Bond, 2004.

Glacial Maximum

A single mass of ice covered southern and eastern Yukon during the glacial maximum. The ice thickness was >1350 m over Whitehorse, as indicated by the

elevation of a local glacier erratic (Bond, 2004). Nunataks were likely rare at this time due to extensive ice cover (Bond, 2004).

Deglaciation

McConnell deglaciation in the Whitehorse area is divided into six stages, which are identified based on changes in ice flow, glacial readvances, periods of dynamic equilibrium, and glacial lake development (Bond, 2004).

The Early Holocene and Current Interglacial

Glaciers melted by approximately 10.7 ka and climate reconstructions based on pollen analyses suggest a "thermal maximum" of warm, wet climate between 8-2.5 ka with cooler, moister conditions beginning at 6 ka (Anderson et al., 2002; Ogden, 2006). Cool periods with adequate precipitation to favor ice persistence and growth have existed since 8 ka, with the possible exception of the Medieval Warm Period between 1030 and 1440 (Ogden, 2006). The Little Ice Age (LIA) followed the Medieval Warm Period leading to lower temperatures until its termination at ~1900 (Ogden, 2006); since 1900, and especially during the past 50 years, warming ensued, leading to melting of ice patches across southwestern Yukon (Farnell et al., 2004).

References Cited

Anderson, L., Abbott, M., Finney, B., and Edwards, M.E. 2002. The Holocene lake-level history of Marcella Lake, southern Yukon Territory, Canada. *In*: The Geological Society of America Northeastern Section- 37th Annual Meeting, Springfield, Massachusetts, Session No. 19 Program Abstract.

Bond, J.D. 2004. Late Wisconsinan McConnell glaciation of the Whitehorse map area (105D), Yukon. *In* Yukon Exploration and Geology 2003, D.S. Emond and L.L. Lewis (eds.), Yukon Geological Survey, p. 73-88.

Jackson, L.E., Ward, B., Duk-Rodkin, A., and Hughes, O.L., 1991. The Last Cordilleran Ice Sheet in Southern Yukon Territory. Gėographie physique et Quaternaire, v. 45, pp. 341-354.

Farnell, R., Hare, P.G., Blake, E., Bowyer, V., Schweger, C., Greer, S., and Gothardy, R., 2004. Multidisciplinary investigations of Alpine ice patches in southwest Yukon, Canada: paleoenvironmental and paleobiological investigations. Arctic, v. 57, n. 3, pp. 247-259.

Huscroft, C. Ward, B.C., Barendregt, R.W., Jackson, L.E. Jr., and Opdyke, N.D., 2004. Pleistocene volcanic damming of Yukon River and the maximum age of the Reid Glaciation, west-central Yukon. *Canadian Journal of Earth Sciences,* v. 41, n. 2, pp. 151-164.

Huscroft, C., Ward, B.C., Jackson, L.E. Jr., and Tarnocai, C.E., 2006. Investigation of high-level glaciofluvial terraces and re-evaluation of the established soil stratigraphy for Early and Middle Pleistocene surfaces, central Yukon, Canada. *Boreas*, v. 35, pp. 96-105.

Matthews, J.V., Schweger, C.E., and Hughes, O.L., 1990. Plant and insect fossils from the Mayo Indian Village section (central Yukon): new data on middle Wisconsinan environments and glaciation. *Gėographie physique et Quaternaire*, v. 44, pp. 15-26.

Ogden, A., 2006. Backgrounder: Climate, Climate Variability and Climate Change in the Southwest Yukon. Environment Canada Northern Climate ExChange, 24 p.

Schweger, C.E., 1997. Late Quaternary Palaeoecology of the Yukon: A Review. *In* Insects of the Yukon, H.V. Danks and J.A. Downes (eds.), p. 59-72.

Smith, C.A.S., Meikle, J.C., and Roots, C.F. (eds), 2004. Ecoregions of the Yukon Territory: Biophysical properties of Yukon landscapes. Agriculture and Agri-

Food Canada, PARC Technical Bulletin No. 04-01, Summerland, British Columbia, 313 p.

CHAPTER 3

FIELD SAMPLING METHODS AND LABORATORY ANALYSES

Field Site Description

The Wheaton Glacier (informal name) showed physical characteristics of a non-temperate glacier and is located approximately 80 km south-south west of Whitehorse, Yukon Territory, Canada (Figure 3.1A). The Wheaton Glacier evolved from occupying one large catchment (4 km^2) to two smaller catchments (each 2 km^2) due to glacier thinning and net mass loss, forming two lobes separated by a medial moraine (Figure 3.1A). The east lobe was drained via a single main outlet stream (Figure 3.1B) while the west lobe of the glacier terminated into a young (< 10 yrs.) proglacial lake (Figure 3.1C).

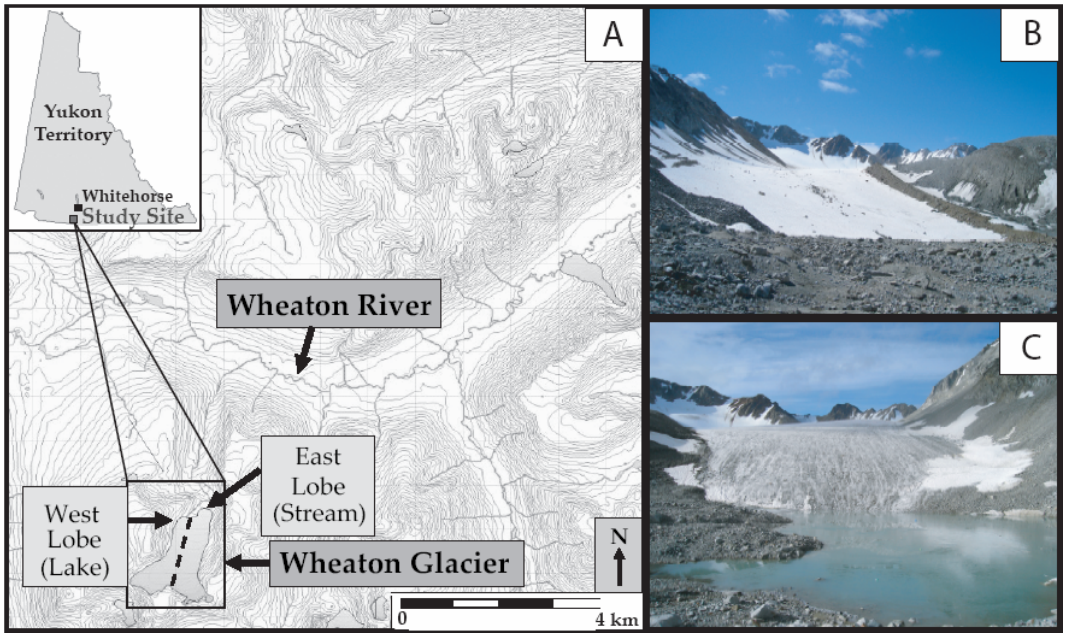


Figure 3.1: (A) Wheaton Glacier location map (modified from J. Bond, unpublished); contour interval is 100 ft. Photographs of the (B) east lobe on 18 July 2006 and (C) west lobe on 1 August 2006.

This study compared the hydrology and dissolved ion and organic carbon dynamics across three subcatchments during the period from 22 June to 16 August 2006. Solute chemistry was measured in three proglacial streams: the East Lobe Stream (ELS), which was the major drainage for the east lobe, the Upper West Lobe Stream (UWLS), which drained the upper west lobe, and the Lake Outlet Stream (LOS), which drained the proglacial lake at the terminus of the west lobe. The lake was fed by the lower portion of the west lobe (Figure 3.2A).

Catchment Characteristics: Glacial Retreat, Lake Profile, and Weather

The duration and frequency of sampling for major variables for the field season (23 June–16 August) is noted in Table 3.1. Stream gauging and electrical conductivity (EC) monitoring stations were constructed on the three proglacial streams (Figure 3.2). The ELS was a proglacial stream stemming directly from the east lobe of the glacier and represented the major drainage from the east lobe (Figure 3.2B). The UWLS was a proglacial stream stemming directly from the west lobe of the glacier and was located along the west side of the medial moraine between the ELS and LOS (Figure 3.2C). The UWLS was the major drainage for the upper portion of the west lobe. The LOS drained the proglacial lake at the terminus of the west lobe which was fed by the lower portion of the west lobe (Figure 3.2D).

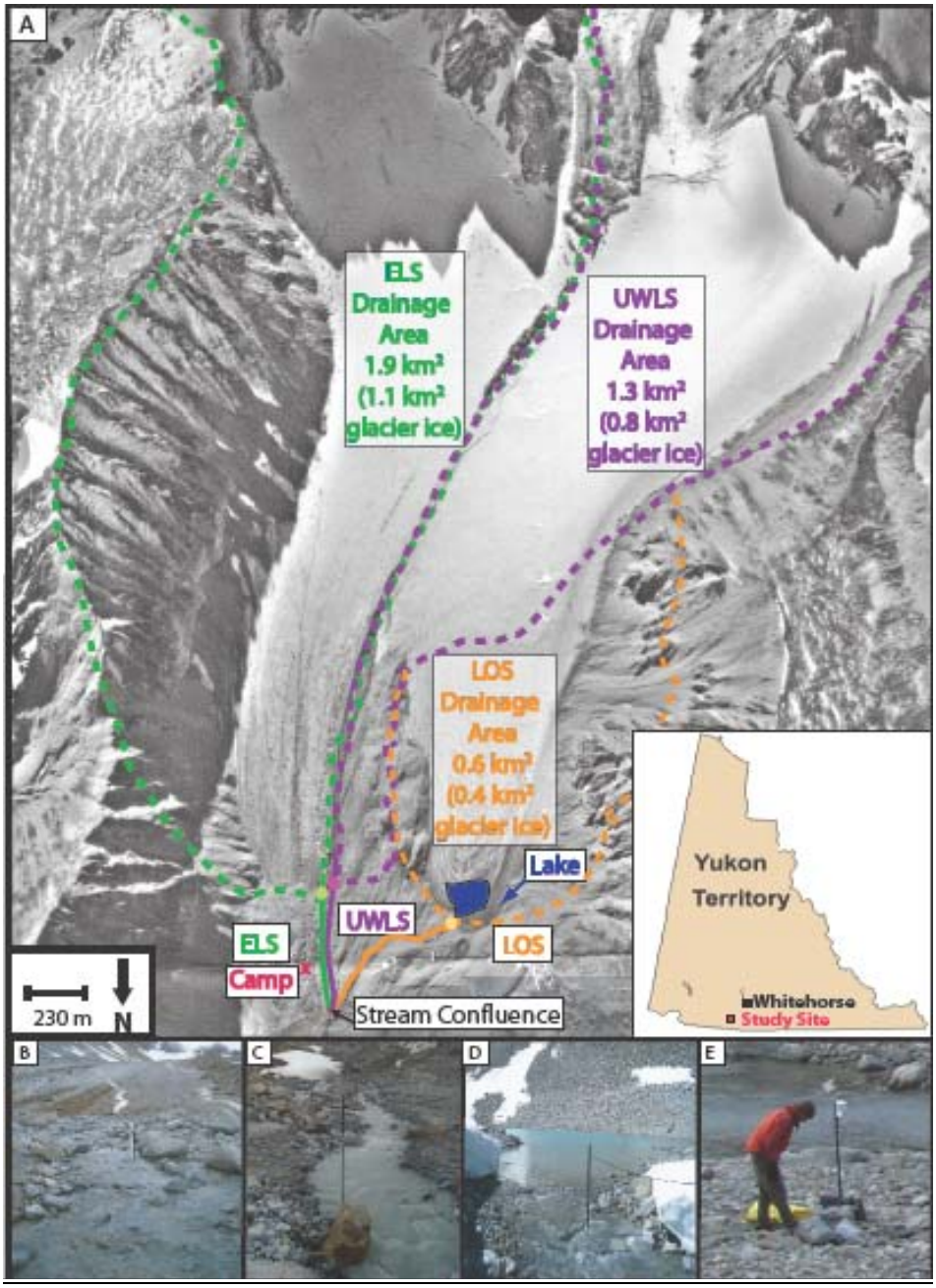
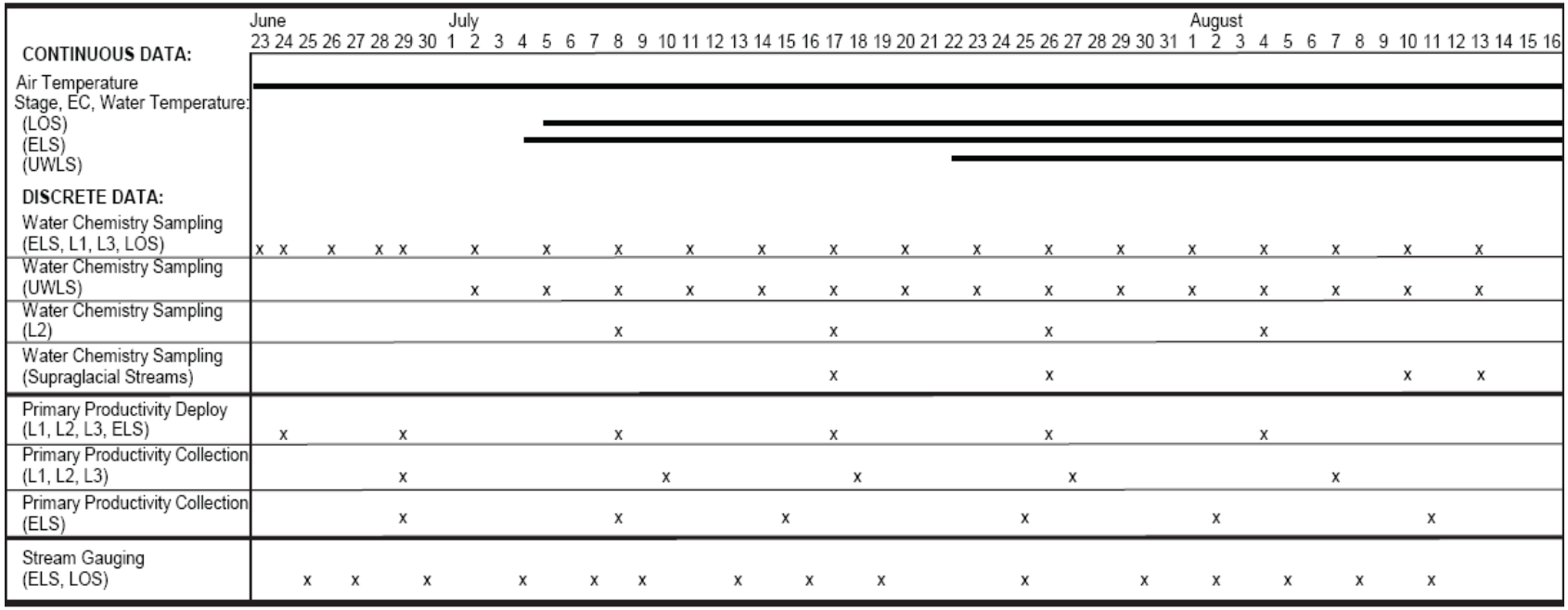


Figure 3.2: (A) September 1995 aerial photograph (# A28240-88) of the Wheaton Glacier catchment (National Air Photo Library, 1995) with drainage areas delineated and streams outlined in green, purple, and orange. Stream gauging and EC monitoring stations (dots) for the (B) East Lobe Stream (ELS), (C) Upper West Lobe Stream (UWLS), and (D) Lake Outlet Stream (LOS) are shown. The (E) temperature monitoring station was set up ~10 m N of the LOS monitoring station. Rebar pole height was ~1.5 m (B, C, D, E).

Table 3.1: Sampling frequency chart. Continuous data collection depicted by solid lines. Discrete sampling is indicated by "x." Sampling location abbreviations are as follows: ELS- East Lobe Stream; UWLS- Upper West Lobe Stream; LOS- Lake Outlet Stream; L1- Lake 0.5 m depth; L2- Lake 1.5 m depth; L3- Lake 5.0 m depth.



Glacial Retreat

Glacial retreat was determined by measuring the distance between several cairns set up on both the east and west lobe proglacial areas during a four-day field excursion in June 2004 (Skidmore, M.L., personal comm.) and during the June-August 2006 field season (Figure 3.4). Two cairns were constructed during the 2004 field season, one marking the terminus on 16 June 2004, and a second marking the September 1995 terminus, as determined from aerial photography (Photo A28240-88, National Air Photo Library, 1995) on 18 September 1995 (Figure 3.3). A third cairn was constructed at the terminus location on 1 July 2006, and a fourth cairn was constructed on 16 August 2006 (the end of the field season) (Figure 3.3). Frontal retreat of the glacier was 56 m between September 1995 and July 2004 and 30 m between July 2004 and August 2006 on each lobe for a total of 86 m between September 1995 and August 2006 (Figure 3.3). Frontal retreat between 1 July and 16 August 2006 was 7 m for the east lobe and 3 m for the west lobe.

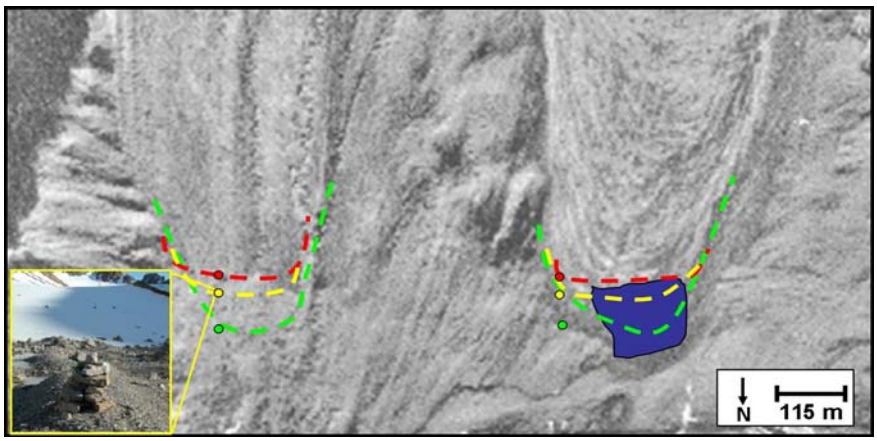


Figure 3.3: Glacier termini locations in September 1995 (green), June 2004 (yellow), and August 2006 (red) based on cairns (dots) constructed from a 1995 aerial photograph (# A28240-88, National Air Photo Library, 1995), June 2004 field season and 2006 field season, respectively. Lake location is indicated in blue on the west lobe.

Lake Physical Characteristics

The dimensions of the lake and lake water depths were measured on 1 July and 3 August 2006 (Figure 3.4A). Lake dimensions were measured by walking a 30 m measuring tape along the shoreline parallel to the long axis of the lake and by measuring a length of string stretched across a transect in the middle of the lake using a boat to get across the lake. The long axis of the lake was 116 m and the short axis was 85 m (Figure 3.4A). Water depths were measured across four transects in the lake from a boat using a calibrated plumb line (Figure 3.4A). The lake dimensions and water depths did not exhibit measurable changes between 1 July and 3 August.

Lake water volume was approximately 16100 m^3, based on adding water volumes approximated using the bathymetric map created with the plumb line measurements (Figure 3.4B); the area within each contour line was multiplied by the average depth between contours to determine lake volume. Light attenuation depths through the lake water column were also measured in these locations using a Secchi disk (Figure 3.4B). The Secchi disk disappears from view when light transmission through the water column falls to 1-15% of its original intensity (Wetzel, 2001).

Temperatures were taken at the LOS with a portable EC probe designed for low conductivity solutions with a thermistor (Campbell Scientific, #CS547a). Continuous records of water temperature were also obtained from TruTrack capacitance rods (TruTrack Ltd., #WT-HR 64K), which were laboratory calibrated to 0°C using an ice-water slurry.

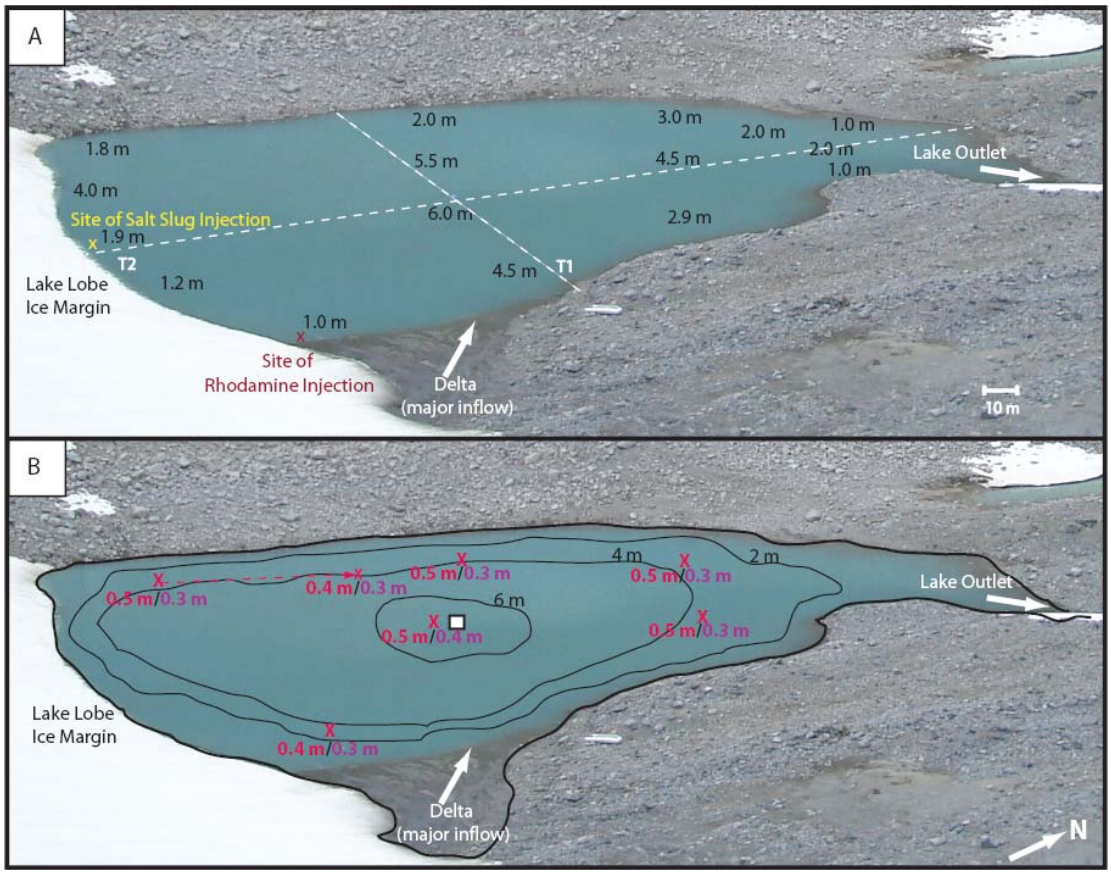


Figure 3.4: (A) The proglacial lake, with lake depths, major inflow and outflow locations, sites of tracer injections, short axis of the lake (T1), and the long axis of the lake (T2). (B) A coarse bathymetric map of the lake based on water depths from (A). The site of chemistry sampling and primary productivity assays is indicated by the white box. Pink "X"s represent sediment trap locations, pink numbers indicate Secchi disk depths measured at 10am and 3pm on 1 July and purple numbers indicate Secchi disk depths measured at 11am on 3 August. The sediment trap on the upper left corner of the figure moved via current along the dotted line between the time of deployment and collection.

Six suspended sediment traps were deployed in the lake (Figure 3.3B) from 5 July until 13 August 2006 to determine relative sedimentation rates throughout the lake. Sediment traps were constructed using a 1 L soda bottle (diameter = 6.5cm) funnel connected to a 50 mL Falcon tube (general design based on traps designed by Cockburn, J.M.H., personal comm.). The traps were set between 0.1 and 0.3 m from the lake bed using fishing weights to sink the funnel system and a soda bottle float to keep the trap

upright. The sediment trap Falcon tubes were collected every 1-2 weeks and new tubes were redeployed to keep a continuous record of sedimentation. The tubes were capped, Parafilm sealed, and stored in a sample cooler upon collection. Sediment was allowed to settle out of suspension in the Falcon tubes and was quantified using calibrated volume demarcations on the tubes. Sediment volumes collected in the Falcon tubes were converted to depths by dividing total sediment collected by the area of the sediment trap opening ($3.25^2\pi = 33.18 cm^2$).

Weather

Continuous measurements of air temperature were taken from 22 June-16 August using a Campbell 107 temperature probe with radiation shield; 30 minute averages from 180 10-second scans were recorded using a Campbell CR10X datalogger. The probe and shield were mounted on a piece of rebar at approximately 1.5 m above the ground surface, which was located approximately 10 m north of the LOS monitoring station just north of the western lobe terminus of the glacier (Figure 3.2E). Measurement accuracy with the Campbell 107 temperature probe was ±0.4°C over the range of -24°to 48°C (Campbell Scientific, 2000). Qualitative records of weather and precipitation events were recorded daily and used to assess generally clear vs. generally cloudy days. Rainwater was collected at camp (Figure 3.2A) using a 5-inch diameter funnel attached to a 50 mL Falcon tube, but rainwater volume could not be assessed due to tipping of the rain gauge collector which resulted in spillage and thus greatly underestimated precipitation.

Hydrology Methods

Stream Gauging

Stage height was continuously measured and recorded at the LOS, ELS, and UWLS using TruTrack capacitance rods with internal data loggers (Figure 3.2B-D). The stage heights for each stream were logged between 22 June-16 August (LOS), 24 June-16 August (ELS), and 22 July-16 August (UWLS). The rods were mounted with cable ties to a piece of rebar that had been hammered into a relatively flat area of the stream bed in order to obtain consistent cross-sectional area measurements and velocity depth profile and for its proximity to the stream bank for easy downloading access. The rods had internal data loggers and were programmed to collect stage height every 30 minutes, averaging 180 10-second measurements. Manual stage height measurements were collected at least once daily at each stream, next to the TruTrack rod, for comparison with the TruTrack readings.

Each TruTrack rod was calibrated for stage height measurement in the laboratory following the manufacturer's instructions (Omnilog version 1.53) prior to field deployment. Calibration involved immersing each rod into a tube containing 0.3 m and 0.5 m water and programming the internal loggers accordingly. The rods were then checked for accuracy by re-immersing them in water depths of 0.1 m, 0.3 m, and 0.5 m. These calibrations were rechecked at the end of the field season by immersing each rod in a series of known water depths of 0.1 m, 0.2 m, and 0.3 m. The TruTrack capacitance rods have a ± 1 mm water height resolution and a ± 0.3°C linear accuracy over a range of

0°-70°C (Intech Instruments Ltd., 2005). This accuracy was replicated in the laboratory calibrations over a range of 0-25°C.

Stream width, depth, and velocity measurements were taken every two to four days (Table 3.1) to generate stage-discharge rating curves for the ELS, UWLS, and LOS. These parameters were measured using a protocol similar to that used by the USGS (Carter and Davidian, 1989). Stream width was measured by stretching a 15 m tape across each stream using a transect marked by two cairns, one on each side of the stream; the transect was located within 0.5 m of the TruTrack rod. Depth and velocity measurements were taken every 10 cm and 15 cm across the ELS and LOS, respectively, equating to 10-15 point measurements per stream transect, using a General Oceanics current meter fixed to a metered steel rod. The velocity measurements were taken at approximately 60% stream depth, measuring the number of rotations per minute at each point across the transect.

High suspended sediment load in the UWLS clogged the propeller on the current meters, preventing use of the General Oceanics instruments, so surface velocity was measured by timing a floating plastic bottle over a 15 m stretch of the stream and taking the average of three runs. The UWLS surface velocity was multiplied by a correction factor of 0.85 to obtain an average velocity (Gordon et al., 2004). A rating curve was derived for each stream using a best-fit equation (power for ELS and LOS; logarithmic for UWLS) for the ELS, LOS, and UWLS, between stage heights recorded by the TruTrack rods and the velocity-area measurements (Figure A.1, Appendix). Accuracy of

the velocity-area method for discharge determination was estimated at ± 10-20% (Dingman, 2001; Lafreniere, 2003; Irvine-Fynn et al., 2005).

Lake Water Residence Time and Groundwater Connectivity Among the Subcatchments (Salt and Rhodamine Tracers)

A salt slug consisting of 10 kg water softener salt dissolved in 40 L lake water (for a final solution of 98250 ppm Na^+ and 151750 ppm Cl^-, or 4.3 x 10^6 μeq L^{-1} of each ion) was prepared in two 20 L plastic jugs and added to the lake at 1.5-2 m depth at the center of the ice margin (Figure 3.4A) at 10 am on 6 August, 2006, to determine the residence time for water storage in the lake and the degree of connectivity between the lake and the ELS and UWLS via groundwater. The concentration of the salt slug in the lake was 10 kg salt: 1.61 x 10^7 kg lake water (see lake physical characteristics section above), which corresponds to an increase of 10.6 μeq L^{-1} Na^+ and Cl^-, assuming the slug fully mixed with all water within the lake (see Appendix for calculations and assumptions). Samples were prepared in the laboratory from the same water softener salt used for the tracer injection and were run on a Metrohm Peak ion chromatograph (diluted to 0.1 ppm, 1 ppm, and 12 ppm salt) to determine constituent ions in the salt, of which the only two measurable ions were Na^+ and Cl^-. Discrete samples taken at 10 am on 6 (LOS), 7, 10, and 13 August (LOS, ELS, and UWLS) were run on the ion chromatograph to determine when the slug exited the lake and groundwater travel times based on Cl^- and Na^+ concentrations.

A 500 mL Rhodamine WT slug (500 mL liquid Rhodamine WT stock, 20% active ingredient, mixed with 10 L lake water, prepared in a 20 L plastic jug) was released at the

lake delta, the major water inlet, at 9am on 14 August to determine lake water residence time and major flow paths in the lake (Figure 3.5). 20 mL water samples were taken every 30-45 minutes over the subsequent 12.75 hour period and a single sample was taken on 16 August from the LOS in HDPE scintillation vials and all samples were stored in the dark until they were analyzed at Montana State University-Bozeman. Rhodamine concentrations were measured using a Turner Designs (model 10-AU-005-CE) Digital Fluorometer calibrated using 5 ppb, 50 ppb, and 100 ppb standards prepared from the same Rhodamine WT stock that was used in the field. Calculations and assumptions for the rhodamine tracer experiment are detailed in the Appendix.

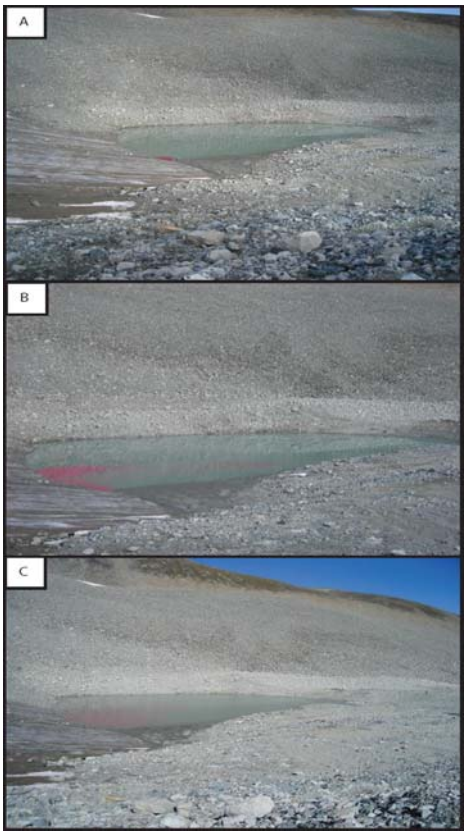


Figure 3.5: (A) A 500 mL rhodamine slug was injected at the delta at 9am. (B) The rhodamine dispersion at 10 am and (C) 12 pm.

Water Chemistry Sampling

Water samples were taken from the ELS, UWLS, LOS, lake surface, and at 5 m depth in the lake every three days from 23 June-13 August, 2006 (Table 3.1). Water samples were also taken from the lake at 1.5 m depth every 9 days, corresponding with primary productivity assays. Water from 1.5 m and 5 m depths in the lake was collected using a 460 mL stainless steel Solinst (model 429) point source bailer, rinsed twice with sample before final collection. Samples were collected in 1 L Nalgene bottles rinsed three times with sample and filled brim-full. Samples were kept at near-freezing temperatures until they were filtered; filtration was done within 3 hours of collection and sample bottles were shaken prior to filtration to re-suspend sediment in the sample. 500 mL of sample was filtered through a 0.4 μm Nuclepore filter (Millipore cat. no. 109817-1) for dissolved ion chemistry using a 500 mL Nalgene filter system and vacuum hand pump. Filtrate was aliquoted into five 20 mL HDPE scintillation vials, each rinsed three times with filtrate; four vials were retained for laboratory analysis of major dissolved ion concentrations and the fifth for laboratory analysis of electrical conductivity (EC). The filtration unit was rinsed with field-generated deionized water and wiped with Kim-wipes between samples.

Approximately 10 mL of filtrate was collected in a 20 mL scintillation vial for pH analysis using an Orion 290A pH meter and Thermo Orion 91-07 Triode Probe. 100 mL of filtrate was analyzed for dissolved inorganic carbon as bicarbonate using a Hach digital titration kit with Bromcresol Green–Methyl Red indicator to an endpoint of pH 4.9

(as specified in the Hach digital titrator manual). Filters were retained in 1.5 mL Eppendorf tubes to determine the mass of suspended sediment. Suspended sediment mass was determined by drying the sample filters at 100-110°C for 8-14 hrs. in pre-weighed crucibles, weighing the crucible and sample filter and subtracting the average of four blank filters (2 field DI water blanks, 2 laboratory prepared blanks of clean filters).

Water samples for dissolved and particulate organic carbon (DOC and POC, respectively) were collected in parallel with the ion chemistry samples. Samples were collected from each environment in 250 mL borosilicate bottles, which were initially combusted at the Skidmore laboratory at 550°C for 4 hrs. Subsequently, the bottles were rinsed three times with sample and filled brim-full; each bottle was used at only one location for the duration of the season. Samples were filtered within 3 hours of collection.

120-150 mL of sample was filtered through a 0.4 μm Nuclepore filter using a 500 mL Nalgene filter system and hand pump for DOC analysis during the first half of the season (23 June-23 July). Filtrate was aliquoted brim-full into 40 mL precombusted (550ºC, 4 hours) amber borosilicate EPA vials, each rinsed three times with filtrate. The filtration system was rinsed between samples with 5 mL 3% H_2O_2 and 15 mL field generated deionized water followed by three rinses with the subsequent sample and its filtrate. Deionized water was prepared in the field by passing excess filtrate from DOC and dissolved ion filtrations through a Cole-Parmer Monobed deionizer (cat. no. EW-01503-00).

During the second half of the season (23 July-16 August), DOC samples were filtered as follows: 120-150 mL of sample was filtered through a precombusted (550ºC, 4 hours) GF/F filter (nominal pore size 0.7 μm) with a 15 mL glass filter system and hand pump. The top and bottom chambers of the glass filtration system were rinsed with ~10 mL field generated deionized water and 5 mL 3% H_2O_2. The top chamber was then rinsed three times with ~10 mL of sample. The GF/F filter was then placed onto the filtration unit and 10 mL of sample was filtered through the apparatus and used to rinse the side arm flask that collected filtrate; this was repeated for a total of three 10 mL rinses with sample filtrate. Filtrate was aliquoted brim-full into 40 mL precombusted (550ºC, 4 hours) amber borosilicate EPA vials. GF/F filters were retained in precombusted (550ºC, 4 hours) foil packets for POC analysis. EPA vials were Parafilmed and all samples (dissolved ion, carbon, and sediment) were kept in a cooler at near-freezing temperatures until they were transported to the Skidmore Laboratory and stored at 4°C prior to analysis. Measured DOC concentrations were consistent before and after the transition between filter papers with slightly different pore sizes (0.4μm Nuclepore and 0.7 μm (nominal) GF/F filters). Therefore, it was assumed that the small increase in the filter pore size mid-season did not significantly influence the measured DOC concentrations.

Primary Productivity and Cell Biomass

Primary productivity assays were deployed at three water depths (0.5m, 1.5m, and 5m) in the middle of the lake (Figure 3.3B) and in the ELS, near the gauging station (Figure 3.2A and B). Incubations lasted at least 24 hours in each location (Table 3.1);

greater incubation periods occurred during overcast days to ensure a measurable amount of ^{14}C uptake. Assays were performed with 0.5 mL 100 μCi ^{14}C bicarbonate aliquots prepared from a 5 mCi stock solution (Sigma-Aldrich, Ontario, Canada) in the Foght laboratory, University of Alberta, Canada, and a method modified from the McMurdo Long Term Ecological Research program limnological methods manual (Priscu, 2005).

Water samples from the three lake depths were collected into a set of three 125 mL borosilicate bottles (acid washed with 10% HNO_3 bath and rinsed three times with deionized and Milli-Q water in the laboratory); two of the bottles were clear and the third was amber and covered in electrical tape to prevent light penetration. Discrete samples of surface water (0.5 m) were taken by filling sample bottles directly from the lake. Water from 1.5 m and 5 m depths was collected with the Solinst bailer, rinsed twice with sample. Each bottle was then inoculated with 0.5 mL 100 μCi ^{14}C bicarbonate, capped, and inverted 10 times to ensure thorough mixing. All inoculations were done in the pre-dawn hours (4-6am). Bottles were attached to a weighted line and floated using a carboy at the location of sampling. ELS samples were submerged in 5-20 cm stream water and attached to a line tied to a rock on the bank.

40 mL of water from each environment was also collected into pre-combusted amber borosilicate EPA vials and fixed with 3 mL 0.2 μm filter sterilized formaldehyde for cell enumeration. Primary productivity samples were incubated in their collection environment for at least 24 hours (L1, L2, L3) and 7 days (ELS) before they were collected at pre-dawn hours for filtration (Table 3.1). Samples were filtered within 3 hours of collection through a 0.4 μm Nalgene nuclepore filter with a Nalgene filtration

system and vacuum hand pump used exclusively for radiolabel analyses. The filtration unit was rinsed three times with field deionized water between samples and wiped dry with KimWipes.

Filters were retained in 20 mL HDPE scintillation vials and purged of excess ^{14}C by acidifying the filters with 1 mL 3.7% HCl sterilized with a 0.2 μm Whatman filter; addition of the HCl drives off excess aqueous ^{14}C-bicarbonate as CO_2. Field blanks were also prepared on 24 July and 11 August, with the same method as above, but substituting 100 mL field-deionized water for sample. Samples were kept at near-freezing temperatures throughout the filtration process and the filters were stored on ice until processing in the Department of Biological Sciences, University of Alberta, Canada.

The author's initial intent was to compare rates of primary productivity between the lake and the ELS. However, using a bottle method in the stream as for lake sampling resulted in unrealistic conditions relative to the flowing streamwater at the ELS. These conditions included isolation from flow, streamwater residence time of one-week, and solar-induced warming of the tops of the borosilicate bottles during low flow. This prevented a feasible comparison between the two environments. Thus, while primary productivity data was collected from the ELS stream, it was not explored further in this thesis; a graph of primary productivity rates for the three lake depths and the ELS is provided in the Appendix as Figure A.2.

Water Chemistry Laboratory Analyses

Ion Chemistry

Concentrations of major ions in water samples were determined using a Metrohm-Peak ion chromatograph with protocols based on the manufacturer's instructions. The eluent flow rate was 0.7 mL min^{-1} and 1.0 mL min^{-1} for anions and cations, respectively. The sample loop was 250 µL for all samples and standards. The concentrations of major cations, including sodium (Na^{+}), calcium (Ca^{2+}), magnesium (Mg^{2+}), ammonium (NH^{4+}), and potassium (K^{+}) were measured with a Metrosep C-2-250 analytical column (4 x 250 mm). Cation eluent consisted of 4 mmol L^{-1} tartaric acid/0.75 mmol L^{-1} dipicolinic acid solution. Anions, including fluoride (F^{-}), chloride (Cl^{-}), nitrate (NO_3^{-}), phosphate (PO_4^{3-}), and sulfate (SO_4^{2-}) were measured with a Metrosep A-2-250 (4 x 250 mm) analytical column in chemical suppression mode with 100 mM H_2SO_4. Anion eluent consisted of a solution of 3.2 mmol L^{-1} sodium carbonate/1.0 mmol L^{-1} sodium hydrogen carbonate.

Final concentrations for each ion were calculated with a linear equation derived from the standard curve of the peak area vs. concentration (mV sec^{-1} vs. mg L^{-1}) for each analyte (0.01 to 10 mg L^{-1}). The coefficient of variation was used as a measure of precision and was found to be < 3% for all ions, except K^{+}, which was 6%. Accuracy was calculated as the relative mean error with respect to known standards (Fluka Inc., cat. nos. 89886 and 89316) and was < 1-5% for all major cations and anions. Laboratory standards, prepared with NaCl, KNO_3, KH_2PO_4, Na_2SO_4, $MgCl_2$, KCl, NH_4Cl, and $CaCl_2$, certified standard solutions (Fluka Inc., cat. nos. 89886 and 89316; Hamilton Inc.,

cat. no. 09821), and blanks were analyzed at the beginning, during (every ten samples), and end of each run for quality assurance and quality control.

Charge Balance

Charge balance error was calculated using the equation:

$$CBE = (\Sigma^+ - \Sigma^-)/(\Sigma^+ + \Sigma^-) \times 100\%$$

where Σ^+ is the sum of measured cations and Σ^- is the sum of measured anions. Major ions were measured by ion chromatography and bicarbonate through titration. Table A.1 (see Appendix) lists measured ions and the associated CBE for each sample. CBE varied between -12.9 and 27.5% for all samples, with the mean CBE = 12.8% (n = 73). Error in CBE was likely related to error in titrating to end point to determine bicarbonate concentrations (Skidmore, 1995).

Particulate Organic Carbon (POC)

GF/F filters from dissolved organic carbon filtration were individually wrapped in pre-combusted (550°C, 4 hrs.) aluminum foil immediately after filtration in the field and stored on ice for the duration of the field season. They were stored at -80°C upon return to the Skidmore Laboratory, Montana State University-Bozeman. POC was measured by mass loss on ignition, with a method similar to that of Heiri et al., (2001). Filters and their foil packets were dried in an oven at 105°-110°C for 24 hours and subsequently weighed. They were then combusted at 550°C for 4 hrs and reweighed to determine mass lost on ignition by mass difference between pre- and post- combusted foil-filter packets.

Dissolved Organic Carbon (DOC)

Samples were analyzed for DOC content at the Aiken USGS water analysis laboratory at the University of Colorado-Boulder, after being shipped on ice from the Skidmore Laboratory at Montana State University-Bozeman. All samples were analyzed at room temperature.

DOC was measured on an Oceanography International (OI) Model 700 carbon analyzer using the persulfate wet oxidation method. A 5 mL sample loop and a peristaltic pump autosampler were used to transport sample into a gas-tight reaction vessel where 0.5 mL 5% H_3PO_4 was added to the sample. The sample was then purged with N_2 for 2 minutes, removing inorganic carbon, and 0.5 mL of 0.42 M sodium persulfate solution was added. Total reaction time was approximately 5 minutes. 15-30 mL of sample were aliquoted into combusted (550°C, 4 hours) 30 mL glass vials, and duplicate analyses were performed using the OI700 analyzer. Laboratory prepared standards: 0.2-5.2 ppm DOC, caffeine, IC check (sodium bicarbonate and sodium carbonate solution), KHP (potassium hydrogen phthalate), and Laboratory Fortified Blank (5.2 mg/L sodium benzoate) and blanks were measured at the beginning and end of each run, and two blanks and three standards were analyzed every ten samples.

A subset (24) of samples was analyzed by combustion using a Shimadzu total carbon and total nitrogen analyzer; these samples were measured in triplicate and approximately 25 mL of sample was aliquoted per triplicate determination. Laboratory prepared standards and blanks were measured at the beginning and end of each run, and two blanks and three standards were analyzed every ten samples. Final DOC

concentration was determined using a linear regression of the machine-measured DOC of standard concentrations, 0.2-5.2 ppm, relative to the actual concentrations, 0.2-5.2 ppm.

Primary Productivity

Primary productivity samples were analyzed at the Department of Biological Sciences, University of Alberta, Edmonton, Canada, on 7 July 2006 (18 samples) and 21 August 2006 (73 samples). 10 mL ACS Fluor was added to each scintillation vial and the vial was inverted 10-15 times to thoroughly mix the Fluor with the filter paper and sample. Filters dissolved upon addition of the Fluor. Samples were dark adapted inside a Beckman LS3801 Liquid Scintillation Counter for 60 minutes prior to counting. Samples were counted twice, once after the 60 minute dark adaptation, and again after 24 hour dark adaptation; both adaptations yielded similar counts. Samples were counted at room temperature. All sample results were converted to a daily productivity rate using the equation:

$$\mu g\ C\ l^{-1}\ d^{-1} = \left(\frac{(DPM_L - DPM_D)\ a \cdot b}{A_{14C}\left(Vol\ ^{14}C(ml)\right)\left(\frac{2.2 \times 10^6\ dpm}{1\mu Ci}\right)\ t} \right) \left(\frac{24hrs}{d} \right)$$

where DPM_L is the average disintegrations per minute (dpm) of the light bottles, DPM_D is the average dpm of the dark bottles, a is the concentration of naturally occurring dissolved inorganic carbon at each respective depth (from Hach titrations) in mgL^{-1}, b is the isotopic discrimination factor for ^{14}C radiolabeled carbon (1.06), A_{14C} is the specific

activity of the ^{14}C in μCi, 2.2 x 10^{-6} is a conversion constant, and *t* is the incubation time (hrs) (equation modified from Priscu, 2005).

Cell Enumeration

The number of cells in discrete samples was measured with a method similar to that of Porter and Feig (1980). 10 mL of each sample was stained with 1 mL of 0.1 mg ml^{-1} 0.2 μm filter sterilized DAPI (4', 6-diamidino-2-phenylindole) and dark adapted for 15 minutes. Each stained sample was filtered onto a 25 mm diameter, 0.22 μm black polycarbonate filter (Poretics, cat. No. K02BP02500) with a filtration manifold and vacuum (25 kPa). Procedural blanks were also made with a pre-sterilized phosphate-buffered saline (PBS) solution as a substitute for the water sample. Filters were mounted onto glass slides and kept in the dark and frozen until they could be viewed with a microscope. All filtering and staining was conducted within a Labconco ^{TM} class 100 purified air bench, equipped with a germicidal UV-lamp.

Cells were viewed using epifluorescence microscopy with a Nikon Optiphot microscope equipped with a DM510 filter cube (Nikon) at a final magnification of 1000X. Bacterial cells in a total of 20 fields of view (one field of view at 1000X = 16,741 μm^2) were counted for each sample slide, distinguishing between cocci, bacilli, and filamentous bacteria. The average number of cells in each sample was calculated by multiplying the average number of cells in the 20 viewed fields by the total number of possible fields ($A = \pi(8\ mm)^2$ or 2.011 x 10^8 μm^2; only 16 mm of the 25 mm filter was covered in cells). Cell numbers are reported as the number of cells mL^{-1} of water.

Analysis of the field and laboratory blanks indicated that cellular contamination associated with bottle preparation, staining, filtering, and microscopy was < 75 cells mL^{-1} in all samples.

References Cited

Campbell Scientific Inc., 2000. Model 107 Temperature Probe Instruction Manual. 8 p.

Carter, R.W. and Davidian, J., 1989. U.S. Geological Survey, Techniques for Water-Resources Investigations, Book 3, Chapter A6. 13 p.

Dingman, L.S., 2001. Stream-gauging methods for short-term studies. In Physical Hydrology, 2nd ed. Prentice-Hall: Englewood Cliffs; pp. 608-623.

Gordon, N.D., McMahon, T.A., Finlayson, B.L., Gippel, C.J., and Nathan, R.J. 2004. Stream Hydrology: An Introduction for Ecologists. 2nd ed. San Francisco: John Wiley and Sons. 448 p.

Heiri, O., Lotter, A.F., and Lemcke, G. 2001. Loss on ignition as a method for estimating organic and carbonate content in sediments: reproducibility and comparability of results. *Journal of Paleolimnology*, v. 25, pp. 101-110.

Intech Instruments Ltd., 2005. TruTrack Data Logger: Water Level/Temperature Model WT-HR Datasheet. Accessed at: http://www.intech.co.nz/products/minipd/datasheets/WT-HR.pdf

Irvine-Fynn, T.D.L., Moorman, B.J., Willis, I.C., Sjogren, D.B., Hodson, A.J., Mumford, P.N., Walter, F.S.A., and Williams, J.L.M. 2005. Geocryological processes linked to High Arctic proglacial stream suspended sediment dynamics: examples from Bylot Island, Nunavut, and Spitsbergen, Svalbard. *Hydrological Processes*, v. 19, pp. 115-135.

Lafreniere, M.J., 2003. Hydrological and hydrochemical investigations in a glacial lake catchment: Implications for organochlorine transport. PhD Dissertation: Department of Earth and Atmospheric Sciences, University of Alberta, Edmonton. 209 p.

National Air Photo Library (Centre for Topographic Information, Natural Resources Canada), 1995. Photo A28240-88. Scale = 1:20,000. Taken 18 September, 1995.

Omnilog Data Management Program version 1.53.1154

Porter, K.G. and Feig, Y.S., 1980. The Use of DAPI for Identifying and Counting Aquatic Microflora. *Limnology and Oceanography*, v. 25, pp. 943-948.

Priscu, J.C., 2005. Limnological Methods for the McMurdo Long Term Ecological Research Program, 2005 (Draft). Accessed at: http://www.homepage.montana.edu/~lkbonney/DOCS/LTER%20methods%20web%20page/Method%20_Oct05_AC.pdf

Skidmore, M.L., 1995. The hydrology and hydrochemistry of a high Arctic glacier. Master's Thesis: Department of Geography, University of Alberta, Edmonton. 114 p.

Wetzel, R.G., 2001. Limnology: Lake and River Ecosystems. 3rd ed. Academic Press: San Diego. 1006 p.

CHAPTER 4

RESULTS

Meteorological Conditions and Hydrology

Half-hourly recorded temperatures at the Wheaton Glacier terminus varied between -2 and 12°C from 22 June-16 August, with an average of 2.4, 6.1, and 3.6°C for 22-30 June, July, and 1-16 August, respectively. Mean air temperatures at Whitehorse, Yukon Territory, Canada, during the 2006 field season (23 June-16 August 2006) were similar to mean air temperatures from 1971-2000 (Figure 4.1). Since Whitehorse is 80 km N-NW of the Wheaton Glacier, it was assumed that Whitehorse had similar temperature records as the Wheaton Glacier and thus the 2006 field season was not unusual in terms of air temperature.

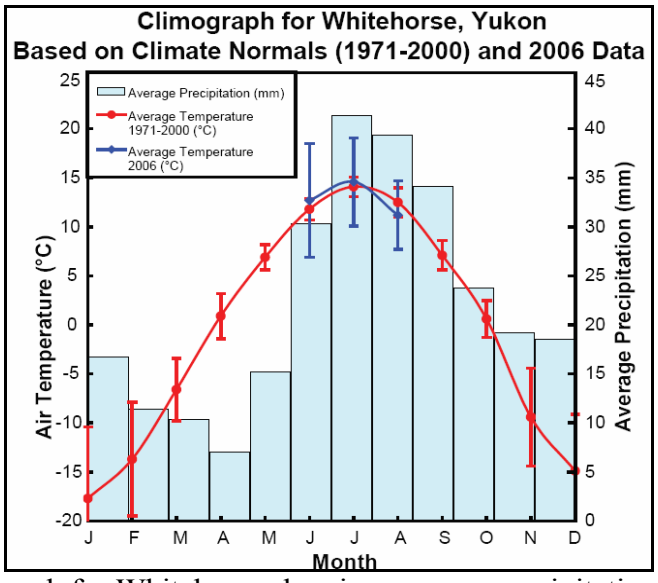


Figure 4.1: Climograph for Whitehorse showing average precipitation (blue bars) and average temperature from 1971-2000 (red line) and average temperature for the 2006 field season (blue line). Error bars indicate 1 standard deviation. Data accessed online from records courtesy of Environment Canada (http://climate.weatheroffice.ec.gc.ca/) (2006).

Stream Discharge

Night-time freeze-up of the gauged streams and low discharge from the streams prevented a reliable record for stage heights using the TruTrack capacitance rods during the early season (23 June-3 July). Thus, discharge data records for the East Lobe Stream (ELS) and Lake Outlet Stream (LOS) began on 4 July and 5 July, respectively, when streamflow was sufficient to be recorded by the TruTrack rods (Figure 4.2A). Upper West Lobe Stream (UWLS) discharge records began on 22 July (Figure 4.2A), when a third TruTrack rod was available to continuously monitor stage height at the UWLS.

Ratings curves were constructed for the ELS, LOS, and UWLS using manual discharge measurements. The velocity-area method (Carter and Davidian, 1989) was used to determine discharge based on channel width, stage height, and water velocity. The ratings curve was constructed by deriving a best fit regression line from the manually collected discharge data and the continuous measurements of stage height from the TruTrack capacitance rods; the ELS rating curve had an R^2 value of 0.49 (n = 13), the LO stream rating curve had an R^2 value of 0.81 (n = 9), and the UWLS rating curve had an R^2 value of 0.83 (n = 4) (see Appendix Figure A.1). Error associated with the TruTrack rod was ± 1 mm water height resolution (Intech, 2005). Error associated with the discharge measurements using the velocity-area method was estimated to be ±10-20% for the ELS and LOS (Dingman, 2001; Lafreniere, 2003; Irvine-Fynn et al., 2005). However, the error in using the ratings curves for predicting discharge for a given stage at times in between discrete measurements may be as high as ± 50% for the UWLS especially at low discharge, primarily due to a small n (Appendix Figure A.1).

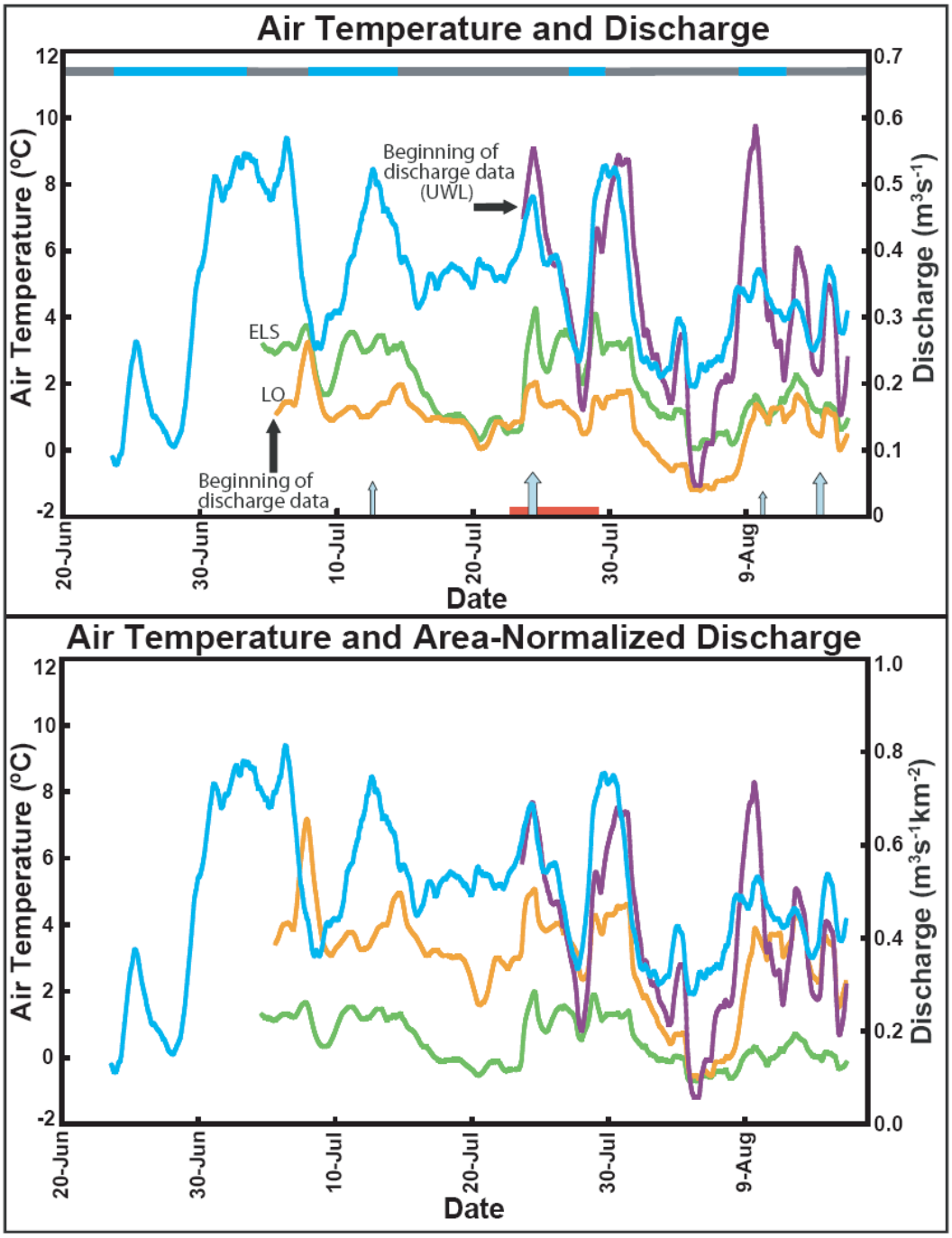


Figure 4.2: Moving average (period = 24 hrs) of (A) air temperature (blue), ELS discharge (green), LOS discharge (orange), and UWLS discharge (purple) for June-August, 2006. Precipitation events are depicted by relative magnitude by blue arrows; the snow to ice transition on the glacier surface at the west lobe and lower third of the east lobe is depicted by a red line just above the x-axis (23 July-29 July); clear (blue) and overcast (gray) days are indicated by the line at the top of the graph. (B) Moving average of (period = 24 hrs) air temperature and area-normalized discharge.

The lowest discharge at the ELS, LOS, and UWLS occurred at the beginning of the field season, 22-30 June, although these discharges were too low to be measured with available instrumentation. Maximum discharge occurred in July for both ELS and LOS and absolute discharge from the ELS was consistently higher than the LOS throughout the field season (Figure 4.2A). The three highest daily average discharges for the ELS were 0.30 $m^3 s^{-1}$ (28 July), 0.28 $m^3 s^{-1}$ (7 July), and 0.28 $m^3 s^{-1}$ (10 July) and 0.26 $m^3 s^{-1}$ (7 July), 0.19 $m^3 s^{-1}$ (23 July), 0.19 $m^3 s^{-1}$ (14 July) for the LOS. The discharge peaks in all streams on 24 July were likely, in part, a result of the precipitation event (blue arrow above 24 July) in Figure 4.2A.

Area-normalized discharge (Figure 4.2B) was calculated by dividing measured discharge by the drainage area for each stream, which normalizes discharge to account for different sized catchments. The drainage areas delineated in Figure 3.2A were equal to 1.9 km^2 for the ELS, 0.6 km^2 for the LOS, and 1.3 km^2 for the UWLS (Figure 3.2). Glacial ice covered 58%, 62%, and 67% of the ELS, LOS, and UWLS drainage areas, respectively (Figure 3.2). Drainage areas and extent of glacial ice cover were determined from the 1995 aerial photograph of the catchment (photo # A28240-88, National Air Photo Library, 1995).

The extent of ice cover in each subcatchment may have affected area-normalization of discharge since glacier ice contributes meltwater even after snowpack has melted from the valley walls. However, since the area of glacier ice cover in each catchment was within 10% of one another, it was assumed that this method for area normalization was reasonable. The drainage areas that were used are the largest estimate

of drainage area since they include both rock and snow/ice in the contributing area and thus they provide the lowest estimate of area-normalized discharge. When area-normalized, the LOS had a higher discharge than the ELS (Figure 4.2B). The UWLS had a similar discharge as the LOS, but appeared flashier than the LOS, as indicated by the 28 July low, and 10 August peak in discharge (Figure 4.2B).

A transition from predominant snow-cover to exposed ice on the glacier surface at the east and west lobe termini occurred between 23-29 July (Figure 4.3), as indicated by the red line in Figure 4.2A; this transition will be referred to as the period of rapid snowline retreat. The area of glacial ice in each catchment was calculated from the 1995 aerial photograph (Photo A28240-88, National Air Photo Library, 1995; Figure 3.2A) and combined with field observations of the snow line to approximate the percentage of ice exposure relative to the total glacier size. By the end of the field season, ice exposure on the glacier surface was approximately the lower three-quarters of the east lobe and of the lower UWLS drainage area, and > 90% of the ice in the LOS drainage area (Figure 4.3). The ice exposure during the second half of the field season reduced surface albedo on the lower half of the glacier from approximately 74% to approximately 29% relative to the snow covering the ice at the beginning of the season (Table 4.1).

Correlation coefficients (r) between air temperature and discharge were calculated using the CORREL function in Microsoft Excel using the half-hourly discharge and air temperature records. Lag times were determined by shifting windows of discharge values through time to best correlate with air temperature measurements. Devore and Peck (2007) define the strength of r: $0 \leq r \leq 0.49$ as weakly correlated, $0.5 \leq r \leq 0.79$ as

moderately correlated, and $0.8 \leq r \leq 1$ as strongly correlated; these definitions will be used henceforth when referring to correlation strength. 30-minute air temperature records were moderately correlated with 30-minute discharge measurements with a lag time of 3 hours for the ELS ($r = 0.52$), 4 hours ($r = 0.52$) for the LOS, and 2 hours ($r = 0.78$) for the UWLS when using the data set as a whole with a single lag interval for all data (4 July-16 August for ELS and LOS and 23 July-16 August for UWLS).

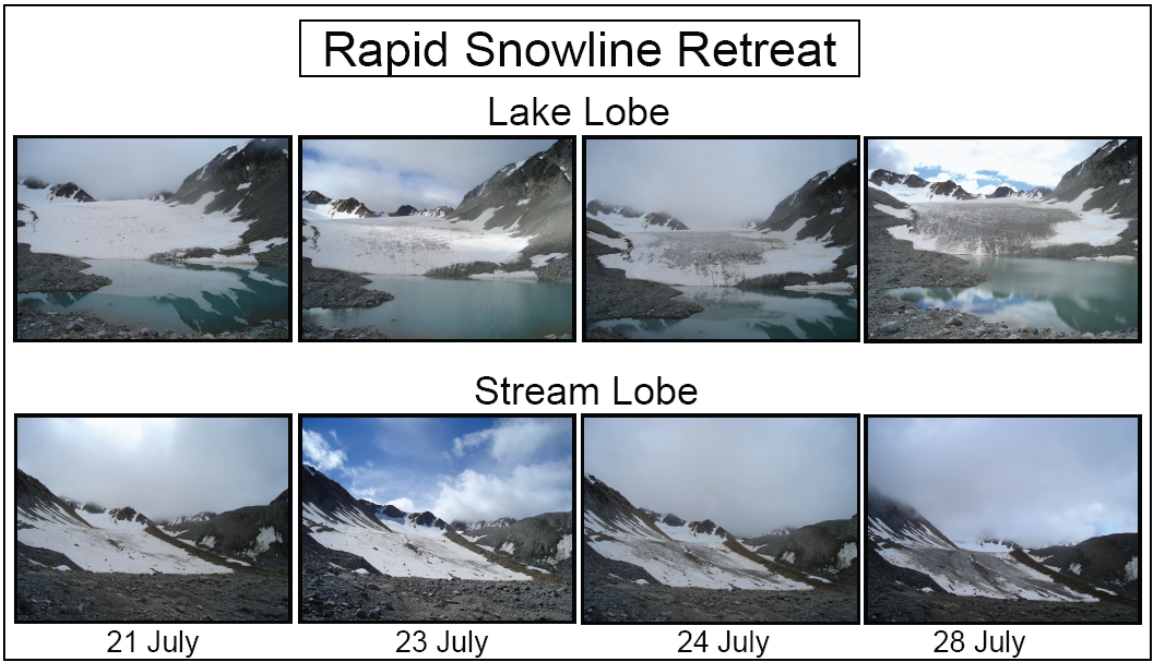


Figure 4.3: Rapid snowline retreat on the west (lake) and east (stream) lobes. Photos were taken at ~ 7am. The rapid snowline retreat began on 21 July (stream) and 23 July (lake), but note the dramatic change in ice exposure between 23 and 24 July.

Table 4.2: Albedo (%) for various glacial surfaces (modified from Paterson, 1994).

Surface Cover	Range	Mean
Dry snow	80-97	84
Melting snow	66-88	74
Firn	43-69	53
Clean ice	34-51	40
Slightly dirty ice	26-33	29
Dirty ice	15-25	21
Debris-covered ice	10-15	12

However, a stronger correlation existed between air temperature and discharge fluctuations after the initiation of the rapid snowline retreat during 23 July-16 August than before it (4 July-22 July). Table 4.2 indicates the best-fit lag time between air temperature and discharge for the ELS, LOS, and UWLS and how the correlation coefficient changes if the data frame is shifted an hour earlier or one or two hours later than the best-fit time. The air temperature-discharge correlation coefficients declined slowly from the optimum time for the ELS and LOS prior to the surface ice exposure. For instance, after 4.5 hrs, $r = 0.39$ for the ELS and $r = 0.21$ for the LOS; after 6.5 hrs, $r = 0.29$ for the ELS and $r = 0.09$ for the LOS. During and after the rapid snowline retreat, the ELS and LOS correlation coefficients declined by 0.01-0.2 for a lag time of minus one hour but dropped dramatically to 0.02 for the lag time plus one hour (Table 4.2). The discharge record for the UWLS began during the rapid snowline retreat and hence, there was no lag time recorded before the retreat was initiated. However, the UWLS contributing area did not transition between snow cover to ice cover as dramatically as the ELS and LOS contributing areas for the majority of the field season.

Table 4.2: Best fit lag times between air temperature and discharge for each stream based on correlation coefficients.

	Best fit lag time (hrs)	Correlation Coefficient at Time Intervals			
ELS		**-1**	**0**	**+1**	**+2**
4 July-22 July	9	0.49	0.5	0.49	0.47
23 July-16 Aug	2	0.69	0.7	0.02	0.003
LOS					
4 July-22 July	10	0.36	0.37	0.36	0.33
23 July-16 Aug	2	0.7	0.72	0.02	0.01
UWLS					
23 July-16 Aug	1.5	0.73	0.77	0.002	0.002

Water Temperature

24-hour moving averages of water temperature for each stream indicated temperature fluctuations between 0 and 2.3°C (Figure 4.4A). The UWLS water temperature record began on 23 July, when instrumentation was available to measure and record stream temperature on a continuous basis. The mean water temperatures were 1.4°C ($\sigma = 0.6$) for the LOS (29 June-16 August), 0.3°C ($\sigma = 0.2$) for the ELS (29 June-16 August) and 0.4°C ($\sigma = 0.3$) for the UWLS (23 July-16 August), where σ indicates one standard deviation.

The LOS was consistently warmer than the ELS and UWLS. The latter two streams had similar water temperatures for the duration of the UWLS temperature record, except for a peak in UWLS water temperatures from 4-5 August (Figure 4.4A). The peak could be attributed to low water volume and discharge in the UWLS at that time. Thus, water storage in the lake and low discharge lead to higher stream water temperatures.

Diurnal cycles in water temperature existed in all three streams throughout the field season and a subset used as an example of these diurnal cycles is shown from 1-7 August in Figure 4.4B. Diurnal changes in air temperature and water temperature were positively correlated. Correlation analysis between water temperature and air temperature did not indicate a particular lag time interval was more significant than another for up to a 12-hour lag (as indicated by applying the Excel CORREL function to air and water temperature records and shifting the data frame through 30-minute intervals).

Correlation coefficients were calculated between the continuous air and water temperature datasets to determine if water storage in the lake affected lake water temperature compared with stream water temperature. Correlations between air and water temperatures were 0.37 for the ELS, 0.66 for the LOS, and 0.04 for the UWLS, indicating a moderate correlation for the LOS and a poor correlation for ELS and UWLS air vs. water temperatures.

The lake had a low albedo compared with the glacier surface and stored meltwater; thus meltwater was warmed in the lake by solar radiation prior to its export via the LOS. In contrast, meltwater from the ELS and UWLS drained directly from the glacier without significant storage. Thus, while solar radiation was a component of the energy budget that resulted in melting the ice and snow to contribute to discharge, it did not subsequently warm the water to a great extent in the headwaters of the ELS and UWLS. Hence, solar radiation likely contributed to the good correlation between LOS water temperatures with air temperature since LOS discharge was sourced from the lake.

Suspended Sediment and Lake Sediment Deposition

The UWLS contained the greatest concentration of suspended sediment, as evidenced by field observations of highly turbid water (Figure 4.5) and suspended sediment measurements (Figure 4.6). A time-series of suspended sediment concentrations (SSC) for all sampling locations are shown in Figure 4.6 and a table of SSC is provided in Table A.4 (Appendix).

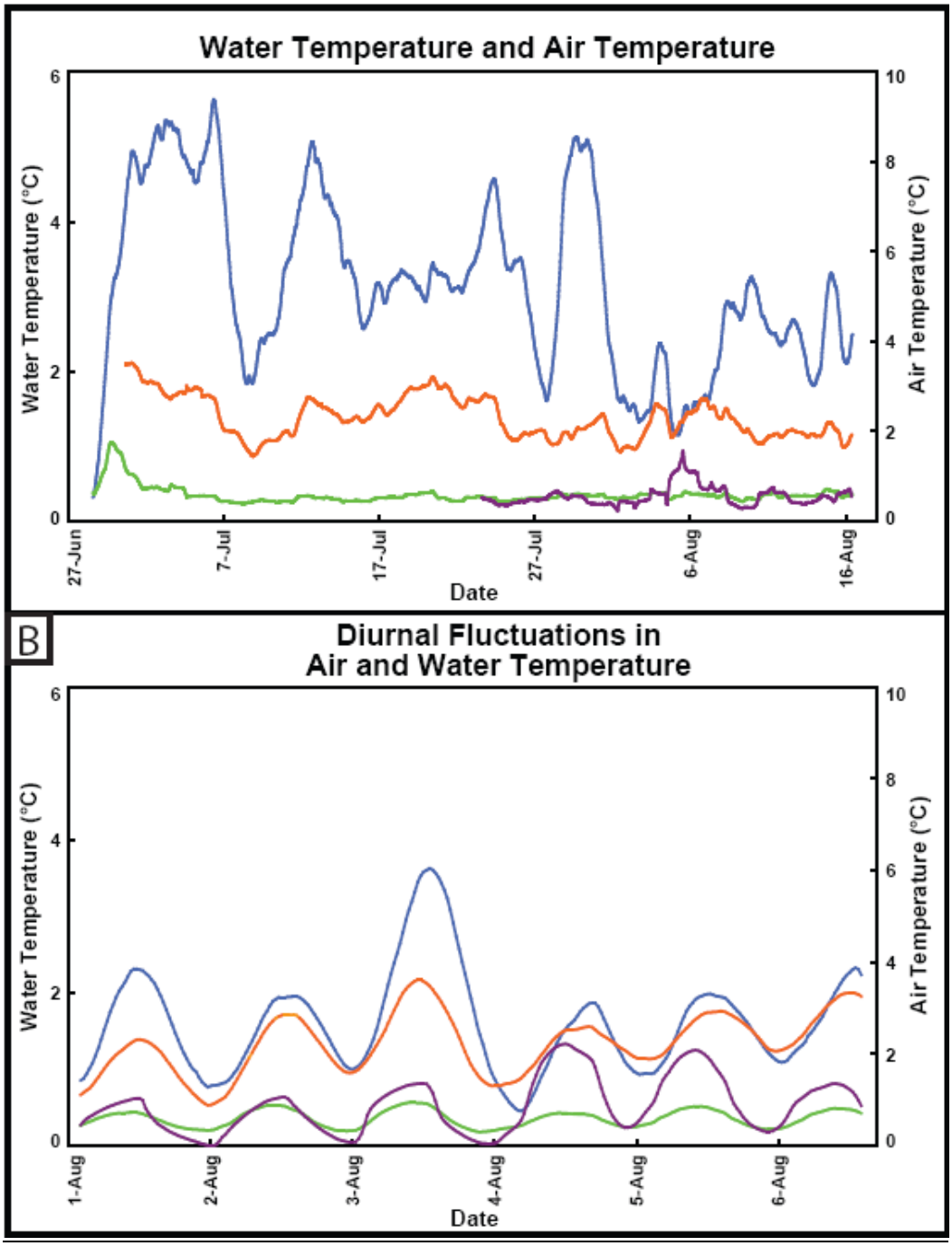


Figure 4.4: ELS (green), UWLS (purple), and LOS (orange): (A) 24-hr moving average of water and air (blue) temperature. (B) 12-hr moving average of diurnal fluctuations in water and air (blue) temperature 1-7 August.



Figure 4.5: UWLS was the most turbid of the three streams.

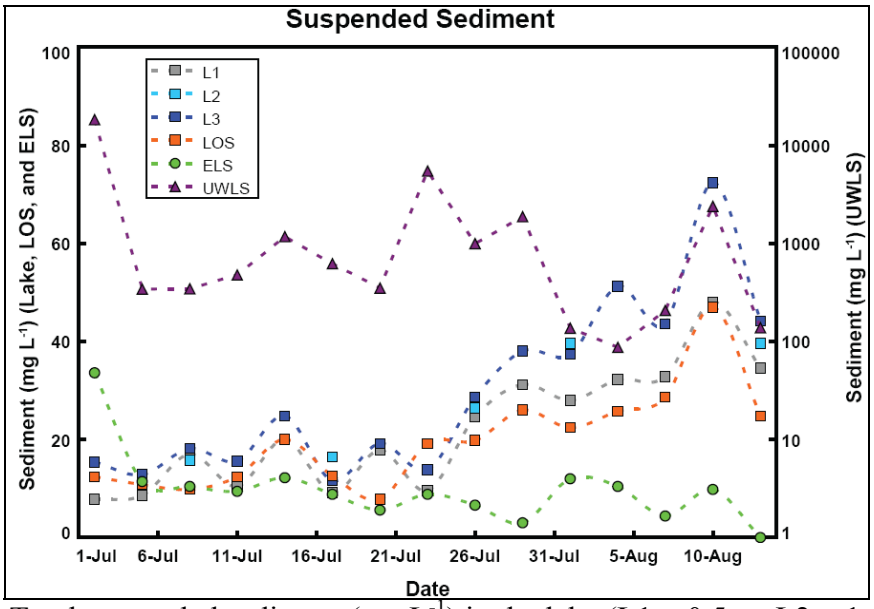


Figure 4.6: Total suspended sediment (mg L^{-1}) in the lake (L1 = 0.5 m, L2 = 1.5 m, and L3 = 5 m depth), LOS, ELS, and UWLS. Note that the UWLS is plotted on a logarithmic secondary axis.

SSC began to increase in the lake and LOS on 26 July (Figure 4.7), which corresponded to the rapid snowline retreat and ice marginal and proglacial sediment exposure (Figure 4.3). Regression analysis between discharge and SSC revealed that SSCs of the proglacial streams were related to discharge with $R^2 = 0.25$ for LOS ($p = 0.08$), $R^2 = 0.22$ for ELS ($p = 0.1$), and $R^2 = 0.36$ for UWLS ($p = 0.15$) (Figure 4.7). SSC was positively correlated with discharge in the ELS and UWLS whereas it was negatively correlated with discharge in the LOS (Figure 4.7).

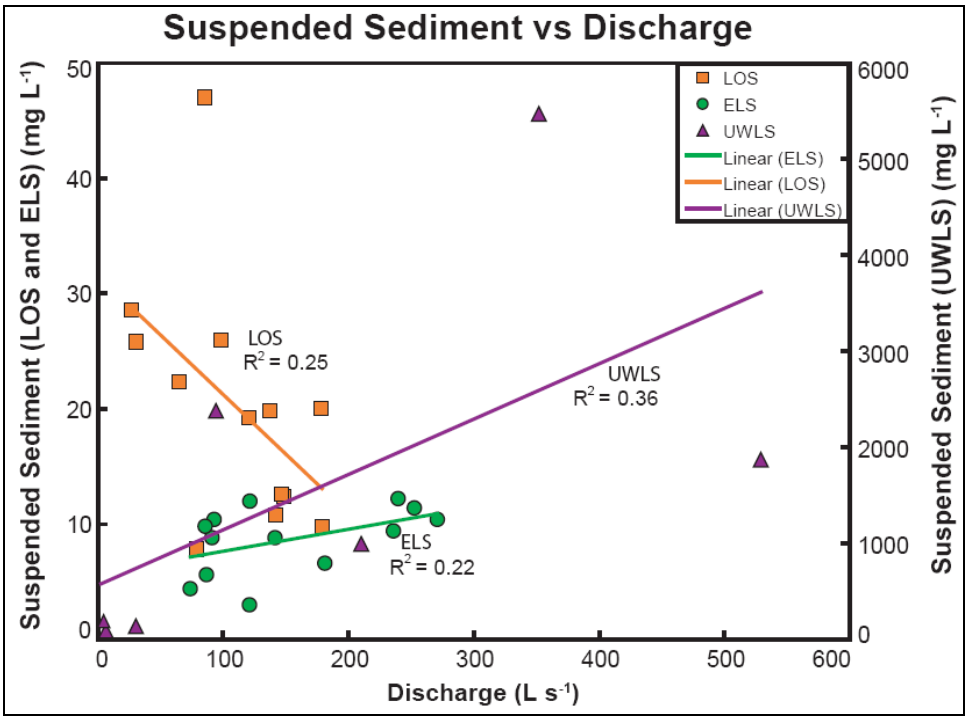


Figure 4.7: Scatterplot of SSC and discharge. Note the secondary axis for the UWLS SSC, which was 1-2 orders of magnitude higher than in the LOS and ELS.

The greatest amount of sediment accumulated at the lake delta, followed by the area closest to the lake outlet (Figure 4.8). The site of water chemistry sampling in the

middle of the lake and the site at the western glacial margin accumulated the least amount of sediment.

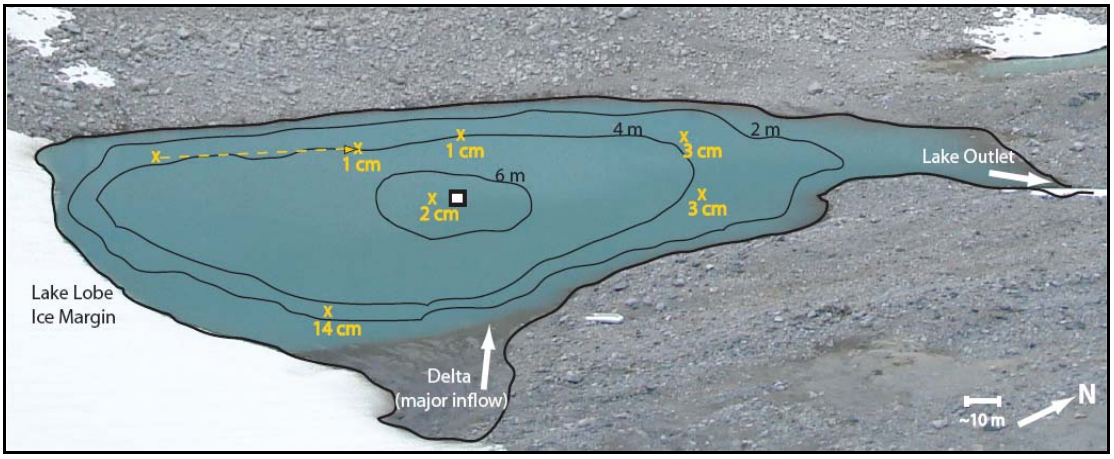


Figure 4.8: Sediment trap locations and depth of sediment collected (cm) from each trap 5 July-13 August, 2006. The yellow arrow indicates the movement of one sediment trap due a lake current. Note that the scale bar only pertains to the long axis of the lake.

Rhodamine Tracer: Surface
Water Flow Path and Residence Time

The rhodamine slug was released at the major lake inlet near the delta on the eastern-most ice marginal section of the lake (Figure 4.8). Observations of the dispersal of the slug indicated that the majority of surface water flowed from the delta towards the central-ice margin before it dispersed and generally flowed towards the LOS (see Figure 3.5). Rhodamine was also used to determine lake water residence time.

Rhodamine leaving the lake via the LOS through time is shown in Figure 4.9. The rise to peak export concentration occurred between 7.5-8.5 hrs after the initial release, however, the tail of the rhodamine peak was not observed over the initial 12.75 hr sampling duration. Thus, the dashed orange line represents a hypothesized tail based on the best-fit exponential decay curve of rhodamine concentration derived from

concentration measurements from the peak of export until the last discrete sample. The mean residence time for the lake water, the time at which half of the injected rhodamine slug exited the lake, was ~ 2.2 days. The shape of the entire curve, measured and extrapolated, is similar to those measured using LiBr tracers as indicators of water residence time at other small lakes (Cole and Pace, 1998) and alpine lakes (Thies et al., 2002) which provides confidence in the shape of the extrapolated portion of the curve.

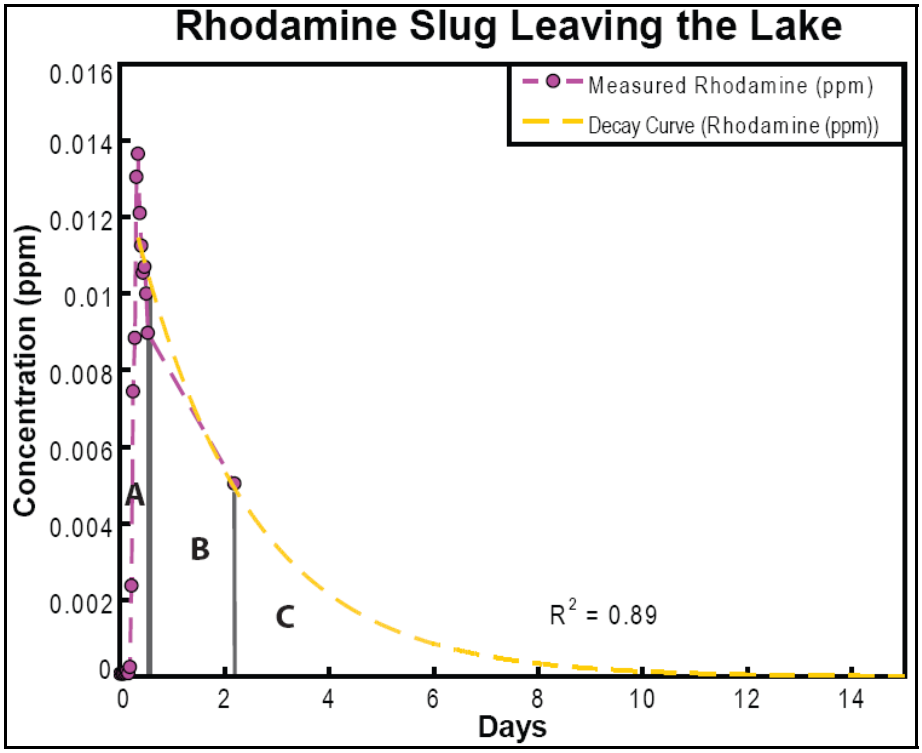


Figure 4.9: Rhodamine export from the lake. The area under the dashed pink line (A) is based on discrete samples taken every 30-45 minutes (pink dots). The gold dashed line represents a hypothetical curve based on an exponential decay equation derived from discrete samples taken from 14 August 4:45pm through 16 August 9:30am.

The area under the pink curve (A) is based on discrete samples (pink dots) taken every 30-45 minutes from the LOS (Figure 4.9) and accounts for 16% of the slug leaving the lake over the 12.75 hr sampling period on 14 August. Area B shows rhodamine concentrations for the period 14 August, 9:15pm until 16 August, 9:30am using an

exponential decay fit between points (Figure 4.9). The combined maximum area under the curves in regions A and B accounts for ~50% of the initial rhodamine slug leaving the lake by 9:30am 16 August. The remaining dashed curve that bounds area C (Figure 4.9) is a hypothesized tail based on a best-fit exponential decay equation that was derived from the measured concentrations from the peak to the last discrete sample ($R^2 = 0.89$).

50% of the tracer mass added had been exported from the lake after 2.2 days, based on the discrete samples taken from the LOS, corresponding to Areas A and B, Figure 4.9. The fractal tail of the decay curve would account for the remaining 50% of the tracer mass, area C Figure 4.9, if the entire tracer exited the lake via the LOS. Alternatively, some of the 50% of the rhodamine tracer that remained unaccounted for may have been trapped in stagnant lake waters at the base of the lake water column since the final density of the rhodamine slug was ~1.008 g cm^{-1} (the Rhodamine WT concentrate has a density of 1.16 g cm^{-3} and 500 mL was added to 10 L lake water to prepare the slug for injection) or been lost to groundwater recharge.

Water Chemistry

pH and Electrical Conductivity

pH ranged between 6.6-7 for all samples throughout the field season. Table A.2 (Appendix) shows the average of two pH measurements taken for each sample. EC ranged between 6.4-19.1 µS cm^{-1} for all samples, with the UWLS having the greatest range of EC (Figure 4.10 and Table A.3, Appendix). Figure A.3 (Appendix) indicates a significant linear relationship between the measured total dissolved solids (TDS) and EC

for the LOS ($R^2 = 0.81$, $p < 0.01$), ELS ($R^2 = 0.75$, $p < 0.01$), and UWLS streams ($R^2 = 0.92$ and $p = 0.02$).

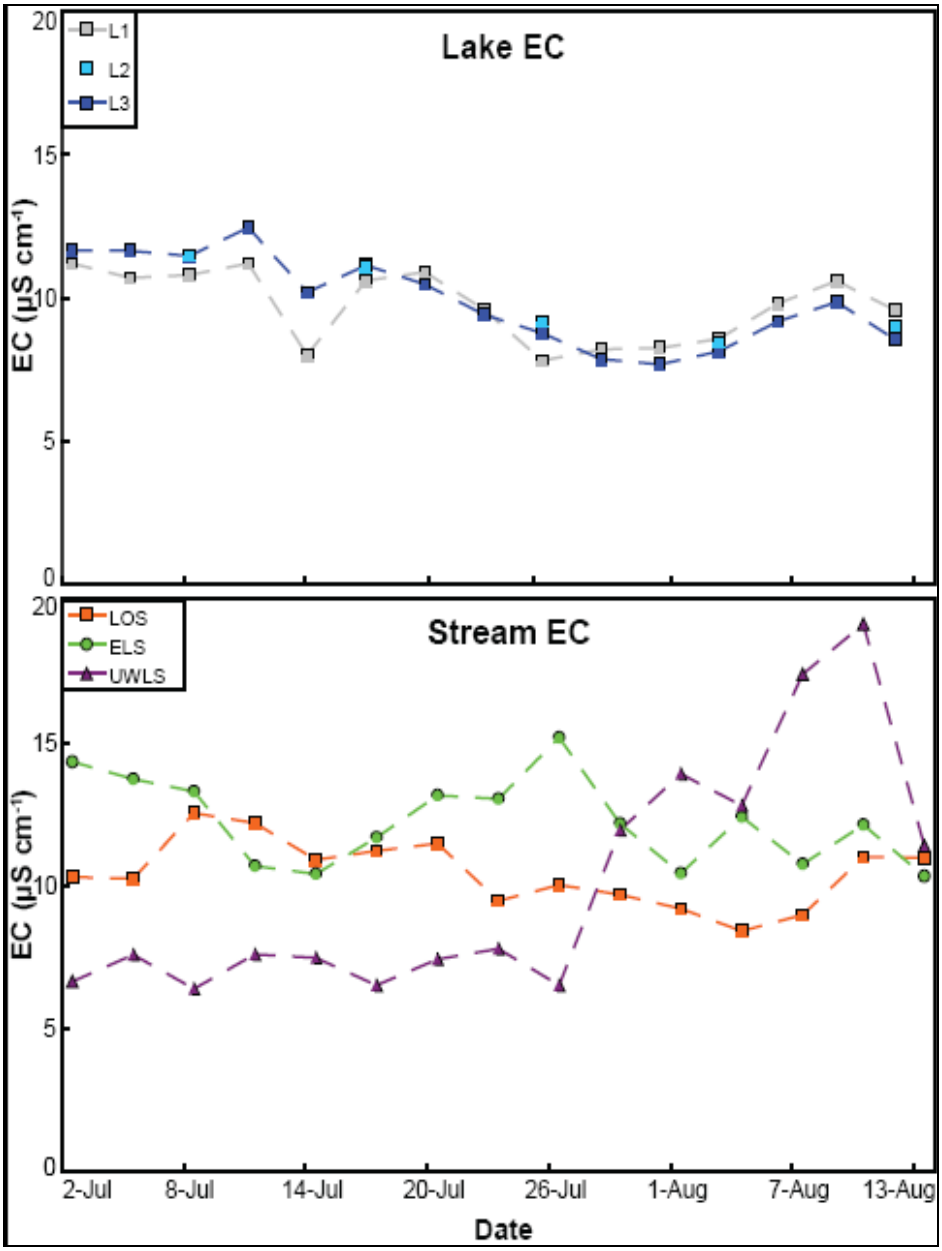


Figure 4.10: Time-series plot of electrical conductivity (EC) in µS cm^{-1} for the lake and streams.

Ion Chemistry

The predominant ions in the ELS, LOS, and UWLS were Ca^{2+}, HCO_3^-, Na^+, and SO_4^{2-} (Table 4.3). The ratio of atmospheric and crustal contributions to dissolved salts in the meltwater can be evaluated with the equation $(Cl^-)/\Sigma(anions)$ under the assumption that there was negligible naturally-occurring halite in the catchment (modified from Skidmore, 1995) and thus Cl^- was atmospherically derived rather than crustally derived. Applying this calculation in the Wheaton Glacier catchment indicated that 1-4% of all anions were derived from the atmospheric component, thus, most anions were crustally derived. This assumption appeared justifiable based on the observed catchment lithology.

There were strong statistically significant correlations between cations (Ca^{2+}, Na^+, K^+, and Mg^{2+}) and HCO_3^- (Table 4.4), which are likely indicative of key weathering reactions in the catchment. These weathering reactions will be explored further in the Discussion chapter. The statistically significant relationships between SSC and ion concentrations were negative in the LOS and positive in the ELS and UWLS (Table 4.4) which follows the trend between SSC and discharge in these streams (Figure 4.7). A time-series of dissolved ion concentrations in the ELS, LOS, UWLS, and lake over the melt season are shown in Figures 4.11, 4.12, 4.13, 4.14, and 4.15. Regression relationships between each ion and discharge are shown in Figure A.5 (Appendix); ion concentrations were not significantly related to discharge. The dominant ion

concentrations were more consistent in the LOS and varied to a lesser degree compared with the ELS and UWLS over the melt season (Table 4.5).

Table 4.3: Median ion concentrations (µeq L^{-1}) for the ELS, LOS, UWLS, and snow. Range of each dissolved ion is shown in parentheses. $n = 15$ for all ions except Cl^- and Na^+ ($n = 12$) which exclude data after the salt slug addition; $n = 2$ for snow.

Ion	ELS	LOS	UWLS	Snow
HCO_3^-	106.5 (77-157)	106.5 (83-126)	72.9 (62-144)	no data
SO_4^{2-}	13 (10-24)	12.7 (7-20)	0.1 (0-0.2)	0.8
F^-	31 (20-44)	2.1 (1.4-3.5)	7.1 (6-12)	0.5
Cl^-	1.6 (0.9-1.9)	1.4 (1.1-1.9)	1 (0.9-1.5)	2.8
NO_3^-	3 (0-6.5)	1.6 (0.7-2.5)	0 (0-1)	1.5
Ca^{2+}	124.9 (100-156)	138.2 (116-172)	99.9 (80-243)	3
Na^+	21.6 (17-30)	13.8 (11-17)	10.3 (7.9-24)	5.2
K^+	4.4 (2.4-6.3)	3.8 (2.6-6.3)	8.3 (5.3-15)	2.6
Mg^{2+}	2.9 (2.4-6.8)	2.9 (2.4-6.8)	1.6 (0.8-6.3)	1.2

Table 4.4: Solute matrix showing r (upper right) and p-values (lower left) among major dissolved ions and suspended sediment concentrations (SSC). Correlations with a significant p-value ($p \leq 0.1$) are bolded and in larger font.

LOS	Na^+	K^+	Ca^{2+}	Mg^{2+}	Cl^-	NO_3^-	SO_4^{2-}	HCO_3^-	SSC
Na^+	-	-0.14	**0.84**	0.10	**0.54**	**0.74**	**0.73**	**0.64**	**-0.63**
K^+	0.67	-	**-0.49**	-0.03	**-0.23**	**-0.44**	-0.27	-0.49	**0.57**
Ca^{2+}	< 0.01	0.05	-	0.32	**0.55**	**0.85**	**0.84**	**0.89**	**-0.71**
Mg^{2+}	0.75	0.93	0.22	-	0.12	0.12	**0.55**	0.32	-0.22
Cl^-	0.07	< 0.01	0.06	0.71	-	**0.76**	**0.58**	**0.57**	**-0.87**
NO_3^-	< 0.01	0.09	< 0.01	0.65	< 0.01	-	**0.61**	**0.79**	**-0.88**
SO_4^{2-}	< 0.01	0.30	< 0.01	0.03	0.05	< 0.01	-	**0.84**	**-0.51**
HCO_3^-	0.03	0.11	< 0.01	0.32	0.05	< 0.01	< 0.01	-	**-0.74**
SSC	0.03	0.03	< 0.01	0.43	< 0.01	< 0.01	0.05	< 0.01	-

ELS	Na^+	K^+	Ca^{2+}	Mg^{2+}	Cl^-	NO_3^-	SO_4^{2-}	HCO_3^-	SSC
Na^+	-	**0.74**	**-0.51**	-0.24	-0.05	0.20	**0.59**	**0.67**	0.14
K^+	< 0.01	-	-0.09	0.31	0.29	0.29	**0.68**	**0.79**	0.06
Ca^{2+}	0.09	0.76	-	0.01	0.41	0.28	-0.10	-0.10	0.24
Mg^{2+}	0.46	0.27	0.97	-	0.34	0.44	**0.78**	0.20	0.29
Cl^-	0.87	0.37	0.19	0.28	-	**0.77**	**0.53**	0.43	**0.72**
NO_3^-	0.53	0.30	0.31	0.10	< 0.01	-	**0.56**	**0.67**	**0.74**
SO_4^{2-}	0.05	< 0.01	0.73	< 0.01	0.08	0.03	-	**0.87**	0.33
HCO_3^-	0.02	< 0.01	0.75	0.53	0.17	0.02	< 0.01	-	0.24
SSC	0.67	0.84	0.36	0.30	< 0.01	< 0.01	0.24	0.41	-

UWLS	Na^+	K^+	Ca^{2+}	Mg^{2+}	Cl^-	NO_3^-	SO_4^{2-}	HCO_3^-	SSC
Na^+	-	**0.73**	**0.96**	**0.93**	-0.41	**0.71**	**0.73**	**0.91**	-0.24
K^+	< 0.01	-	**0.94**	**0.85**	-0.34	**0.53**	**0.75**	**0.82**	-0.15
Ca^{2+}	< 0.01	< 0.01	-	**0.93**	-0.34	**0.66**	**0.83**	**0.96**	-0.17
Mg^{2+}	< 0.01	< 0.01	< 0.01	-	-0.30	**0.69**	**0.80**	**0.82**	-0.06
Cl^-	0.19	0.27	0.28	0.37	-	0.40	-0.19	-0.34	**0.86**
NO_3^-	< 0.01	0.04	< 0.01	< 0.01	0.20	-	**0.77**	**0.57**	0.26
SO_4^{2-}	< 0.01	< 0.01	< 0.01	< 0.01	0.56	< 0.01	-	**0.74**	-0.05
HCO_3^-	< 0.01	< 0.01	< 0.01	< 0.01	0.28	0.03	< 0.01	-	-0.23
SSC	0.46	0.59	0.54	0.84	< 0.01	0.35	0.85	0.47	-

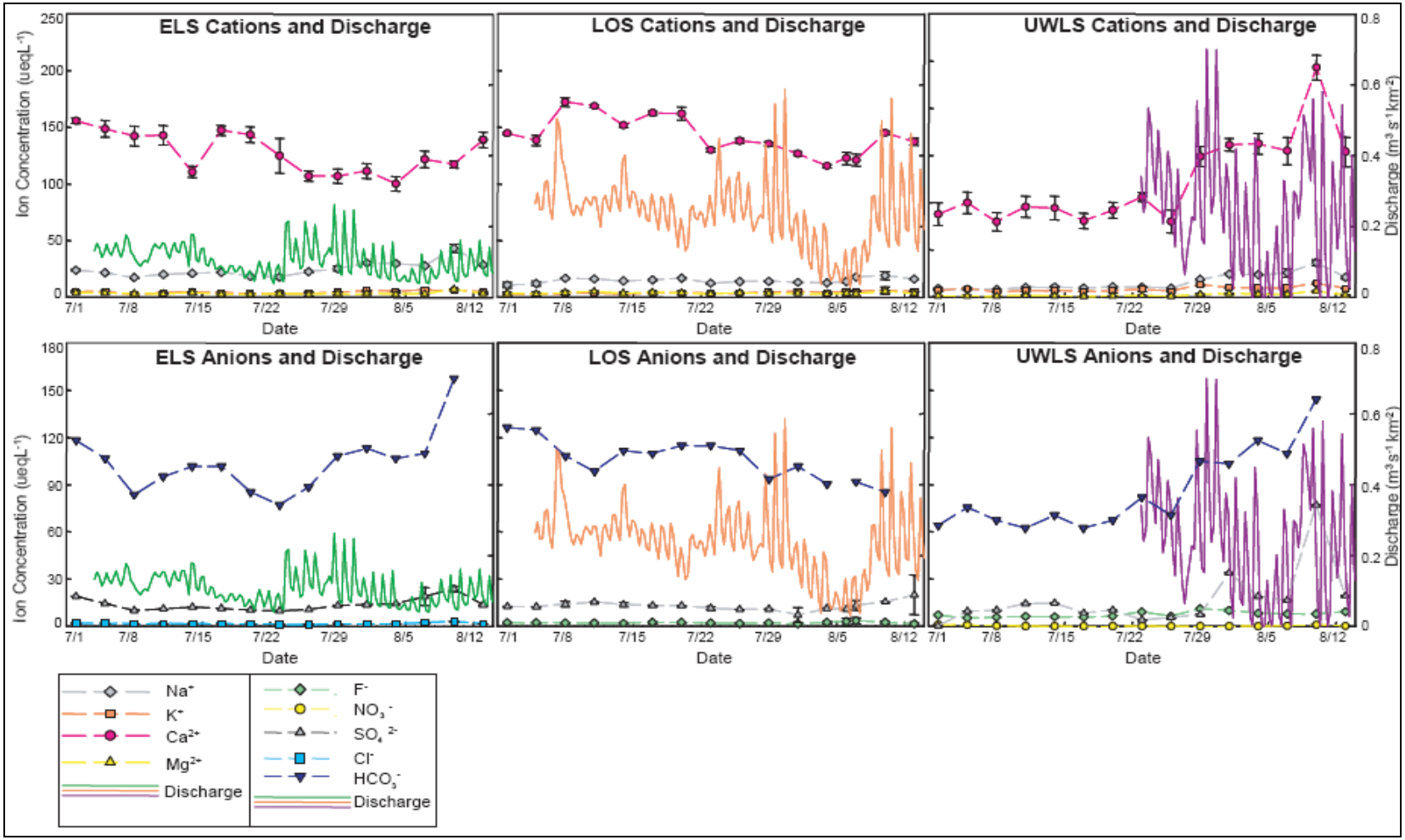


Figure 4.11: Concentration of ions in the ELS, LOS and UWLS over the melt season as determined using a Metrohm Peak ion chromatograph and [HCO_3^-] via acid titration. Area normalized discharge from figure 4.2B for comparison. Concentration data were based on quadruplicate samples; error bars indicate 1 standard deviation from the mean of quadruplicate samples.

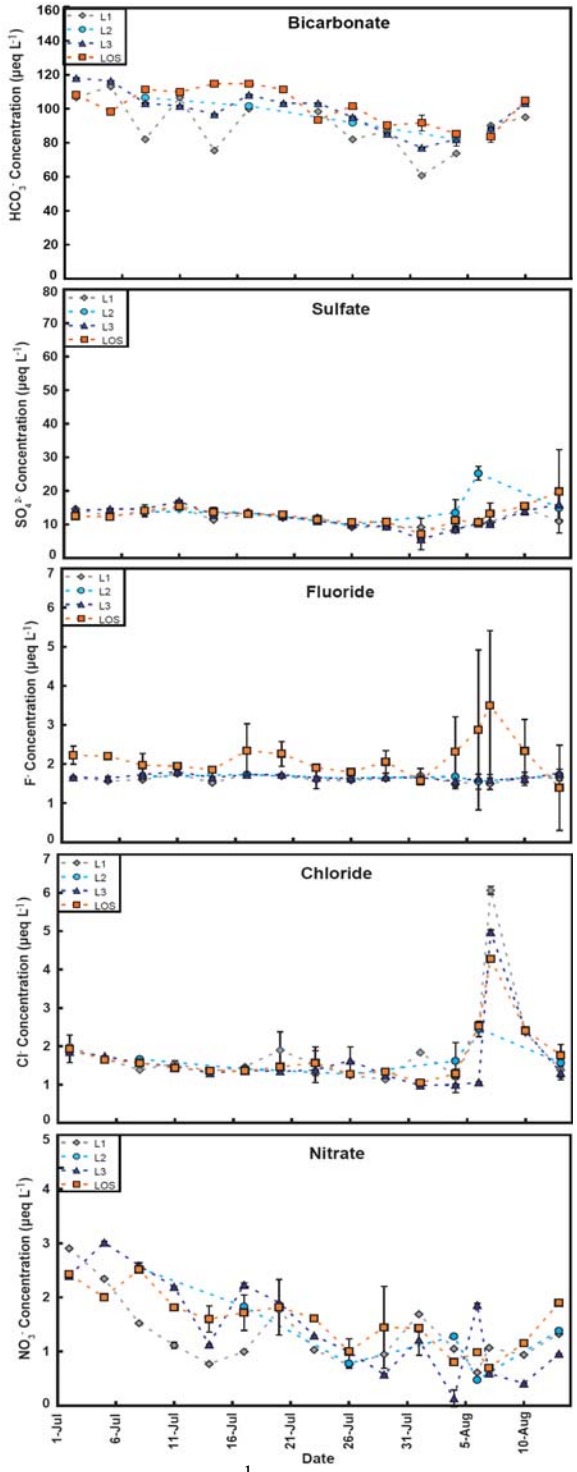


Figure 4.12: Anion concentrations (μeqL^{-1}) for the lake water samples. L1 indicates surficial lake waters, L2 is 1.5 m water depth, L3 is 5 m water depth, and LOS is Lake Outlet Stream. Bicarbonate was measured once in the field. Error bars on SO_4^{2-}, F^-, Cl^-, and NO_3^- denote 1 standard deviation from the mean of quadruplicate samples. Note the different y-axis scales.

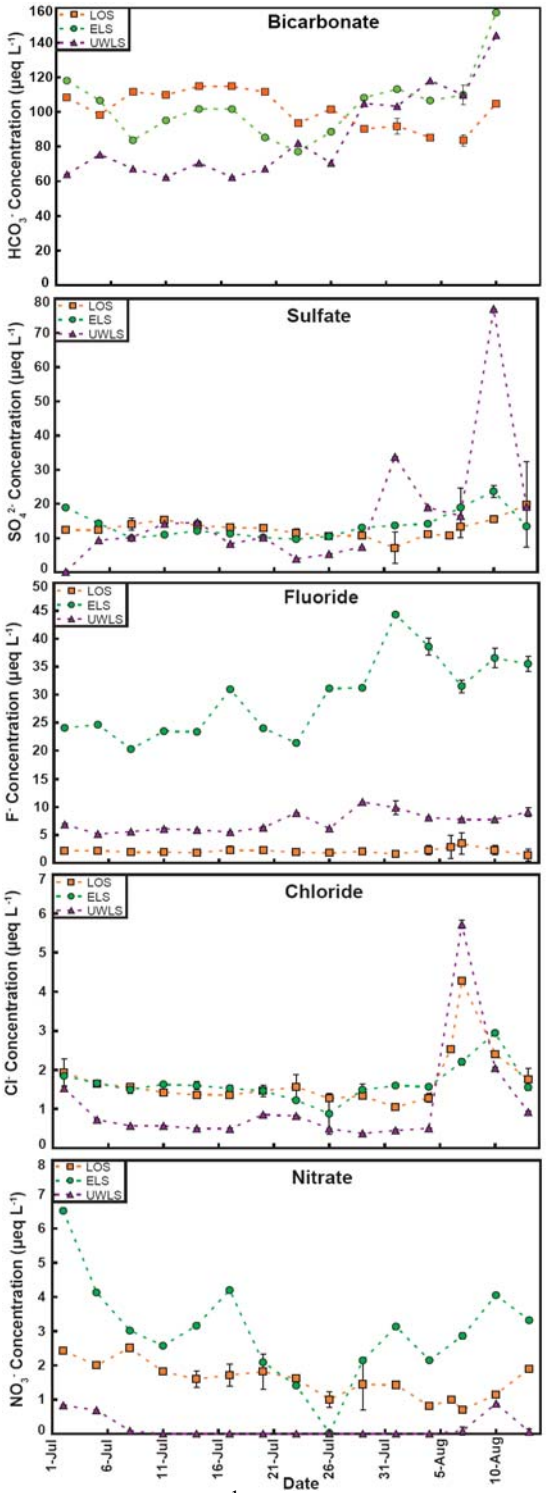


Figure 4.13: Anion concentrations (μeqL^{-1}) for LOS, ELS, and UWLS. Single measurements of bicarbonate concentration were made on each sample. Error bars on SO_4^{2-}, F^-, Cl^-, and NO_3^- denote 1 standard deviation from the mean of quadruplicate samples. Note the difference in y-axis scales.

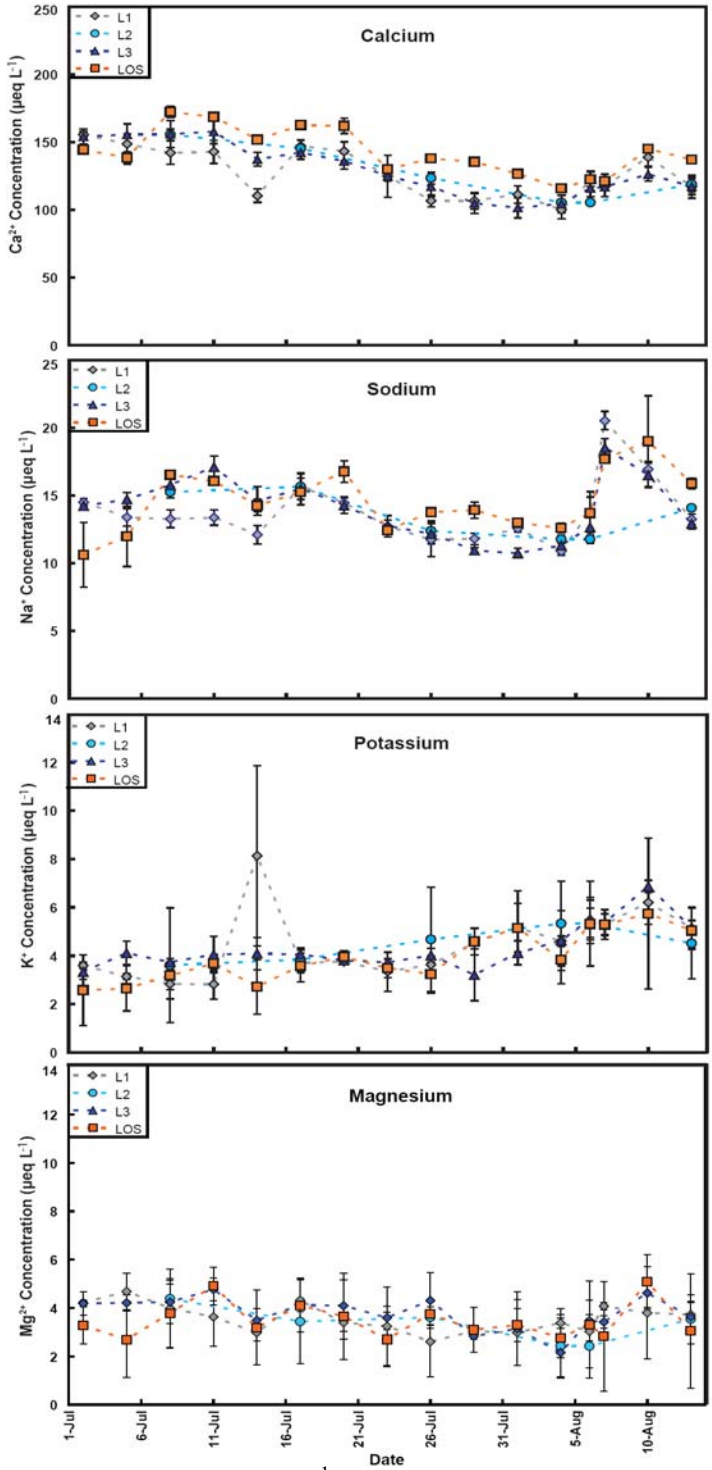


Figure 4.14: Cation concentrations (μeqL^{-1}) for the lake. L1 indicates surficial lake waters, L2 is 1.5 m water depth, L3 is 5 m water depth, and LOS is Lake Outlet Stream. Error bars denote 1 standard deviation from the mean of quadruplicate samples. Variability in Mg^{2+} is likely due to sample concentrations near the detection limit of the ion chromatograph. Note the difference in y-axis scales.

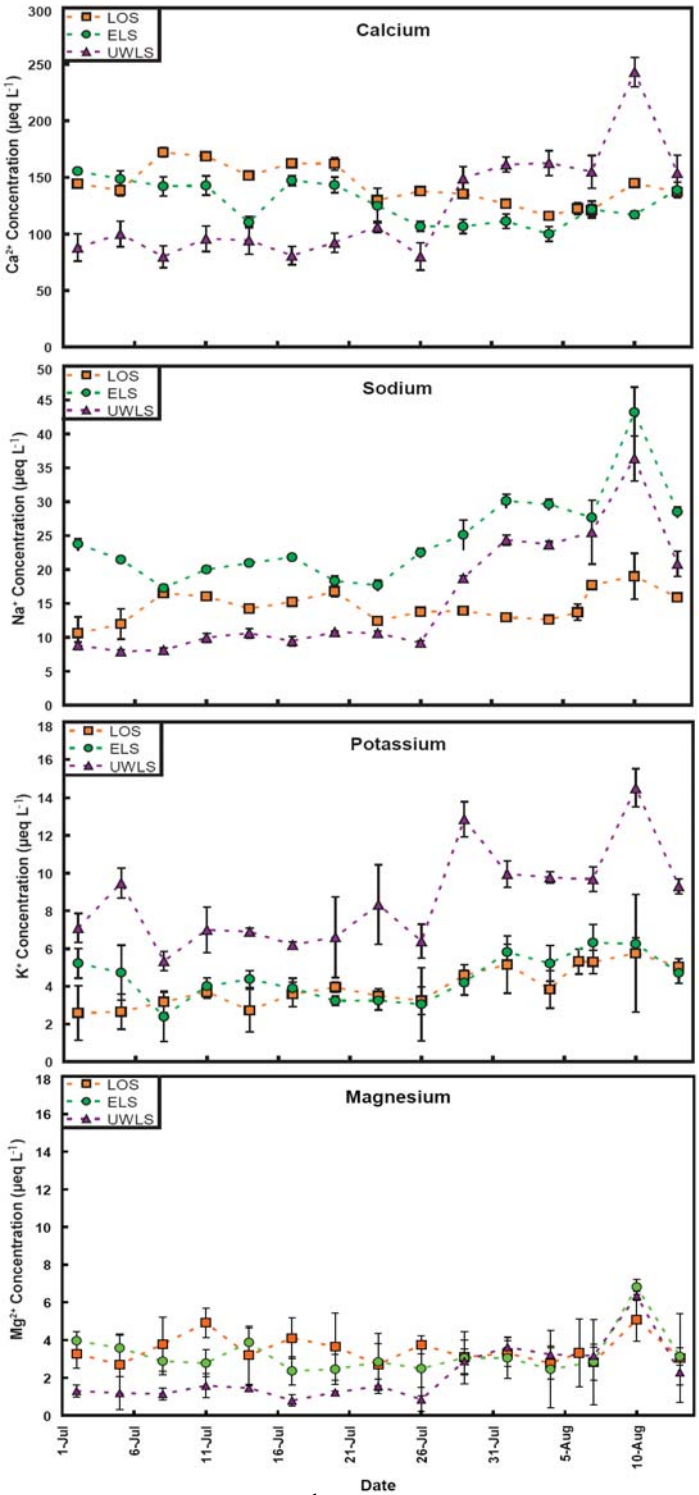


Figure 4.15: Cation concentrations (μeqL^{-1}) for LOS, ELS, and UWLS. Error bars represent 1 standard deviation from the mean of quadruplicate samples. Variability in Mg^{2+} is likely due to sample concentrations near the detection limit of the ion chromatograph. Note the difference in y-axis scales.

Table 4.5: Variations in major dissolved ions in each stream from June-August 2006.

Stream	Ion Concentration Fluctuations (μeq L^{-1})			
	HCO_3^-	Ca^{2+}	SO_4^{2-}	Na^+
LOS	<31	<53	<13	<8
ELS	73	56	14	26
UWLS	82	162	33	28

Chloride is a conservative environmental tracer, meaning it is not utilized by biota and is relatively inert, (e.g. Hodson et al., 2005) and Cl^- concentrations remained relatively constant before the salt slug addition on 6 August. Nitrate, a common limiting nutrient in aqueous systems (Wetzel, 2001), remained above 1 μeq L^{-1} throughout the field season in the ELS and LOS, with the exception of July 26 for the ELS. Nitrate concentrations were consistently higher in the ELS than the LOS with the exception of July 26 for the ELS and were near zero for the UWLS. Phosphate, the most common limiting nutrient in aqueous systems (Wetzel, 2001), was below detection limits (< 0.01 ppm) using ion chromatography. HCO_3^- provides pH buffering ability to the lake water and represents the major proton accepting species at pH 6.7-6.9 (Wetzel, 2001).

Fluoride concentrations were higher in the ELS than the other sampling environments (Figure 4.11), which may be due to a possible occurrence of fluorite, biotite and muscovite micas, (Bond, J, personal comm.; White, 2002), and cryolite (Na_3AlF_6) within the east lobe of the catchment. An extensive literature search produced no published evidence of cryolite deposits in the Yukon, but cryolite has been found in association with pegmatites in Greenland, Quebec, and Colorado (Schumann, 1985;

Ralph and Ralph, 2008) and pegmatites also exist within the Wheaton catchment, based on field observations. A significant regression relationship between Ca^{2+} and F^- (R^2 = 0.28, p = 0.05) and between Na^+ and F^- (R^2 = 0.64, $p < 0.01$) indicates that fluorite, biotite, and/or cryolite may have contributed to the F^- anomaly (Figure A.6, Appendix). However, a detailed geologic map of the catchment was not available to identify the likely a geologic source for this difference in fluoride concentrations between the two lobes.

Salt Tracer and Ion Chemistry

A peak in Cl^- and part (~3-5μeq) of the Na^+ peak on 7 August in the lake, LOS, and UWLS samples were potentially a result of the 10 kg salt slug released on 6 August at depth in the lake (Figure 4.13). A portion of the Na^+ peak in the UWLS and ELS on 7 and 10 August, respectively, could be attributed to the salt slug addition (approximately 5 $\mu eq L^{-1}$), but these peaks may have been augmented by other variable(s) such as the hydrolysis of the Na-aluminosilicate mineral, albite. If the original salt slug had fully mixed with the lake water, the concentrations of Cl^- and Na^+ would have increased by 10.6 $\mu eq\ L^{-1}$ (see Lake Physical Characteristics section in Methods chapter and Appendix).

Cl^- concentrations in the LOS rose on 7 August and returned to concentrations similar to those prior to salt slug release by 13 August. This indicated a residence time of at least 3 days for detectable concentrations of the salt slug in the lake and LOS. Cl^-, presumably from the salt slug, appeared in the UWLS and ELS on 7 August and peaked

in the UWLS and ELS on 7 and 10 August, respectively. This indicated potential groundwater travel of lake water to the UWLS and ELS.

Analysis of the 1995 aerial photograph and photos taken from the helicopter indicated that the UWLS and ELS sampling sites are slightly down-valley from the injection point of the salt in the lake and thus the groundwater source region (Figure 4.16). The lake was also ~25 m higher than the UWLS (and ELS) thus providing a hydraulic head to drive groundwater flow from the lake to the UWLS and ELS (Figure 4.16). Hydraulic conductivity of the glacial sediments was calculated using Darcy's law with the following assumptions: 1) the flow was in a straight line vector from the lake to the UWLS and ELS (Figure 4.16) and there was negligible dispersion in the subsurface (i.e. a 2-D flow model) and 2) transit time for the salt slug via groundwater was 1 day, which was the time between salt injection in the lake and detection of elevated Cl^- concentrations in the UWLS and ELS (see Appendix for full calculations).

The calculated hydraulic conductivity was ~ 8 cm s^{-1}, which is an order of magnitude higher than reported hydraulic conductivities for glacial sands and gravels (10^{-3} – 10^{-1} cm s^{-1}) and approximately two orders of magnitude below values for glacial clay non-aquifers (10^3 cm s^{-1}) (values from Assaad et al., 2004). While high, these calculations indicate a groundwater flow path for the salt tracer is a feasible explanation for the spike in Cl^- and a portion of the spike in Na^+ in the UWLS and ELS.

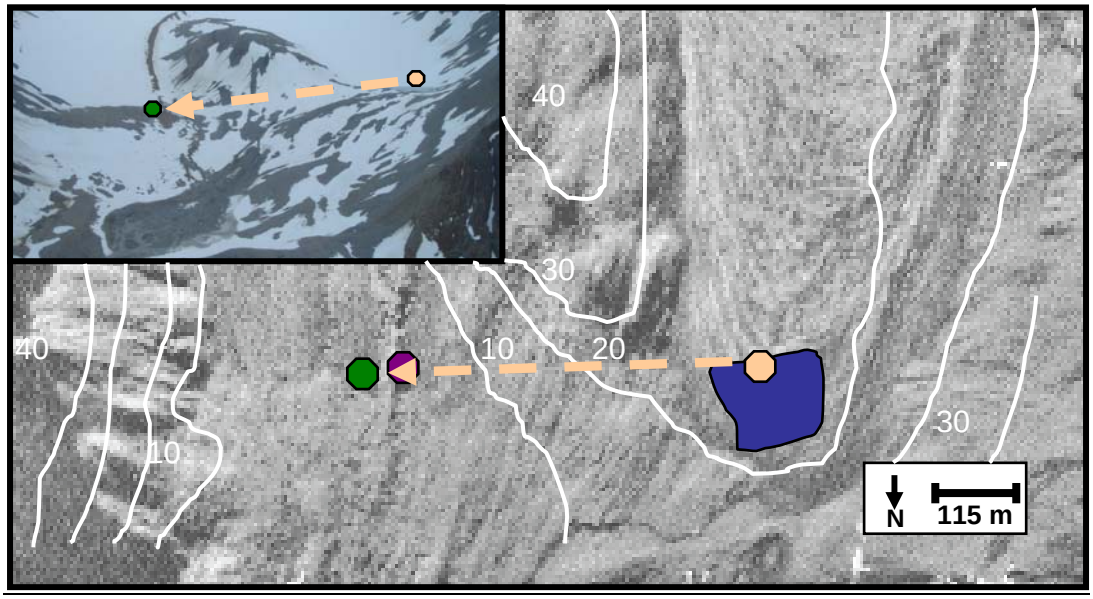


Figure 4.16: Possible salt injection groundwater flow path (arrow); green dot is the ELS sampling site, purple dot is the UWLS sampling site, and the tan dot indicates site of salt tracer injection (aerial photograph # A28240-88, National Air Photo Library, 1995). Inset and estimated contour lines (based on field observations) show that the lake is at a slightly higher elevation than the ELS sampling site. CI = 10 m, assume ELS is the 0 m reference point.

A two-component mixing model (Equation 1) was used to determine percent contributions of groundwater to the overall discharge in each stream (UWLS and ELS) and the extent of connectivity among the lake, UWLS, and ELS via groundwater.

$$\%Q_{GW} = (C_t - C_o) / (C_n - C_o) * 100\% \qquad \text{(Equation 1)}$$

where $\%Q_{Gw}$ is the percent contribution of groundwater to overall stream discharge measured with the salt tracer, C_t is the total concentration of Cl^- in the discrete sample from each stream on 7, 10, and 13 August as measured on the ion chromatograph, C_o is the background concentration of Cl^- in each stream (determined by subtracting the 4

August [Cl^-] from the 7, 10, and 13 August [Cl^-]; the 4 August sample was used because it was the last sample taken from all three streams prior to the salt slug addition), and C_n is the groundwater contribution, which was assumed to be 10.6 μeq L^{-1} from the salt tracer mixing fully with the lake water, as stated above (see Appendix for calculations).

Assuming the salt slug fully mixed with the lake water, the model predicted that 51% of UWLS discharge was derived from groundwater sourced from the lake (Table 4.6). This contribution appeared to be too high and potentially implausible since the discharge hydrograph from the UWLS was extremely variable (Figure 4.2) and it was difficult to envision such variability if groundwater flow was such a large component of UWLS discharge. Furthermore, the salt slug was released at the south end of the lake at a depth of 1-1.5 m below the water surface, thus this more dense saline input may have sunk to the lake bottom and entered the groundwater flow system after only mixing with a fraction of the total lake volume. Therefore, the assumption of full mixing with the entire lake prior to its entering the groundwater flowpath as in Equation 1 seemed unlikely.

The mixing model was evaluated for concentrations (C_n) of the groundwater contribution of 53 and 106 μeq L^{-1}, which would result from mixing of the salt slug with 20% or 10% of the total lake volume, respectively, prior to entering the groundwater flow system. The two component mixing model assumes that the end members are constant (Collins, 1979) and it is recognized that this analysis is therefore a simplification of the true mixing conditions, but it does provide a first order constraint on possible groundwater contributions to the UWLS and ELS. The lower mixing efficiencies

resulted in predicted values for the groundwater contribution from the lake to the UWLS and ELS that were < 10% of total discharge (Table 4.6). A groundwater contribution of < ~10% was more consistent with observations on the diurnal variability in stream discharge in the ELS and UWLS (Figure 4.4), and fell within literature values for groundwater connectivity in the headwaters of glacerized alpine catchments, which has been documented as < 40% (Brown et al., 2006; Brown et al., 2007).

Table 4.6: Percent contribution of total discharge that comes from groundwater for each stream based on the salt slug travel from the lake to the UWLS and ELS assuming dilution efficiency of 100%, 20%, and 10%.

	% Contribution from GW		
Dilution efficiency	100%	20%	10%
µeq L-1	10.6	53.0	106.0
	ELS		
	7%	1%	1%
	14%	3%	1%
	0%	0%	0%
	LOS		
	32%	5%	3%
	12%	2%	1%
	5%	0%	0%
	UWLS		
	51%	8%	5%
	15%	1%	1%
	4%	0%	0%

Carbon Chemistry: Dissolved Organic Carbon

Dissolved organic carbon (DOC) concentrations were blank subtracted (0.2 ppm, based on Milli-Q blanks) and most were below 0.2 ppm, with all samples below 0.85 ppm (Figure 4.17). These results are typical of remote glacial alpine environments with little human influence and with limited allochthonous sources of carbon such as vegetation (Karlsson et al., 2001; Tockner et al. 2002; Lafreniere, 2003; Barker et al.,

2006). The DOC record appears to have had three distinct periods: measurable quantities of DOC (1-17 July), depletion of DOC (20 July-4 August), and an increase in DOC in the lake, LOS, and UWLS (7-10 August). The highest DOC values were observed in the UWLS.

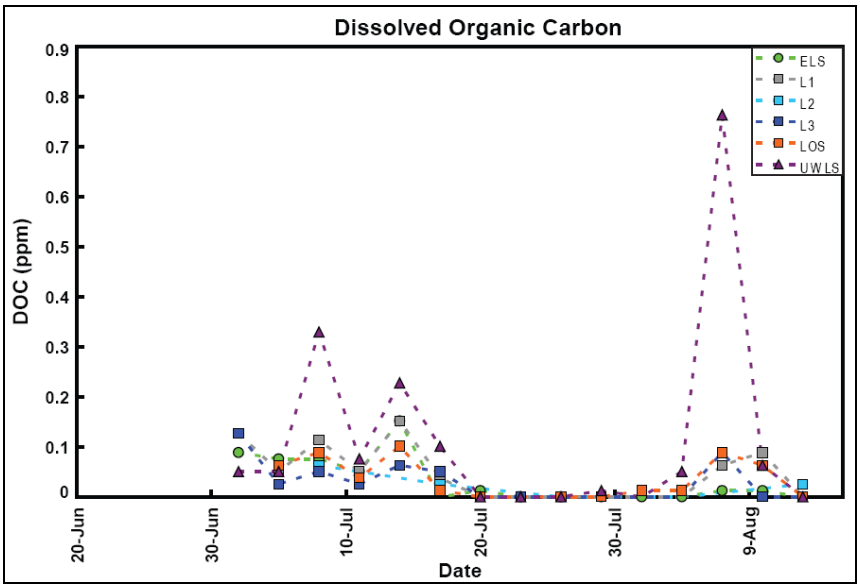


Figure 4.17: DOC concentrations.

Carbon Chemistry: Particulate Organic Carbon

Particulate organic carbon (POC) was quantified by loss on ignition (LOI) in a method similar to that of Heiri et al. (2001). LOI for POC in field blanks indicated no measurable contamination occurred. Results are shown in Table 4.7.

Table 4.7: Particulate organic carbon as determined by mass loss on ignition.

	POC (mg L^{-1})							
Sample Location	23-Jul	26-Jul	29-Jul	1-Aug	4-Aug	7-Aug	10-Aug	13-Aug
L1	5	6	2	75	33	4	5	10
L2	-	7	-	-	-	-	-	11
L3	1	6	9	6	8	7	13	14
LOS	0	3	7	8	-	5	10	14
ELS	4	8	4	7	3	2	8	15
UWLS	11	8	22	-	5	11	15	11

Cell Enumeration

Bacterial cell enumerations indicated a relatively consistent number of bacterial cells in the LOS and within the lake and an increase followed by a decrease in bacterial cell numbers in the ELS over the field season (Figure 4.18). Bacterial cell numbers ranged between 6.7 x 10^4 cells (L3) and 9.9 x 10^4 (L3) mL^{-1} in the lake, 6.4 and 9.7 x 10^4 in the LOS, and 2.8 and 6.0 x 10^4 in the ELS. Contamination during slide preparation was < 75 cells mL^{-1}, as determined by analysis of procedural blanks (see Methods chapter).

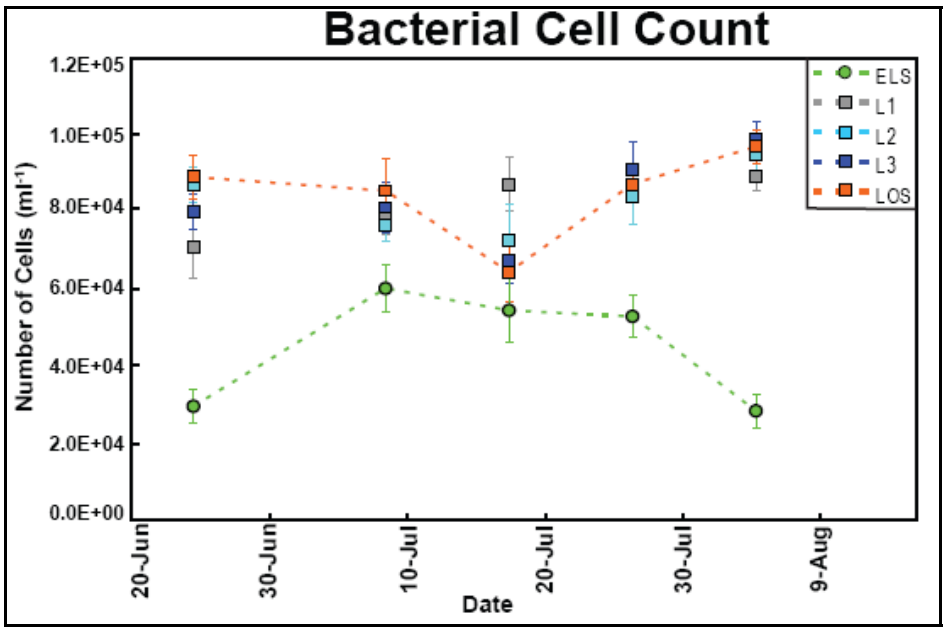


Figure 4.18: Bacterial cell enumerations through the field season. Note there is no data for L1 on 26 July due to loss of sample.

Primary Productivity

Primary productivity was highest at the beginning of the season and occurred at the greatest rate at 0.5 m water depth, L2 (Figure 4.19). Surface waters (L1) and L2 had

highest rates of primary productivity (Figure 4.19). The lowest rate of primary productivity occurred at 5 m water depth, L3, which also corresponds with the lowest amount of light availability (Figures 3.4B and 4.19). The primary productivity incubations on 25 June, 29 June, and 26 July occurred on mostly sunny days, while those on 8 July, 17 July, and 4 August occurred on mostly cloudy days (Figure 4.2A). The greatest rates of productivity occurred in surface waters (L1 and L2) on 25 June, 29 June, and 26 July, which corresponded with days with the most available sunlight to facilitate primary productivity (Figures 4.2A and 4.19).

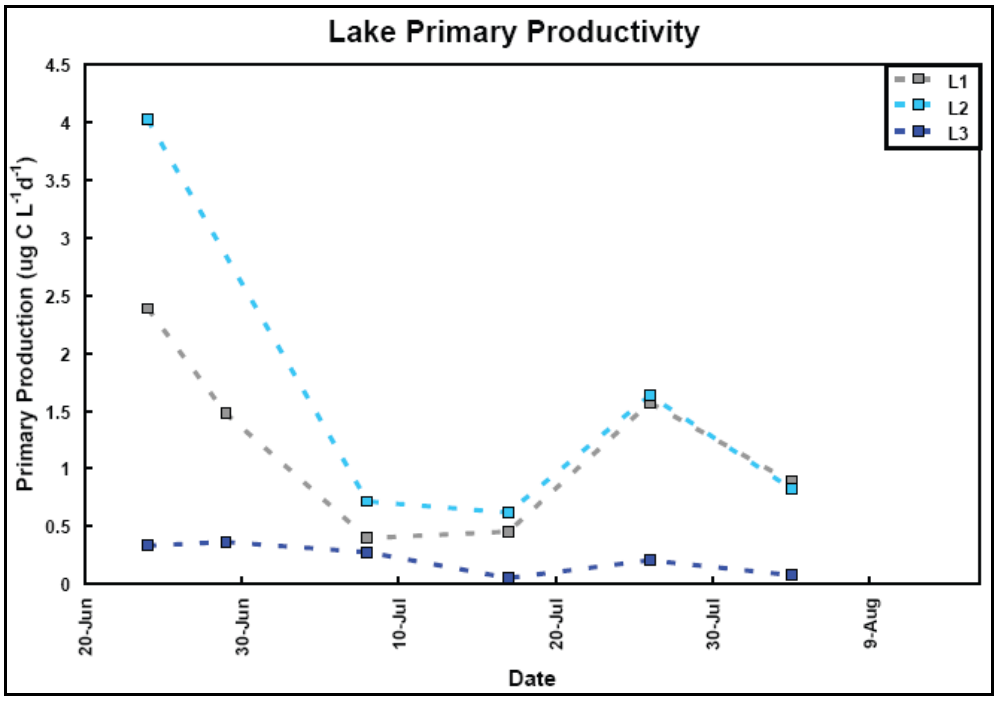


Figure 4.19: Rates of primary productivity in the lake at surface (L1), 1.5 m (L2), and 5 m (L3) water depths after 24-hour incubations in each environment following inoculation with ^{14}C bicarbonate.

References Cited

Assaad, F.A., LaMoreaux, P.E., and Hughes, T.H., 2004. Field Methods for Geologists and Hydrogeologists. New York: Springer-Verlag. 378 p.

Barker, J.D. Sharp, M.J., Fitzsimons, S.J., and Turner, R.J., 2006. Abundance and Dynamics of Dissolved Organic Carbon in Glacier Systems. *Arctic, Antarctic, and Alpine Research*, v. 38, pp. 163-172.

Brown, L.E., Hannah, D.M., Milner, A.M., Soulsby, C., Hodson, A.J., and Brewer, M.J., 2006. Water sources dynamics in a glacierized alpine river basin (Taillon-Gabietous, French Pyrenees). *Water Resources Research*, v. 42, W08404.

Brown, L.E., Milner, A.M., and Hannah, D.M., 2007. Groundwater influence on alpine stream ecosystems. *Freshwater Biology*, v. 52, pp. 878-890.

Carter, R.W. and Davidian, J., 1989. U.S. Geological Survey, Techniques for Water-Resources Investigations, Book 3, Chapter A6.

Cole, J.J. and Pace, M.L., 1998. Hydrologic variability of small northern Michigan lakes measured by the addition of tracers. *Ecosystems*, v. 1, pp. 310-320.

Collins, D.N., 1979. Hydrochemistry of meltwaters draining from an alpine glacier. *Arctic, Antarctic, and Alpine Research,* v. 11, pp. 307-324.

Devore J. and Peck, R., 2007. Statistics, 5th ed. Belmont: Brooks/Cole—Thompson Learning Inc. 763 p.

Dingman, L.S., 2001. Stream-gauging methods for short-term studies. In Physical Hydrology, 2nd ed. Englewood Cliffs: Prentice-Hall; 608-623.

Environment Canada, 2006. National Climate Archive. Accessed at: http://climate.weatheroffice.ec.gc.ca/ [20 September 2006].

Heiri, O., Lotter, A.F., and Lemcke, G., 2001. Loss on ignition as a method for estimating organic and carbonate content in sediments: reproducibility and comparability of results. *Journal of Paleolimnology*, v. 25, pp. 101-110.

Hodson, A.J., Mumford, P.N., Kohler, J., and Wynn, P.M., 2005. The High Arctic glacial ecosystem: new insights from nutrient budgets. *Biogeochemistry*, v. 72, pp. 233-256.

Intech Instruments Ltd., 2005. TruTrack Data Logger: Water Level/Temperature Model WT-HR Datasheet. Accessed at: http://www.intech.co.nz/products/minipd/datasheets/WT-HR.pdf [14 September 2007].

Irvine-Fynn, T.D.L., Moorman, B.J., Willis, I.C., Sjogren, D.B., Hodson, A.J., Mumford, P.N., Walter, F.S.A., and Williams, J.L.M. 2005. Geocryological processes linked to High Arctic proglacial stream suspended sediment dynamics: examples from Bylot Island, Nunavut, and Spitsbergen, Svalbard. *Hydrological Processes*, v. 19, pp. 115-135.

Karlsson, J. Jonsson, A., and Jansson, M., 2001. Bacterioplankton production in lakes along an altitude gradient in the Subarctic North of Sweden. *Microbial Ecology*, v. 42, n. 3, pp. 372-382.

Lafreniere, M.J., 2003. Hydrological and hydrochemical investigations in a glacial lake catchment: Implications for organochlorine transport. PhD Dissertation, University of Alberta. 209 p.

McKnight T.L. and Hess, D., 2004. Physical Geology: A Landscape Appreciation, 7th ed. Upper Saddle River: Pearson Education, Inc. 631 p.

National Air Photo Library (Centre for Topographic Information, Natural Resources, Canada)., 1995. Photo A28240-88. Scale = 1:20,000. Taken 18 September, 1995.

Paterson, W.S.B., 1994. The Physics of Glaciers, 3rd ed. New York: Pergamon Press. 480 p.

Ralph, J. and Ralph, I., 2008. Cryolite. Accessed at: http://www.mindat.org/min-1161.html [13 January 2008].

Schumann, W., 1985. Handbook of Rocks, Minerals, and Gemstones. New York: HarperCollins Publishers and Houghton Mifflin Co. 380 p.

Skidmore, M.L., 1995. The hydrology and hydrochemistry of a high Arctic glacier. Master's Thesis: Department of Geography, University of Alberta, Edmonton. 114 p.

Thies, H., Nickus, U., Arnold, C., and Psenner, R., 2002. A hydrological tracer experiment with LiCl in a high mountain lake. *Hydrological Processes*, v. 16, pp. 2329-2337.

Tockner, K.T. Malard, F., Uehlinger, U., and Ward, J.V., 2002. Nutrients and organic matter in a glacial river-floodplain system (Val Roseg, Switzerland). *Limnology and Oceanography*, v. 47, pp. 266-277.

Wetzel, R.G., 2001. Limnology: Lake and River Ecosystems. 3rd ed. San Francisco: Academic Press. 1006 p.

White, G.V., 2002. Industrial Minerals, Gems, and Minor Metals in the Yukon. Whitehorse: GV White Resources Limited. 244 p.

CHAPTER 5

DISCUSSION

The East Lobe Stream (ELS), Upper West Lobe Stream (UWLS), Lake Outlet Stream (LOS), and the lake exhibit several differences in biogeochemical characteristics, measured over a period from late June to mid August, 2006. These characteristics demonstrate the interplay between physical characteristics (e.g. water temperature), chemistry (e.g. solute composition), and biology (e.g. microbial communities). The ELS, UWLS, and LOS represent outlet streams for three distinct proglacial subcatchments. The ELS is fed by meltwater sourced directly from a supraglacial stream on the east lobe of the glacier and drains a lobe that transitions from full snow cover in late June to approximately 25% snow cover by mid-August; the UWLS is fed by the upper section of a lobe that is snow covered for most of the melt season and its source water has a high degree of contact with the medial moraine and unconsolidated proglacial sediments; the LOS drains a lake which is fed by the lower section of a lobe that transitions from snow cover to > 90% ice cover by mid-August. This chapter describes the major similarities and differences in hydrology, chemistry, and biology to address the overarching theme of the thesis: to evaluate how differing proglacial environments affect discharge, dissolved ion concentrations, and carbon dynamics in a glaciated sub-Arctic catchment. The study tested the following hypotheses:

(H1) The Wheaton Glacier is non-temperate.

Biogeochemical and hydrological analysis of proglacial stream water chemistry was used to assess whether there was a significant subglacial component to the out-

flowing streams at the Wheaton Glacier and thus whether the glacier is non-temperate with little to no water flowing at its base.

(H2) Water storage time differences between the proglacial streams vs. lake produce more consistent discharge and dissolved ion concentrations in the LOS, and lower SSC in the LOS relative to the ELS and UWLS.

Lake water residence times were measured using salt and rhodamine tracers and discharge, dissolved ion concentrations, and SSCs were compared among the ELS, LOS, and UWLS.

(H3) Primary productivity, microbial biomass, and organic carbon are higher in the lake, and LOS relative to the ELS and UWLS.

Bacterial enumerations in the ELS, LOS, and in the lake compared the amount of biomass among the proglacial streams and lake. Discrete samples for organic carbon concentration were compared between the ELS, LOS, UWLS and lake to evaluate this hypothesis.

Thermal Regime of the Wheaton Glacier

The thermal regime of a glacier has a strong influence on the biogeochemistry of a system since it governs how meltwater is routed and stored in the glacial drainage system. Non-temperate glaciers can be either (1) cold-based with no liquid water flowing at the base or (2) polythermal, with a limited drainage systems at the base. Hodgkins (1997) documented a critical ice thickness to reach pressure-melting point of at least 90 m (based on polythermal conditions at this depth at Austre Brøggerbreen, Svalbard) as

necessary for polythermal conditions to exist. Physical features of the Wheaton Glacier such as its small size (4 km^2), lack of crevassing on the glacier surface, and no evidence for subglacial drainage outlets at the terminus suggested that the Wheaton Glacier was non-temperate. This hypothesis was supported by dissolved ion concentration data. Solute concentrations were generally consistent throughout the melt season in the ELS and LOS with a rise in solute concentrations later in the season in the UWLS. An early season flush of solute, which is common at temperate glaciers, is not evident at non-temperate glaciers due to the lack of winter storage of solute-rich meltwaters at the base of the glacier (Hodgkins, 1997; Wadham et al., 1998). Further, dissolved ion concentrations tend to increase during the melt season at non-temperate glaciers as weathering of proglacial sediments increases, which is related to the exposure of proglacial sediment as winter snowpack melts (Hodgkins, 1997; Wadham et al., 1998). This increase in dissolved ion concentrations was observed in the UWLS at the Wheaton Glacier both in the EC record (Figure 4.10) and the discrete ion data (Figure 4.11, 4.13 and 4.15).

Unlike proglacial streams from temperate glaciers which tend to have a steady supply of sediment sourced in part at the glacier bed and transported via the subglacial drainage system (Gurnell et al., 1996), proglacial streams at non-temperate glaciers have limited access to sediment at the glacier bed and thus suspended sediment is available primarily through supraglacial, ice marginal, and proglacial sources (e.g. moraines, debris from valley walls, and unconsolidated proglacial sediment). Sediment availability from these sources generally increases as snowpack melts and supraglacial, ice marginal, and

proglacial sediment is exposed, and when debris avalanches from the valley walls occur (Hodson et al., 1998). A poor-moderate discharge-suspended sediment relationship has been observed in non-temperate glacial systems in Svalbard, which was attributed to sediment availability as the limiting factor in sediment transport (Hodson et al., 1998).

Regression analysis between discharge and SSC revealed that 22-36% of the variability in SSCs in the proglacial streams was related to variability in discharge (Figure 4.7). However, for the LOS, the relationship was negative, i.e. at higher discharges lower SSC was observed. Thus sediment availability is a plausible limiting factor for SSC in all three streams, but to a lesser degree in the UWLS, which had a consistently higher SSC than the other streams by 1-2 orders of magnitude and greater variability in SSC for a given discharge (Figure 4.6). Sediment in the UWLS was sourced from the medial morainal and proglacial areas that were accessed by the stream waters and the stream occupied multiple (braided) channel locations during the melt season (Figure 5.1). In contrast, the ELS flowed supraglacially for a considerable distance with limited access to debris on the glacier surface and proglacially, it occupied a channel with consistent geometry throughout the season. Furthermore, the ELS proglacial stream exhibited significant bed armoring, resulting in little available sediment for stream transport (Figure 3.2B, Figure 4.6). The lake upstream of the LOS provided a sink for sediments in-washed from the main inlet stream to the lake draining across morainal sediments as shown by the significant inlet delta (Figure 3.4). Similar to the ELS, the LOS occupied a channel with consistent geometry throughout the season and exhibited significant bed armoring, resulting in little available sediment for stream

transport (Figure 3.2D). However, there was an increase in SSC in the lake and LOS to consistently higher values during the mid-season, around 26 July (Figure 4.6). This change occurred concurrently with rapid snowline retreat on the lower portion of the west lobe (Figure 4.3) and thus these observations are consistent with those of Hodson et al., (1998) that snow cover is a factor in limiting ice marginal and proglacial sediment availability to streams. The consistent and/or increasing solute concentrations in all three streams and consistent SSC in the ELS and rising SSC in the lake and LOS in response to rapid snowline and sediment exposure support the hypothesis that the Wheaton glacier is non-temperate and does not have a well developed subglacial drainage system.

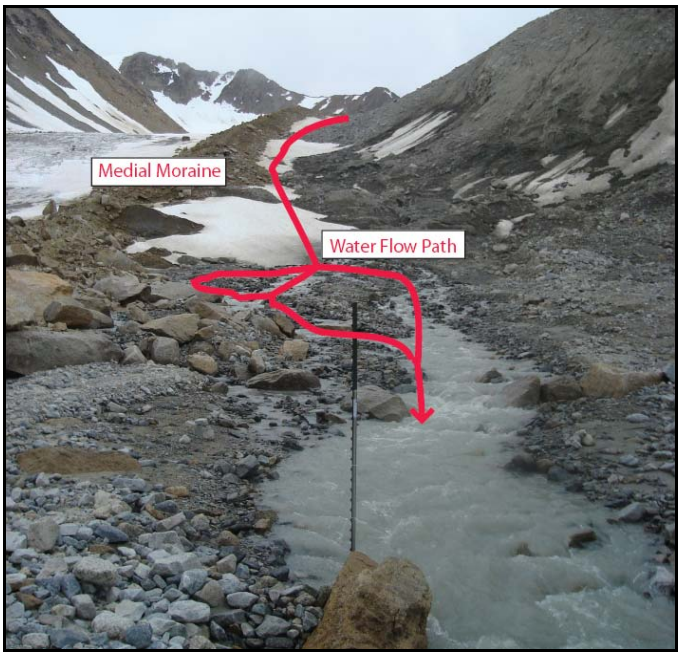


Figure 5.1: Surface flow path for UWLS water (red arrow) along the medial moraine, which provided a stable source for sediment acquisition for the UWLS water.

Meltwater Solute and Biogeochemical Weathering

The Wheaton Glacier catchment aqueous chemistry was dominated by Ca^{2+} and HCO_3^- (Table 4.3). C-ratios, defined as $[HCO_3^-/(HCO_3^- + SO_4^{2-})]$ (Brown, 2002), for the stream solute data indicated that protons were derived mainly from carbonation reactions (dissolution and dissociation of atmospheric CO_2; Equation 1) rather than the oxidation of pyrite (Table 5.1). A C-ratio of 1 represents weathering by carbonation reactions and a ratio of 0.5 represents coupled sulfate oxidation and carbonate dissolution reactions with protons derived from pyrite oxidation (Brown, 2002). Interestingly, peaks in sulfate on 1 and 10 August (Figure 4.13) corresponded with the lowest C-ratios for all streams, thus providing evidence for potential oxidation of pyrite from morainal and proglacial sediments via geochemical and/or microbial processes.

$$CO_{2(g)} + H_2O_{(l)} \leftrightarrow H_2CO_{3(aq)} \leftrightarrow H^+_{(aq)} + HCO_3^-{}_{(aq)} \quad (1)$$

Table 5.1: C-ratios for the ELS, UWLS, and LOS.

	ELS	UWLS	LOS
	C-ratio	C-ratio	C-ratio
2-Jul	0.86	1.00	0.90
5-Jul	0.88	0.89	0.89
8-Jul	0.89	0.87	0.89
11-Jul	0.90	0.81	0.88
14-Jul	0.89	0.83	0.89
17-Jul	0.90	0.88	0.90
20-Jul	0.89	0.87	0.90
23-Jul	0.89	0.95	0.89
26-Jul	0.89	0.93	0.91
29-Jul	0.89	0.93	0.89
1-Aug	0.89	0.75	0.93
4-Aug	0.88	0.86	0.88
7-Aug	0.85	0.87	0.86
10-Aug	0.87	0.65	0.87

White et al., 1999 demonstrated that the weathering of granitoid rocks leached Ca^{2+} and Na^{+} from plagioclase feldspar with a higher proportion of Ca^{2+} than Na^{+} from the plagioclase component in freshly ground rock. The study also showed that excess Ca^{2+} could be attributed to weathering of accessory calcite within fresh granitoids (White et al., 1999). Granitoids were evident within the catchment (Bond, J., personal comm.; Smith et al., 2004); thus, Ca^{2+} and HCO_3^- in the UWLS and LOS may reflect weathering of calcite (Equation 2) and the hydrolysis of silicate minerals (e.g. plagioclase feldspar) may have liberated Na^{+}, Ca^{2+}, and HCO_3^- (Equation 3, modified from a reaction provided by Malard, 2003, at a glacial flood plain). White et al. (2001) provided evidence for plagioclase weathering at circumneutral pH (4.5-7.5) in granitic saprolites and quartz diorites in both laboratory and natural (field) dissolution studies. These weathering reactions were supported by significant correlations between ion concentrations and bicarbonate (Table 4.4).

$$CaCO_{3(s)} + H_2O_{(l)} + CO_{2(aq)} \leftrightarrow Ca^{2+}{}_{(aq)} + 2\ HCO_3^-{}_{(aq)} \qquad (2)$$

Calcium carbonate

$$Na_{(1-x)}Ca_xAl_{(1+x)}Si_{(3-x)}O_{8(s)} + (1+x)\ CO_{2(aq)} + \tfrac{1}{2}\ (11-5x)\ H_2O_{(l)} \rightarrow \qquad (3)$$

Plagioclase (x= mole fraction anorthite)

$$(1-x)\ Na^{+}{}_{(aq)} + x\ Ca^{2+}{}_{(aq)} + (1+x)\ HCO_3^-{}_{(aq)} + 2\ (1-x)\ H_4SiO_{4(aq)} + (1+x)/2\ Al_2Si_2O_5(OH)_{4(s)}$$

Kaolinite

SO_4^{2-} may reflect microbial and geochemical weathering of pyrite (Equation 4) (Montross, 2007) associated with metavolcanics within the catchment (Smith et al., 2004).

$$2\ FeS_{2(s)} + 7\ O_{2(g)} + 2\ H_2O_{(l)} \rightarrow 2\ Fe^{2+}{}_{(aq)} + 4\ SO_4^{2-}{}_{(aq)} + 4\ H^{+}{}_{(aq)} \qquad (4)$$

K^+ and Mg^{2+} were likely products of biotite, muscovite, and chlorite mica weathering (e.g. Equation 5 for generalized biotite weathering from Malard, 2003). Laboratory experiments have demonstrated that biotite undergoes incongruent dissolution at pH ranges of 3-7, with faster rates occurring at lower pH (Acker and Bricker, 1992) and Anderson et al. (2000) demonstrated biotite weathering occurred in young proglacial sediments from an Alaskan glacier, thus biotite could have undergone slow incongruent dissolution in the circumneutral Wheaton Glacier meltwaters.

$$KMg_xFe_{(3-x)}AlSi_3O_{10}(OH)_{2(s)} + (1+2x)\ CO_{2(aq)} + 15/2\ H_2O_{(aq)} + O_{2(aq)} \rightarrow \quad (5)$$

Biotite (x= mole fraction of magnesium)

$$K^+_{(aq)} + x\ Mg^{2+}_{(aq)} + (1+2x)\ HCO_3^-{}_{(aq)} + (3-x)\ Fe(OH)_{2(aq)} + 2\ H_4SiO_{4(aq)} + \tfrac{1}{2}\ Al_2Si_2O_5(OH)_{4(s)}$$

Kaolinite

The Effect of Water Storage Time on Meltwater Biogeochemistry

Mineral weathering, and thus solute production, is controlled by the reactivity (solubility) of the mineral, the rock:water interaction time, and the rock:water ratio. Water storage time differs in the various components of the catchment hydrologic system, e.g. lake vs. streams, and is directly related to rock:water interaction time. Therefore, water storage time is important when considering differences in solute dynamics and mineral weathering in a catchment. Mean water residence time in the lake was at least 2 days based on rhodamine tracer data (Figure 4.9), which was longer than that of the proglacial streams where water flowed downstream without significant storage. The rhodamine tracer was likely a better tracer than the salt slug for assessing mean lake water residence time because it was released at the major inlet delta to the lake, where most meltwater contributions entered. In addition, the rhodamine was not

released at depth, so its slightly higher density than the lake water (1.008 g cm^{-3}) was likely less of a factor than the denser salt slug (1.25 g cm^{-3}) released at 1.5 m water depth in relatively stagnant waters close to the southern margin of the lake.

Stream water temperatures (Figure 4.4) reflect both water residence time and the substrate of the source region for an individual stream. The lake, as a source component for the LOS, resulted in longer water residence times relative to the ELS and UWLS which allowed for warming of the waters due to increased exposure to solar radiation and stream temperatures that were 1^{o} C warmer than the ELS and UWLS. However, the LOS and UWLS showed greater variability in stream water temperature than the ELS (Figure 4.4B). This was likely related to the fact that the ELS stream waters were sourced from snow and ice melt and had a short travel time over proglacial substrate that was not 0^{o} C.

Air temperature and discharge were strongly correlated (Devore and Peck, 2007) in the ELS, LOS, and UWLS. The air temperature and ELS and LOS discharge showed a stronger correlation with a shorter lag time during and after the rapid snowline retreat (23 July-16 August) than before it (4 July- 22 July), which suggests the importance of albedo on melt rate. Correlation coefficient strengths of lag time between air temperature and discharge diminished more quickly after the snow to ice transition than they did before it (Table 4.2). The stronger correlation during and after the rapid snowline retreat was likely due to the effect of albedo on melt rate, where the darker ice melted more quickly than the bright white snow due to lower reflection of solar energy.

The greatest variability in diurnal discharge was observed in the UWLS, followed by the LOS and then the ELS. This suggests that for the west lobe, the presence and

water storage capacity of the proglacial lake reduced diurnal variability in stream discharge. The ELS and LOS discharge records shared a common feature in that the diurnal discharge amplitude was lower in the period 3-23 July relative to that after 23 July. The change in discharge amplitude correlates with the rapid snowline retreat phase (Figure 4.3) and therefore the reduced impact of snowpack water storage as a hydrological buffer in these catchments. The relatively low amplitude in diurnal discharge for the ELS throughout the season potentially reflected the importance of snowcover in its catchment and its water storage properties. The high diurnal variability in the UWLS was somewhat counterintuitive if the stream is fed largely by snowmelt throughout the majority of the season. However, it may be that a good proportion of the source area for the UWLS was in fact icemelt occurring in close proximity to the channel, and that snowmelt from the upper reaches of the UWLS catchment was not a significant proportion of the overall discharge.

It was assumed that the ionic composition of the original meltwater (i.e. snowmelt and icemelt) was the same for each stream since a) the catchment was relatively small and thus each lobe received approximately the same amount and composition of precipitation, and b) there was likely little heterogeneity in catchment lithology for each lobe (with the exception of fluoride). Solute concentrations in the ELS, LOS, and UWLS were of a similar magnitude (Figure 4.11), however, solute concentrations varied to a lesser degree in the LOS than they did in the ELS and UWLS (Table 4.5), which was likely due to the effect of the lake in allowing greater mixing and homogenization of varied source waters due to the increased water storage time. There was a marked

increase in solute concentration in the UWLS after 28 July that did not appear to be directly correlated to discharge (Figure 4.11) or SSC (Figure 4.6). Concentrations of Ca^{2+}, HCO_3^-, SO_4^{2-}, and to a lesser extent Na^+ were the specific ions showing the greatest increase. The increases in sulfate and sodium likely reflected weathering processes (Equations 3 & 4 above) that required longer reaction times than simple carbonate dissolution (Equation 2). This suggests that there was a component of the meltwater with a high solute content in addition to the (relatively) more dilute ice and snowmelt. The high solute content waters were likely generated where the rock:water ratio and/or rock:water contact times were elevated. The timing of the increase in solute concentrations may have been related to a reduction in snow cover and increased access to sediments, but there is not sufficient data on this for the UWLS catchment to analyze this potential linkage.

Meltwater residence times in the lake as well as within the snowpack influenced nutrient concentrations (i.e. nitrate) measured in the meltwater. NO_3^- concentrations in the LOS were consistently lower than in the ELS (Figure 4.13) and were near detection limits in the UWLS for the majority of the field season (Figure 4.13). The lake, LOS and ELS were fed primarily by ice and snowmelt, whereas the UWLS streams waters also had significant interaction with and mobilization of sediments. Therefore it seems reasonable to infer that the water:rock interaction processes were the source of the nitrate depletion, and that microbial activity was the most plausible process. However, no data is available on the microbial biomass as determined by cell concentrations for the UWLS to support this inference. The lower concentration of NO_3^- in the lake and LOS relative

to the ELS may reflect greater microbial uptake in the lake since cell concentrations are up to an order of magnitude higher in the lake and LOS than the ELS (Figure 4.18).

A major determining factor for SSC in each stream was sediment availability, as noted above. SSC was the highest in the UWLS where there was the greatest sediment availability from morainal and proglacial sources. The presence of a proglacial lake also had an effect on SSC. SSC in the ELS and UWLS was positively correlated with discharge, whereas it was negatively correlated with discharge in the LOS (Figure 4.7), likely a result of the settling of suspended sediment in the lake.

The Effect of Water Storage on Organic Carbon and Biota

Dissolved organic carbon (DOC) in the streams appeared to have been influenced by the presence of a proglacial lake, since water storage in the lake facilitated the growth of a larger microbial population in the lake relative to the ELS (Figure 5.2). Based on lake water residence time, the lake also temporarily stored organic carbon produced as biomass by microorganisms and from cell decomposition within the lake. There were three distinct periods in the DOC record, as indicated by Roman numerals in Figure 5.2: period I had measurable amounts of DOC, period II showed a depletion of DOC to detection limits, and period III showed a return to measurable DOC concentrations in the lake, LOS, and UWLS. The decline in DOC during period II indicated that the Wheaton Glacier catchment was likely a DOC-limited system during this period, which is characteristic of high alpine sites with little allochthonous input of carbon due to lack of vegetation in the catchment (Karlsson et al., 2001).

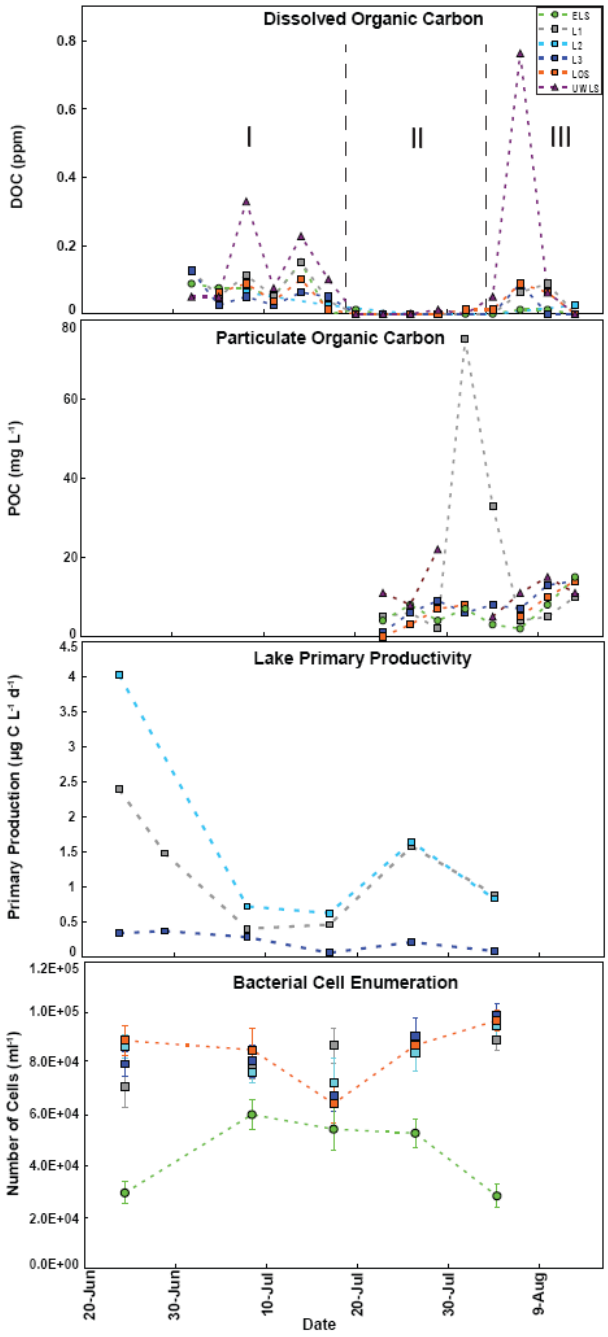


Figure 5.2: Synthesis of organic carbon and biological time series data for the ELS, UWLS, and LOS and within the lake: 0.5 m lake depth (L1), 1.5 m lake (L2), and 5 m lake depth (L3) from 25 June-13 August, 2006.

Decreasing bacterial biomass in the ELS (Figure 5.2) during period III may have resulted in limited regeneration of DOC in the ELS, but this limited regeneration was not significant enough to raise DOC concentrations much above depletion. In contrast, the lake, LOS, and UWLS may have reached carrying capacity, the point at which resource limitation begins to limit population growth (Wetzel, 2001), since they were DOC-limited in period II, until primary productivity and autotrophy could regenerate enough DOC (period III) to support more biota. DOC concentrations were highest and most variable in the UWLS which may reflect the flushing of microbially-derived DOC from the proglacial and medial morainal sediments.

POC concentrations measured from 22 July onwards were relatively consistent and comparable in the ELS and LOS, with a slight increase near the end of the season (Figure 5.2). Thus, the proglacial lake and processes occurring within it did not appear to have a significant effect in modifying the out-flowing POC concentrations relative to the ELS. POC in the UWLS and lake surface waters peaked on 28 July and 1 August, respectively, which may have been caused by POC being transported by increased flow over proglacial sediments (Figure 4.2A) and from the lake inlet delta, and suggests that access to unconsolidated proglacial material was important as a source for POC in the UWLS and the lake.

Water storage in the lake appears to have facilitated the presence of a larger bacterial population in the lake (Figure 5.2). This was in contrast to the ELS, where bacterial abundance declined through the field season after 26 July (Figure 5.2). Bacterial abundance and primary productivity occurring within the lake appears to have

had an impact on nutrient concentrations (e.g. nitrate, Figure 4.13) and dissolved organic carbon (DOC) (Figure 4.17). The data suggest that nitrate was utilized in the lake prior to its export via the LOS and that DOC was replenished to a greater extent in the lake and LOS than in the ELS in August. The increase in DOC in the lake was attributed to primary productivity occurring in the lake (Figure 5.2) and to the greater storage time of this DOC-containing water (Figure 4.9) within the lake relative to the ELS.

Bacterial abundance was low (10^4-10^5 cells ml^{-1}) in the aquatic environments studied at the Wheaton Glacier, but was within the range of values reported for Midre Lovénbreen, Svalbard proglacial lakes and streams, which had ~ 10^4-10^5 cells ml^{-1} (Mindl et al., 2007). Relatively limited bacterial growth in the Wheaton glacier proglacial lake was likely due its low water temperature (1^o C) (Mindl et al., 2007) and limited nutrient (unbound phosphorous was below detection limits of the ion chromatograph and bound phosphorous was not measured) and energy (DOC) sources (Nakano and Ban, 2003; Straškrábová et al, 2006; Amato et al., 2007; Mindl et al, 2007).

Low bacterial abundance also may have been related to the lack of subglacial drainage at the Wheaton Glacier site, as microbial populations have been found to reside within subglacial sediments and meltwater where there is a supply of nutrients from subglacial water and sediment (e.g. Skidmore et al., 2005; Montross, 2007). In contrast, meltwater input was predominantly from snow and icemelt which have low bacterial abundance (Amato et al., 2007) and limited contact with sediments at the Wheaton Glacier, so the influx of microbiota and nutrients to the streams from meltwater was likely small compared with some temperate glaciers with a subglacial input.

Primary Productivity at the
Wheaton Glacier Proglacial Lake

Rates of primary productivity in the Wheaton Glacier proglacial lake were similar to rates observed at several other remote glaciated alpine catchments (Table 5.4; Karlsson et al., 2001). Primary productivity was consistently higher at 1.5 m lake depth than at the surface and 5 m lake depths (Figure 5.2). The 5 m depth likely had the lowest rate of primary productivity because at least 85% of light was absorbed (Wetzel, 2001) by 1.5 meters as evidenced by Secchi disk measurements (Figure 3.4B). Productivity rates and cell concentrations were similar between the lake surface and 1.5 m lake depth (Figure 5.2). The slightly higher rate of productivity at 1.5 m depth may be attributed to photoinhibition of photosynthetic organisms at the lake surface, which was documented in similar alpine lake environments in Banff National Park, Alberta, Canada, by Vinebrooke and Leavitt (1996). In addition, low rates of primary productivity from 8 July-17 July in lake surface waters and at 1.5 m depth may have been due to photoinhibition from high solar irradiance (Vinebrooke and Leavitt, 1996).

Bacterial abundance in Wheaton Glacier aquatic environments was low, though similar numbers (10^4 -10^5 cells ml^{-1}) have been documented at high mountain lakes in Retezat National Park, Romania (Straškrábová et al., 2006) and Lake Toya, Japan (Nakano and Ban, 2003) and from proglacial streams and lakes at the polythermal Midre Lovénbreen glacier, Svalbard (Mindl et al., 2007), however comparable primary productivity values are not available. Nonetheless, it is interesting to note that the number of bacterial cells is approximately an order of magnitude less than those at the

comparative sites in Table 5.2, yet the rate of primary productivity is comparative with these sites (Table 5.2).

The lower concentration of bacterial cells in the Wheaton Glacier proglacial lake may be the result of a variety of possible processes as a single causative factor or in combination: a) the smaller lake area relative to all sites listed in Table 5.2, would affect the extent of the photic zone and/or availability of space to the photosynthetic vs. non-photosynthetic organisms (rates of primary productivity are not area normalized to water volume), b) colder water temperatures relative to the Swiss lakes (Hinder et al., 1999; Karlsson et al., 2001) in Table 5.2, which could limit bacterial growth (Panzenböck et al., 2000), c) grazing on bacteria by larger lacustrine organisms such as flagellates and ciliates (Roberts and Laybourn-Parry, 1999), or d) infection by viruses (Takacs and Priscu, 1998), both of which have been suggested to occur in the McMurdo Dry Valley lakes of Antarctica. Low [DOC] also may have limited bacterial growth in the Wheaton Glacier proglacial lake (Figure 5.2). The Wheaton Glacier proglacial lake was also only ~10 years old at the time of this study so the bacterial population still may have been establishing itself whereas the other lakes are older and have more established bacterial communities. Rates of primary productivity may be similar among the sites since the Wheaton Glacier proglacial lake is relatively shallow and thus the photic zone is deeper in this lake as compared with the others.

Microbial biomass was higher in the lake and LOS relative to the ELS, whereas DOC was comparable in the LOS and ELS prior to 1 August but lower in the ELS thereafter. This data supports hypothesis three (H3) when comparing the LOS and ELS.

However, for the more limited data set that is comparable among the three streams, i.e. only POC and DOC concentrations, there is not such a clear distinction in the influence of the lake. The seasonal pattern of DOC change in the UWLS was similar to that in the ELS and LOS but showed higher concentrations. POC concentrations were relatively similar between the LOS, ELS, and UWLS despite high values recorded within the lake itself. These observations indicate that microbial processes in the lake potentially had an impact on DOC concentrations and thus DOC export from the catchment later in the melt season via the LOS relative to the ELS.

Table 5.2: Rates of primary productivity (PP) for lakes located in mid- and high-alpine sites north of Sweden, Swiss Alps, the high Arctic, the Antarctic peninsula, and this study. Z_m represents maximum lake depth, Z represents mean lake depth, and PP represents rates of primary productivity.

Location	Elevation (m asl)	Area (ha)	Z_m (m)	Z (m)	T (°C)	Bacterial Cells x10^4 mL^{-1}	PP (µgC L^{-1} d^{-1})	Source
Mid-alpine lake N. of Sweden 1	850	1.9	8.2	2.2	7.9 ± 2.0	120 ± 10	1.3 ± 0.4	Karlsson et al., 2001
Mid-alpine lake N. of Sweden 2	865	10.9	10.7	4.5	8.0 ± 1.5	130 ± 10	1.2 ± 0.4	
Mid-alpine lake N. of Sweden 3	993	17.4	15.8	4.7	8.0 ± 1.1	170 ± 20	0.7 ± 0.3	
High-alpine lake N. of Sweden 1	1045	17.4	12	5.3	7.2 ± 1.0	40 ± 0	0.2 ± 0.1	
High-alpine lake N. of Sweden 2	1115	3.8	6.8	1.9	4.9 ± 1.2	60 ± 10	1.3 ± 0.6	
High-alpine lake N. of Sweden 3	1140	26.6	24	8.6	6.4 ± 0.5	50 ± 10	0.3 ± 0.1	
Zeigler Island Franz Joseph Land	-	8.2	-	9	1.1 - 2	73 - 193	7.8 - 41.5	Panzenböck et al., 2000
Jori Lake Eastern Swiss Alps	2512	5.8	22	-	4 - 8	70 - 170	0.3 ± 0.1	Hinder et al., 1999
Antarctic Peninsula 62°57'10"S 60°37'53"W	0	-	1-15 20-60	-	1.25 - 2 0.25 - 1.25	16.5 - 22.5 21.0 - 22.0	10.3-15.9 0.3-5.4	Aristegui et al., 1996
Antarctic Peninsula 64°13'10"S 61°19'18"W	0	-	1-15 20-60	-	1.5 - 1.8 1.0 - 1.5	37.0 - 53.0 30.0 - 65.0	1.2 - 203.0 0.3 - 0.5	
Wheaton Glacier Lake Yukon, Canada	1705	0.9	6.7	2.5	1.4 ± 0.6	6.7 - 9.9 ± 0.9	0.8 ± 0.2	This study

References Cited

Acker, J.G. and Bricker, O.P., 1992. The influence of pH on biotite dissolution and alteration kinetics at low temperature. *Geochimica et Cosmochimica*, v. 56, pp. 3073-3092.

Amato, P., Hennebelle, R., Magand, O., Sancelme, M., Delort, A., Barbante, C., Bourtron, C., and Ferrari, C., 2007. Bacterial characterization of the snow cover at Sptizberg, Svalbard. *FEMS Microbiology and Ecology*, v. 59, pp. 255-264.

Anderson, S.P. 2005. Glaciers show direct linkage between erosion rate and chemical weathering fluxes. *Geomorphology*, v. 67, pp. 147-157.

Arísegui, J., Montero, M.F., Baallesteros, S. Basterretxea, G., and van Lenning, K., 1996. Planktonic primary production and microbial respiration measured by ^{14}C assimilation and dissolved oxygen changes in coastal waters of the Antarctic Peninsula during austral summer: implications for carbon flux studies. *Marine Ecology Progress Series*, v. 132, pp. 191-201.

Barker, J.D. Sharp, M.J., Fitzsimons, S.J., and Turner, R.J., 2006. Abundance and Dynamics of Dissolved Organic Carbon in Glacier Systems. *Arctic, Antarctic, and Alpine Research*, v. 38, pp. 163-172.

Brown, G.H., 2002. Glacier Meltwater Hydrochemistry. *Applied Geochemistry*, v. 17, pp. 855-883.

Brown, L.E., Hannah, D.M., and Milner, A.M., 2003. Alpine Stream Habitat Classification: An Alternative Approach to Incorporating the Role of Dynamic Water Source Contributions. *Arctic, Antarctic, and Alpine Research*, v. 35, pp. 313-322.

Devore J. and Peck, R., 2007. Statistics, 5th ed. Belmont: Brooks/Cole—Thompson Learning Inc. 763 p.

Gurnell, A.M., Hannah, D., and Lawler, D. 1996. Suspended sediment yield from glacier basins. *IAHS Publications*, v. 236, pp. 97-104.

Hinder, B., Baur, I., and Hanselmann, K., 1999. Microbial food web in an oligotrophic high mountain lake (Jöri Lake III, Swizerland). *Journal of Limnology*, v. 58, pp. 162-168.

Hodgkins, R., 1997. Glacier hydrology in Svalbard, Norwegian High Arctic. *Quaternary Science Reviews*, v. 16, pp. 957-973.

Hodgkins, R., Tranter, M., and Dowdeswell, J.A., 1998. The hydrochemistry of runoff from a 'cold-based' glacier in the High Arctic (Scott Turnerbreen, Svalbard). *Hydrological Processes*, v. 12, pp. 87-103.

Hodson, A., Gurnell, A., Tranter, M., and Bogen, J. 1998. Suspended sediment yield and transfer processes in a small High-Arctic glacier basin, Svalbard. *Hydrological Processes*, v. 12, pp. 73-86.

Hodson, A.J. and Ferguson, R.I. 1999. Fluvial suspended sediment transport from cold and warm-based glaciers in Svalbard. *Earth Surface Processes and Landforms*, v. 24, pp. 957-974.

Jones, H.G., 1999. The ecology of snow-covered systems: a brief overview of nutrient cycling and life in the cold. *Hydrological Processes*, v. 13, pp. 2135-2147.

Karlsson, J. Jonsson, A., and Jansson, M., 2001. Bacterioplankton production in lakes along an altitude gradient in the Subarctic North of Sweden. *Microbial Ecology*, v. 42, n. 3, pp. 372-382.

Malard, F., 2003. Groundwater-Surface Water Interactions, Chapter 3 in Ecology of a Glacial Flood Plain: Dordrecht: Kluwer Academic. Ward, J.V. and Uehlinger U. (eds.) p. 37-56.

Mindl, B., Anesio, A.M., Meirer, K., Hodson, A.J., Laybourn-Parry, J., Sommaruga, R., and Sattler, B., 2007. Factors influencing bacterial dynamics along a transect from supraglacial runoff to proglacial lakes of a high Arctic glacier. *FEMS Microbiology and Ecology*, v. 59, pp. 307-317.

Montross, S., 2007. Geochemical evidence for microbially mediated subglacial mineral weathering. Master's Thesis, Montana State University Department of Earth Sciences.

Nakano, A. and Ban, S. 2003. Microbial communities in oligotrophic Lake Toya, Japan. *Limnology*, v. 4, pp.19-24.

Panzenböck, M., Möbes-Hansen, B., Albert, R., and Herndl, G.J., 2000. Dynamics of phyto- and bacterioplankton in a high Arctic lake on Franz Joseph Land archipelago. *Aquatic Microbial Ecology*, v. 21, pp. 265-273.

Ralph, J. and Ralph, I., 2008. Cryolite. Accessed at: http://www.mindat.org/min-1161.html [13 January 2008].

Roberts, E.C. and Laybourn-Parry, J., 1999. Mixotrophic cryptophytes and their predators in the Dry Valley lakes of Antarctica. *Freshwater Biology*, v. 41, pp. 737-746.

Schumann, W., 1985. Handbook of Rocks, Minerals, and Gemstones. New York: HarperCollins Publishers and Houghton Mifflin Co. 380 p.

Skidmore, M., Anderson, S.P., Sharp, M., Foght, J., and Lanoil, B.D., 2005. Comparison of microbial community compositions of two subglacial environments reveals a possible role for microbes in chemical weathering processes. *Applied and Environmental Microbiology*, v. 71, n. 11, pp. 6986-6997.

Smith, C.A.S., Meikle, J.C., and Roots, C.F. (eds), 2004. Ecoregions of the Yukon Territory: Biophysical properties of Yukon landscapes. Agriculture and Agri-Food Canada, PARC Technical Bulletin No. 04-01, Summerland, British Columbia, 313 p.

Straskraboca, V., Cogalniceanu, D., Nedoma, J., Parpala, L., Postolache, C., Tudorancea, C., Vadineanu, A., Valcu, C.M., and Zinevici, V. 2006. Bacteria and pelagic food webs in pristine alpine lakes (Retezat Mountains, Romania). In Banaduc, D., Sirbu, I., Curtean-Banaduc, A. (eds.), *Transylvanian Review of Systematical and Ecological Research*, v. 3, "The Retezat National Park": pp. 1-10.

Takacs, C.D. and Priscu, J.C., 1998. Bacterioplankton dynamics in the McMurdo Dry Valley Lakes, Antarctica: Production and biomass loss over four seasons. *Microbial Ecology*, v. 36, pp. 239-250.

Vinebrooke, R. D. and Leavitt, P.R., 1996. Effects of ultraviolet radiation on periphyton in an alpine lake. *Limnology and Oceanography*, v. 41, pp. 1035-1040.

Wadham, J.L., Hodson, A.J., Tranter, M., and Dowdeswell, J.A., 1998. The hydrochemistry of meltwaters draining a polythermal-based, high Arctic glacier, south Svalbard: I. the ablation season. *Hydrological Processes*, v. 12, pp. 1825-1849.

Wetzel, R.G., 2001. Limnology: Lake and River Ecosystems. 3rd ed. Boston: Academic Press, 1006 pp.

White, A.F., Bullen, T.D., Vivit, D.V., Schulz, M.S., and Clow, D.W., 1999. The role of disseminated calcite in the chemical weathering of granitoid rocks. *Geochimica et Cosmochimica Acta*, v. 63, pp. 1939-1953.

White, A.F., Bullen, T.F., Schulz, M.S., Blum, A.E., Huntington, T.G., and Peters, N.E., 2001. Differential rates of feldspar weathering in granitic regoliths. *Geochimica et Cosmochimica Acta*, v. 65, n. 6, pp. 847-869.

White, G.V., 2002. Industrial Minerals, Gems, and Minor Metals in the Yukon. Whitehorse: GV White Resources Limited. 244 p.

CHAPTER 6

SUMMARY AND CONCLUSIONS

Headwater environments are crucial to a holistic understanding of climate change on glaciated catchments since they are the first in a chain of variables that affect downstream hydrology and biogeochemistry. This study explored the effects of three different proglacial environments including the presence/absence of a proglacial lake on hydrological, geochemical, and biological characteristics at a small, 4 km^2 glacier in the Coast Mountains, Yukon, Canada by testing three hypotheses.

(H1) The Wheaton Glacier is non-temperate.

Observation of aerial photographs suggested that the Wheaton Glacier is a non-temperate glacier due the lack of significant crevassing, evidence of moulins, and subglacial drainge outlets. The glacier appeared to be drained by proglacial streams that were predominantly fed via snow and ice melt. This melt flowed supraglacially and ice marginally before reaching the main proglacial stream channel for the ELS and UWLS as well as the proglacial lake, drained at its outlet by the LOS. Field measurements in June-August 2006 demonstrated consistent and/or increasing solute concentrations in all three streams (LOS, ELS, and UWLS) and consistent SSC in the ELS and rising SSC in the lake and LOS in response to rapid snowline and sediment exposure. These observations support the hypothesis that the Wheaton glacier is non-temperate and does not have a well developed subglacial drainage system.

(H2) Water storage time differences between the proglacial streams vs. lake will produce more consistent discharge and dissolved ion concentrations in the LOS, and lower SSC in the LOS relative to the ELS and UWLS.

The presence of a proglacial lake increased water storage time, based on rhodamine tracer data. Discharge did not appear to be more consistent from the LOS as compared with the ELS despite the presence of the lake as a water storage component in the hydrologic system. Both streams did however show lower amplitude diurnal variability in discharge relative to the UWLS. Solute concentrations in the ELS, LOS, and UWLS were of a similar magnitude, however, solute concentrations varied to a lesser degree in the LOS than they did in the ELS and UWLS. The decreased fluctuation was likely due to the effect of the lake in allowing greater mixing and homogenization of varied source waters due to the increased water storage time.

There was a marked increase in solute concentration in the UWLS after 28 July that did not appear to be directly correlated to discharge or SSC. Concentrations of Ca^{2+}, HCO_3^-, SO_4^{2-}, and to a lesser extent Na^+ were the specific ions showing the greatest increase. The increases in sulfate and sodium likely reflect weathering processes such as pyrite oxidation and silicate dissolution that require longer reaction times than simple carbonate dissolution. This suggests that there is a component of the meltwater with a high solute content in addition to the (relatively) more dilute ice and snowmelt. The high solute content waters are likely generated where the rock:water ratio and/or rock:water contact times are elevated.

Concentrations of the nutrient nitrate were lower on average in the LOS suggesting that the larger bacterial population in the lake relative to the ELS (see H3 below) may utilize more nitrate. The low-energy nature of the lake resulted in the deposition of suspended sediment before its export via the LOS. However, it appeared that the availability of sediment from morainal and proglacial sources was the main determinant for SSC in the UWLS relative to the ELS.

The data largely does not support the hypothesis when comparing discharge, dissolved ion concentrations, and SSC in the ELS and LOS. However, notable differences were observed between the ELS (and LOS) and UWLS in discharge variability, dissolved ion concentrations and SSC, highlighting the importance of flowpath routing, access to morainal sediments and water:rock interactions both in terms of concentration and contact time.

(H3) Primary productivity, microbial biomass and thus organic carbon will be higher in the lake and LOS relative to the ELS and UWLS.

The lake had a larger bacterial biomass than the ELS throughout the season, and its biomass increased slightly as the melt season progressed whereas the ELS bacterial biomass declined. The increasing bacterial biomass in the lake may have affected DOC regeneration in the lake and LOS, especially later in the ablation season which was likely due to productivity (primary productivity and heterotrophy) by biotic communities within the lake. There were no significant differences in POC concentrations among the ELS, UWLS, and LOS, thus the lake and processes therein did not appear to influence POC concentrations relative to streams that simply transitioned from flowing supraglacially to

proglacially. Thus, certain parameters, notably bacterial biomass and DOC, were higher in the lake and LOS relative to the ELS, supporting in part hypothesis three.

This study provided a small-scale example for how differences in proglacial environments and water flow paths can affect headwater hydrology and biogeochemistry and, to the author's knowledge, is the first of its kind to compare the biogeochemistry and carbon dynamics of glacial subcatchments in Coast Mountains, Yukon, Canada. While it is important to note that catchments are unique on the local and regional scale (e.g. bedrock composition, precipitation chemistry), results from this study may be beneficial in assessing the effect of a proglacial lake and water flow paths on hydrology and dissolved ion and carbon dynamics in other alpine catchments undergoing glacial retreat.

APPENDIX A

SUPPLEMENTARY MATERIALS

Tables and Graphs

Table A1: Ion concentrations (blank subtracted) and charge balance errors (CBE) for all samples.

L1	F ueq L-1	Cl ueq L-1	NO3 ueq L-1	PO4 ueq L-1	SO4 ueq L-1	HCO3 ueq L-1	Na ueq L-1	NH4 ueq L-1	K ueq L-1	Ca ueq L-1	Mg ueq L-1	(Cat-An)-Alk	Cat+An	CBE (%)
2-Jul	1.65	1.98	2.90	0.00	14.62	106.52	14.50	0.00	3.60	155.51	4.22	50.15	305.49	16.42
5-Jul	1.57	1.67	2.34	0.00	12.49	113.08	13.39	0.00	3.14	148.60	4.69	38.67	300.96	12.85
8-Jul	1.60	1.38	1.52	0.00	13.40	81.94	13.27	0.00	2.84	142.14	3.99	62.39	262.08	23.81
11-Jul	1.75	1.55	1.11	0.00	15.08	106.52	13.36	0.00	2.82	142.79	3.63	36.59	288.63	12.68
14-Jul	1.52	1.34	0.77	0.00	11.39	75.39	12.10	0.00	8.13	110.40	2.97	43.20	224.00	19.28
17-Jul	1.74	1.46	0.99	0.00	13.10	99.97	15.64	0.00	3.70	147.19	4.31	53.59	288.11	18.60
20-Jul	1.70	1.90	1.77	0.00	11.96	nd	14.44	0.00	3.76	143.34	3.39			
23-Jul	1.59	1.52	1.03	0.00	12.03	98.33	12.73	0.00	3.35	124.87	3.24	29.69	258.69	11.48
26-Jul	1.58	1.24	0.75	0.00	9.19	81.94	11.73	0.00	3.63	106.66	2.61	29.92	219.32	13.64
29-Jul	1.63	1.13	0.94	0.00	9.29	86.86	11.80	0.00	4.53	106.65	3.04	26.16	225.87	11.58
1-Aug	1.72	1.83	1.69	0.00	9.11	60.64	12.56	0.00	5.16	111.26	2.99	56.98	206.95	27.53
4-Aug	1.50	1.23	1.05	0.00	8.29	73.75	10.88	0.00	4.61	99.95	3.38	33.01	204.64	16.13
6-Aug	1.55	2.43	0.61	0.00	10.95	nd	13.79	0.00	5.47	121.57	3.03			
7-Aug	1.49	6.07	1.07	0.00	10.59	90.13	20.52	0.00	5.30	117.07	4.08	37.62	256.33	14.68
10-Aug	1.66	2.35	0.94	0.00	14.71	95.05	16.94	0.00	6.21	138.77	3.79	51.01	280.41	18.19
13-Aug	1.64	1.38	1.32	0.00	10.92	nd	13.25	0.00	5.14	117.12	3.73		154.50	0.00
L2	F ueq L-1	Cl ueq L-1	NO3 ueq L-1	PO4 ueq L-1	SO4 ueq L-1	HCO3 ueq L-1	Na ueq L-1	NH4 ueq L-1	K ueq L-1	Ca ueq L-1	Mg ueq L-1	(Cat-An)-Alk	Cat+An	CBE (%)
8-Jul	1.68	1.66	2.54	0.00	13.83	106.52	15.24	0.00	3.61	155.57	4.38	52.58	305.03	17.24
17-Jul	1.73	1.41	1.83	0.00	13.47	101.61	15.66	0.00	3.84	145.36	3.44	48.25	288.36	16.73
26-Jul	1.62	1.28	0.78	0.00	9.87	91.77	12.38	0.00	4.67	123.38	3.61	38.73	249.37	15.53
4-Aug	1.68	1.62	1.28	0.00	13.46	81.94	11.77	0.00	5.33	105.45	2.42	25.00	224.95	11.11
6-Aug	1.56	2.46	0.47	0.00	25.21	nd	11.77	0.00	5.33	105.45	2.42			
13-Aug	1.72	1.57	1.38	0.00	14.89	nd	14.08	0.00	4.51	118.87	3.54			
L3	F ueq L-1	Cl ueq L-1	NO3 ueq L-1	PO4 ueq L-1	SO4 ueq L-1	HCO3 ueq L-1	Na ueq L-1	NH4 ueq L-1	K ueq L-1	Ca ueq L-1	Mg ueq L-1	(Cat-An)-Alk	Cat+An	CBE (%)
2-Jul	1.66	1.85	2.39	0.00	14.18	117.99	14.22	0.00	3.33	154.12	4.18	37.77	313.94	12.03
5-Jul	1.64	1.74	3.01	0.00	14.49	116.36	14.71	0.00	4.12	155.59	4.21	41.39	315.86	13.10
8-Jul	1.73	1.55	2.58	0.00	14.64	103.24	15.77	0.00	3.74	155.89	4.24	55.89	303.40	18.42
11-Jul	1.80	1.48	2.19	0.00	16.86	101.61	17.09	0.00	4.05	157.63	4.76	59.60	307.48	19.38
14-Jul	1.66	1.29	1.13	0.00	12.84	96.69	14.60	0.00	4.09	137.25	3.49	45.82	273.05	16.78
17-Jul	1.73	1.37	2.23	0.00	13.58	108.16	15.51	0.00	4.05	142.34	4.12	38.94	293.09	13.29
20-Jul	1.73	1.34	1.90	0.00	12.41	103.24	14.26	0.00	3.82	135.94	4.09	37.48	278.74	13.45
23-Jul	1.65	1.38	1.29	0.00	10.97	103.24	12.75	0.00	3.72	124.79	3.59	26.32	263.39	9.99
26-Jul	1.64	1.62	0.99	0.00	9.95	95.05	12.17	0.00	4.02	117.12	4.31	28.36	246.87	11.49
29-Jul	1.66	1.24	0.57	0.00	9.36	85.22	10.95	0.00	3.21	104.71	2.83	23.64	219.76	10.76
1-Aug	1.65	0.98	1.21	0.00	5.58	77.02	10.74	0.00	4.11	101.56	3.14	33.11	206.00	16.07
4-Aug	1.56	1.00	0.13	0.00	8.49	81.94	11.31	0.00	4.63	104.38	2.16	29.36	215.60	13.62
6-Aug	1.63	1.06	1.86	0.00	10.23	nd	12.65	0.00	5.53	115.91	3.47			
7-Aug	1.59	4.97	0.59	0.00	10.13	88.50	18.52	0.00	5.37	116.98	3.42	38.50	250.08	15.40
10-Aug	1.62	2.40	0.41	0.00	14.02	103.24	16.49	0.00	6.87	126.21	4.62	32.49	275.89	11.78
13-Aug	1.77	1.31	0.96	0.00	15.96	nd	12.90	0.00	5.15	117.30	3.63			

Table A.1 (continued)

LOS	F ueq L-1	Cl ueq L-1	NO3 ueq L-1	PO4 ueq L-1	SO4 ueq L-1	HCO3 ueq L-1	Na ueq L-1	NH4 ueq L-1	K ueq L-1	Ca ueq L-1	Mg ueq L-1	(Cat-An)-Alk	Cat+An	CBE (%)
2-Jul	2.2	1.9	2.4	0.0	12.4	108.2	10.6	0.0	2.6	144.4	3.3	33.7	288.1	11.7
5-Jul	2.2	1.6	2.0	0.0	12.3	98.3	12.0	0.0	2.7	138.4	2.7	39.3	272.2	14.4
8-Jul	2.0	1.6	2.5	0.0	14.1	111.4	16.5	0.0	3.2	172.2	3.8	64.2	327.3	19.6
11-Jul	1.9	1.4	1.8	0.0	15.3	109.8	16.1	0.0	3.7	168.7	4.9	63.0	323.6	19.5
14-Jul	1.9	1.4	1.6	0.0	13.7	114.7	14.2	0.0	2.7	151.7	3.2	38.6	305.1	12.7
17-Jul	2.3	1.4	1.7	0.0	13.1	114.7	15.2	0.0	3.6	162.5	4.1	52.2	318.6	16.4
20-Jul	2.3	1.5	1.8	0.0	12.9	111.4	16.8	0.0	3.9	162.0	3.7	56.5	316.3	17.9
23-Jul	1.9	1.6	1.6	0.0	11.4	93.4	12.4	0.0	3.5	130.0	2.7	38.6	258.5	14.9
26-Jul	1.8	1.3	1.0	0.0	10.6	101.6	13.8	0.0	3.2	137.9	3.8	42.4	274.9	15.4
29-Jul	2.1	1.3	1.4	0.0	10.7	90.1	13.9	0.0	4.6	135.4	3.1	51.3	262.7	19.5
1-Aug	1.6	1.1	1.4	0.0	7.1	91.8	13.0	0.0	5.2	126.6	3.3	45.1	251.0	18.0
4-Aug	2.3	1.3	0.8	0.0	11.2	85.2	12.6	0.0	3.8	115.8	2.8	34.2	235.8	14.5
6-Aug	2.9	2.5	1.0	0.0	10.7	nd	13.7	0.0	5.3	122.5	3.3			
7-Aug	3.5	4.3	0.7	0.0	13.2	83.6	17.7	0.0	5.3	120.9	2.8	41.5	252.0	16.5
10-Aug	2.3	2.4	1.2	0.0	15.5	104.9	19.0	0.0	5.7	145.0	5.1	48.6	301.0	16.1
13-Aug	1.4	1.8	1.9	0.0	19.8	nd	15.9	0.0	5.0	137.2	3.0			
ELS	F ueq L-1	Cl ueq L-1	NO3 ueq L-1	PO4 ueq L-1	SO4 ueq L-1	HCO3 ueq L-1	Na ueq L-1	NH4 ueq L-1	K ueq L-1	Ca ueq L-1	Mg ueq L-1	(Cat-An)-Alk	Cat+An	CBE (%)
2-Jul	24.1	1.8	6.5	0.0	18.9	118.0	23.8	0.0	5.2	155.5	4.0	19.1	357.8	5.3
5-Jul	24.6	1.7	4.1	0.0	14.3	106.5	21.5	0.0	4.7	148.6	3.6	27.1	329.6	8.2
8-Jul	20.3	1.5	3.0	0.0	10.0	83.6	17.3	0.0	2.4	142.1	2.9	46.4	283.0	16.4
11-Jul	23.5	1.6	2.6	0.0	10.9	95.1	20.0	0.0	4.0	142.8	2.8	35.9	303.2	11.8
14-Jul	23.4	1.6	3.2	0.0	12.1	101.6	21.0	0.0	4.4	110.4	3.9	-2.2	281.4	-0.8
17-Jul	31.0	1.5	4.2	0.0	11.3	101.6	21.8	0.0	3.9	147.2	2.4	25.7	324.8	7.9
20-Jul	24.0	1.5	2.1	0.0	10.1	85.2	18.3	0.0	3.2	143.3	2.5	44.4	290.2	15.3
23-Jul	21.4	1.2	1.4	0.0	9.6	77.0	17.7	0.0	3.2	124.9	2.8	38.0	259.3	14.6
26-Jul	31.1	0.9	0.0	0.0	10.5	88.5	22.5	0.0	3.0	106.7	2.5	3.8	265.6	1.4
29-Jul	31.2	1.5	2.1	0.0	13.1	108.2	25.1	0.0	4.2	106.6	3.1	-17.0	295.1	-5.8
1-Aug	44.3	1.6	3.1	0.0	13.7	113.1	30.1	0.0	5.8	111.3	3.0	-25.5	326.0	-7.8
4-Aug	38.6	1.6	2.2	0.0	14.1	106.5	29.6	0.0	5.2	100.0	2.5	-25.7	300.2	-8.6
7-Aug	31.5	2.2	2.9	0.0	18.9	109.8	27.6	0.0	6.3	121.6	2.8	-6.9	323.7	-2.1
10-Aug	36.5	2.9	4.0	0.0	23.6	157.3	43.2	0.0	6.3	117.1	6.8	-51.1	397.8	-12.9
13-Aug	35.5	1.6	3.3	0.0	13.4	nd	28.5	0.0	4.7	138.8	3.1			
UWLS	F ueq L-1	Cl ueq L-1	NO3 ueq L-1	PO4 ueq L-1	SO4 ueq L-1	HCO3 ueq L-1	Na ueq L-1	NH4 ueq L-1	K ueq L-1	Ca ueq L-1	Mg ueq L-1	(Cat-An)-Alk	Cat+An	CBE (%)
2-Jul	6.9	1.5	0.8	0.0	0.1	63.9	8.8	0.0	7.1	88.0	1.3	31.9	178.4	17.9
5-Jul	5.2	0.7	0.7	0.0	9.4	75.4	7.9	0.0	9.5	99.9	1.2	27.1	209.8	12.9
8-Jul	5.6	0.6	0.1	0.0	10.1	67.2	8.1	0.0	5.3	79.8	1.1	10.8	178.0	6.1
11-Jul	6.1	0.6	0.0	0.0	14.2	62.3	9.9	0.0	7.0	95.7	1.6	31.0	197.3	15.7
14-Jul	5.9	0.5	0.0	0.0	14.6	70.5	10.6	0.0	6.9	94.4	1.5	21.9	204.8	10.7
17-Jul	5.5	0.5	0.0	0.0	8.3	62.3	9.5	0.0	6.2	80.8	0.8	20.7	173.9	11.9
20-Jul	6.3	0.9	0.0	0.0	10.1	67.2	10.8	0.0	6.6	92.2	1.2	26.3	195.3	13.4
23-Jul	9.0	0.8	0.0	0.0	4.0	81.9	10.6	0.0	8.3	106.1	1.6	30.9	222.3	13.9
26-Jul	6.2	0.5	0.0	0.0	5.3	70.5	9.2	0.0	6.4	80.1	0.8	14.1	178.9	7.9
29-Jul	10.9	0.4	0.0	0.0	7.4	104.9	18.7	0.0	12.9	149.1	2.9	60.0	307.1	19.5
1-Aug	9.9	0.5	0.0	0.0	33.7	103.2	24.4	0.0	10.0	161.4	3.6	52.0	346.7	15.0
4-Aug	8.1	0.5	0.0	0.0	18.9	118.0	23.7	0.0	9.8	162.6	3.2	53.7	344.9	15.6
7-Aug	7.8	5.7	0.1	0.0	16.4	109.8	25.5	0.0	9.7	155.0	3.2	53.5	333.2	16.1
10-Aug	7.8	2.0	0.9	0.0	77.0	144.2	36.4	0.0	14.5	243.2	6.3	68.5	532.3	12.9
13-Aug	9.1	0.9	0.1	0.0	19.1	nd	20.8	0.0	9.3	153.9	2.3			

Table A.2: pH values measured in the field on filtered samples from L1 (lake surface), L2 (1.5 m lake depth), L3 (5 m lake depth). LOS, ELS, and UWLS. pH values listed are averages of two measurements.

pH						
Date	L1	L2	L3	LOS	ELS	UWLS
2-Jul	6.8		6.8	6.8	7.0	6.9
5-Jul	6.8		6.8	7.0	6.9	6.9
8-Jul	6.6	6.6	6.8	6.7	6.8	6.7
11-Jul	6.8		6.7	6.9	6.7	6.8
14-Jul	6.6		6.6	6.7	6.7	6.7
17-Jul	6.7	6.7	6.8	6.8	6.8	6.8
20-Jul	6.6		6.8	6.7	6.7	6.7
23-Jul	6.7		6.8	6.9	6.8	6.8
26-Jul	6.6	6.7	6.8	6.8	6.7	6.7
29-Jul	6.7		6.8	6.9	7.0	6.9
1-Aug	6.7		6.7	6.8	6.9	6.8
4-Aug	6.7	6.7	6.7	6.8	6.8	6.8
7-Aug	6.7		6.8	6.8	6.9	6.9
10-Aug	6.9		6.9	6.9	6.9	7.0

Table A.3: Electrical conductivity (EC) (µS cm^{-1}) measured in the laboratory from filtered field samples from L1 (lake surface), L2 (1.5 m lake depth), L3 (5 m lake depth), LOS, ELS, and UWLS.

EC						
Date	L1	L2	L3	LOS	ELS	UWLS
2-Jul	11.2		11.7	10.3	14.3	6.6
5-Jul	10.7		11.6	10.2	13.3	7.6
8-Jul	10.8	11.5	11.5	12.5	10.4	6.4
11-Jul	11.2		12.5	12.2	11.7	7.6
14-Jul	8.0		10.2	10.9	13.2	7.5
17-Jul	10.6	11.1	11.1	11.2	12.2	6.5
20-Jul	10.9		10.5	11.5	10.8	7.4
23-Jul	9.6		9.4	9.5	10.3	7.8
26-Jul	7.8	9.2	8.8	10.0	12.2	6.5
29-Jul	8.2		7.9	9.7	13.8	11.9
1-Aug	8.2		7.7	9.2	15.3	13.9
4-Aug	8.6	8.4	8.1	8.4	14.6	12.8
7-Aug	9.8		9.2	9.0	14.7	17.4
10-Aug	10.6		9.9	11.0	19.0	19.1

Table A.4: Suspended sediment (mgL^{-1}) for the lake surface (L1), 1.5 m lake depth (L2), 5 m lake depth (L3), LOS, ELS, and UWLS.

Suspended Sediment (mg L^{-1})															
Sample Location	2-Jul	5-Jul	8-Jul	11-Jul	14-Jul	17-Jul	20-Jul	23-Jul	26-Jul	29-Jul	1-Aug	4-Aug	7-Aug	10-Aug	13-Aug
L1	8	9	17	10	20	9	18	10	25	31	28	32	33	48	35
L2			16			16			26		40				40
L3	15	13	18	16	25	12	19	14	29	38	37	51	44	72	44
LOS	12	11	10	12	20	13	8	19	20	26	22	26	29	47	25
ELS	34	11	10	9	12	9	6	9	7	3	12	10	4	10	0
UWLS	18236	342	344	477	1174	621	350	5473	995	1873	136	87	207	2380	138

Table A.5: Regression relationships between discharge and ions in the ELS and LOS determined by LINEST function in Excel. Se-y refers to the standard error on the y-variable (ion concentration).

	ELS			LOS		
	Equation	se-y	R^2	Equation	se-y	R^2
HCO_3	0.00448x + 6.8875	2.1165	0.07	0.0080x + 5.3265	0.8823	0.44
SO_4	0.001x + 0.7916	0.3153	0.16	0.0005x + 0.5606	0.2491	0.04
Cl	0x + 0.0482	0.0151	0.04	- 0.0001x + 0.0611	0.0234	0.10
F	- 0.0011x + 0.7251	0.212	0.25	- 0.0001x + 0.0502	0.0156	0.07
NO_3	0.0001x + 0.148	0.1297	0.02	0.0004x + 0.0518	0.0408	0.48
Ca	- 0.003x + 3.9485	1.1371	0.11	0.00504x + 2.327	0.44	0.55
Na	- 0.0005x + 0.6015	0.1443	0.14	0.0003x + 0.2935	0.0711	0.11
Mg	- 0.0000125x + 0.002	0.0252	0	0.0000486x + 0.03685	0.0158	0.08
K	- 0.0002997x + 0.2163	0.078285	0.2	- 0.0006x + 0.2183	0.0266	0.59

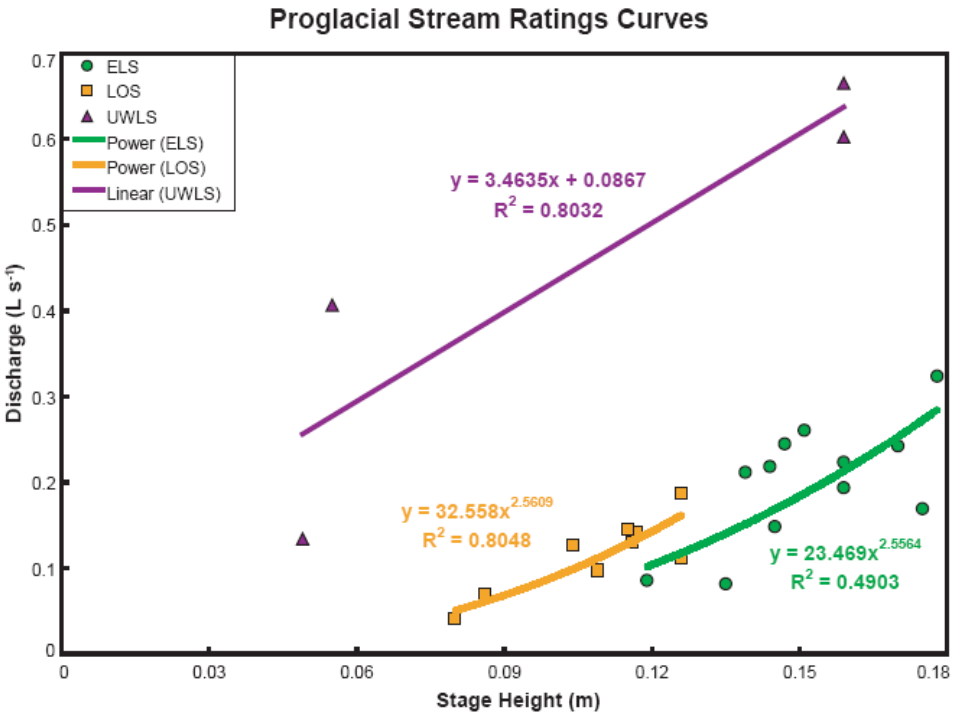


Figure A.1: Proglacial stream ratings curves derived using the velocity-area method.

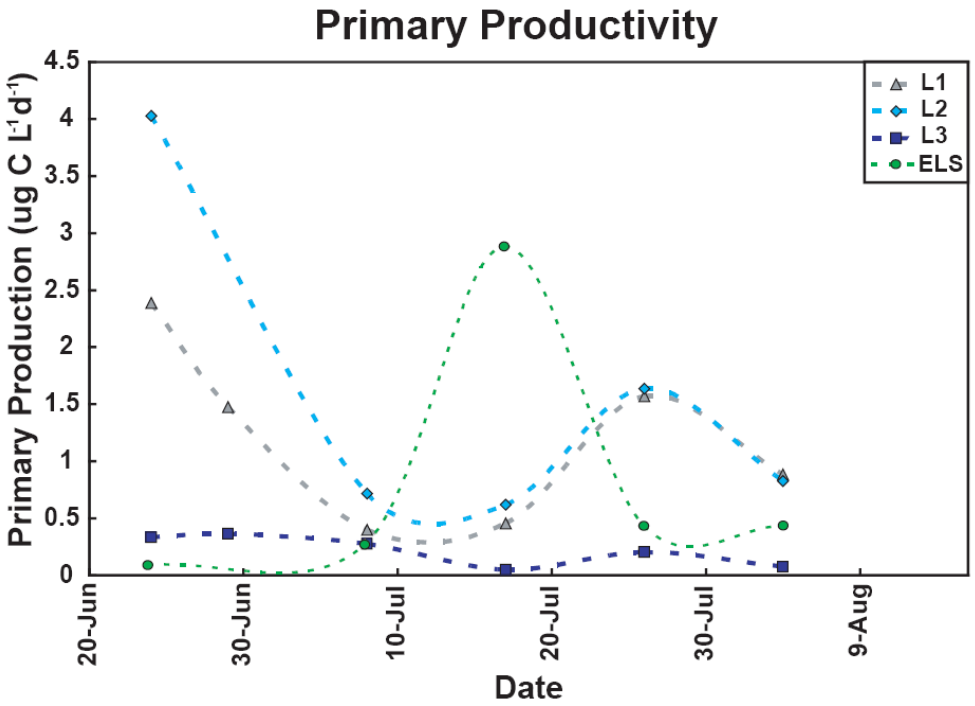


Figure A.2: Primary productivity data for 0.5 m lake depth (L1), 1.5 m lake depth (L2), 5 m lake depth (L3), and ELS.

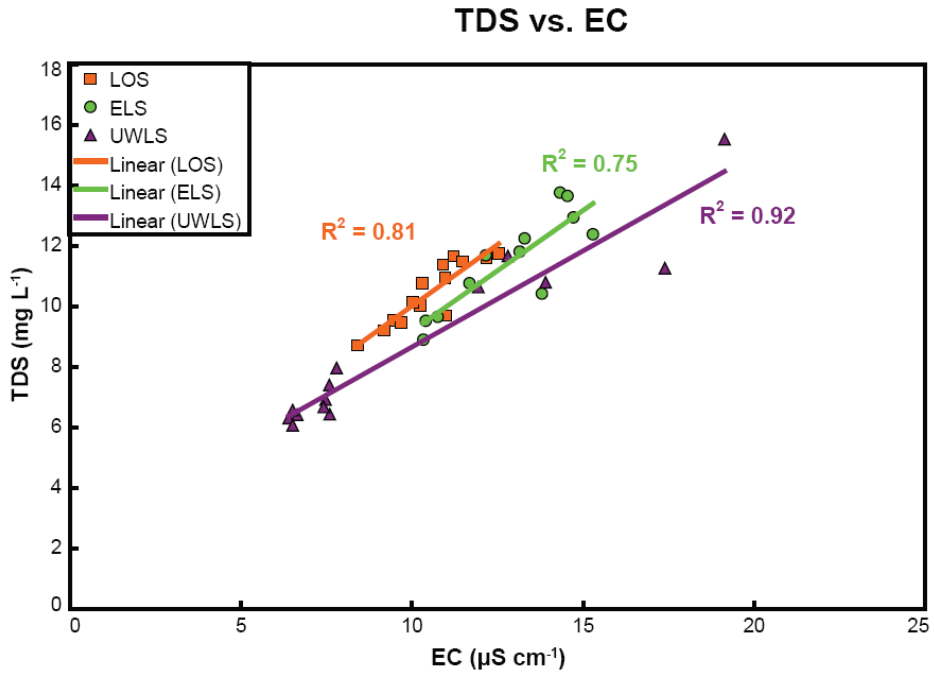


Figure A.3: Regression relationship between total dissolved solids (TDS) and electrical conductivity (EC) for LOS, ELS, and UWLS streams.

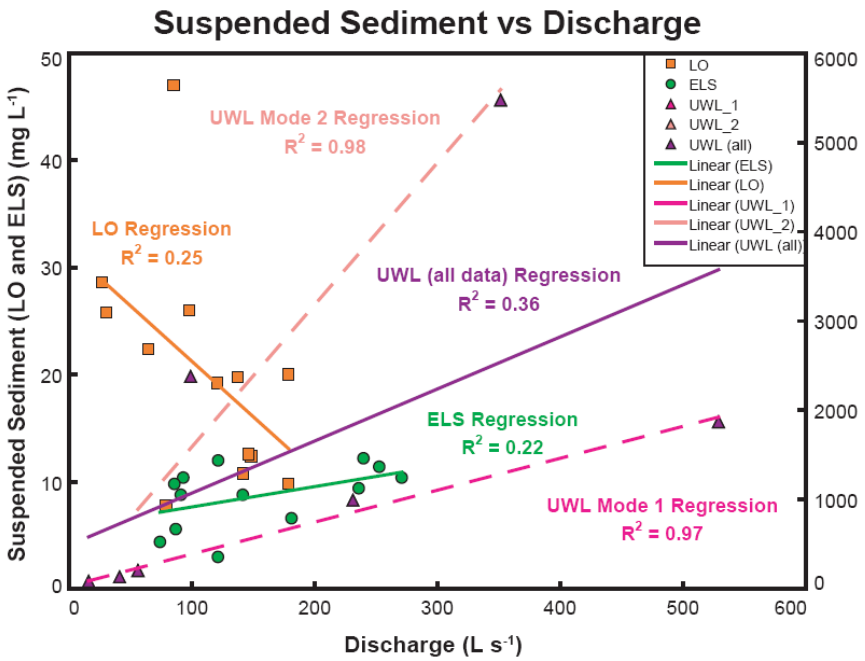


Figure A.4: Regression relationships for LOS, ELS, and UWLS. Dashed lines represent regression line for a bimodal distribution of suspended sediment in the UWLS, which may be dependent on water flowpath or sediment availability from the moraine. Mode 1 data points include data collected on 23 July and 4, 7, and 10 August. Mode 2 data points include data collected on 26 and 29 July and 1 and 4 August.

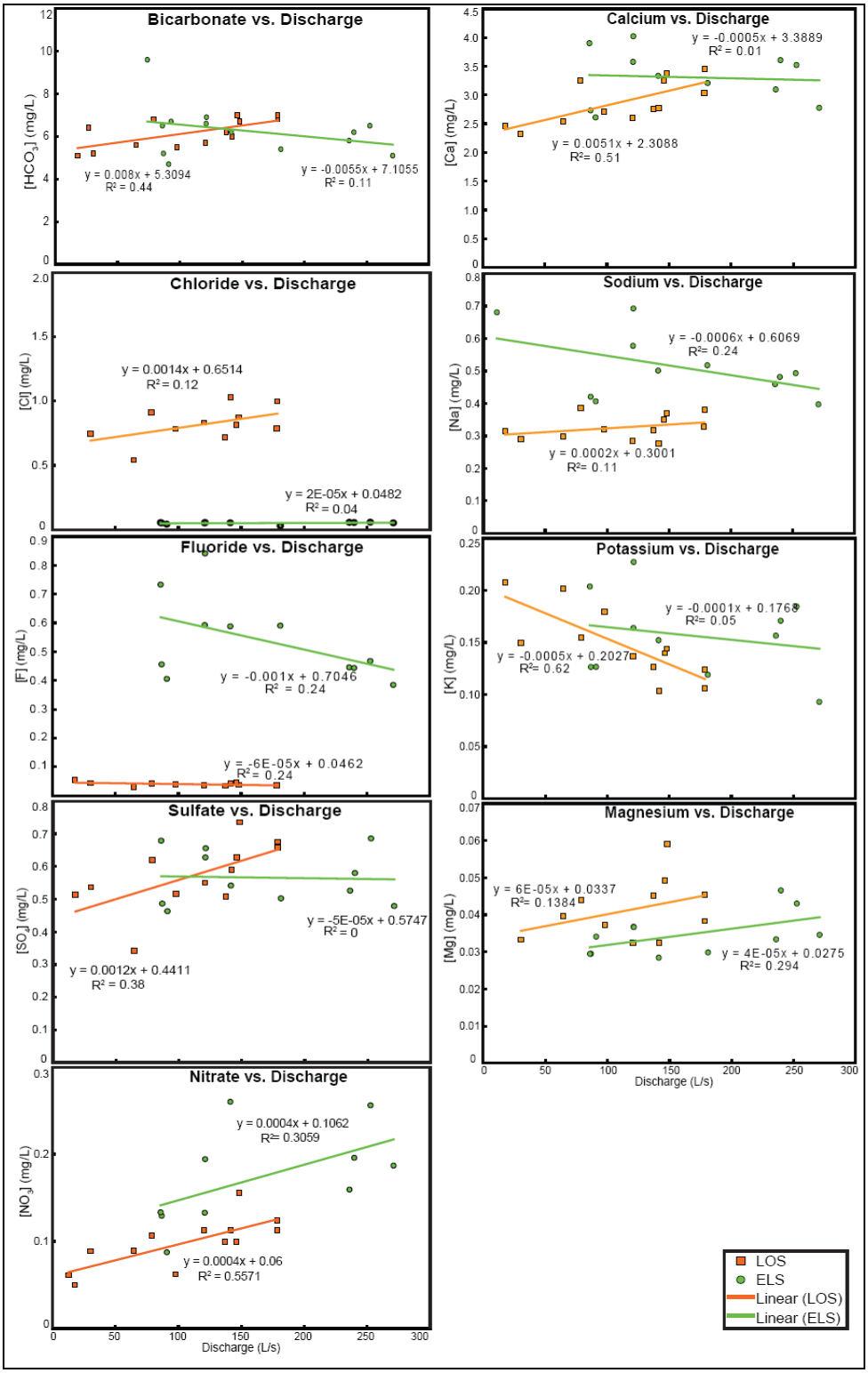


Figure A.5: Ion vs. discharge simple linear regression lines, equations, and R^2 values for the LOS and ELS streams.

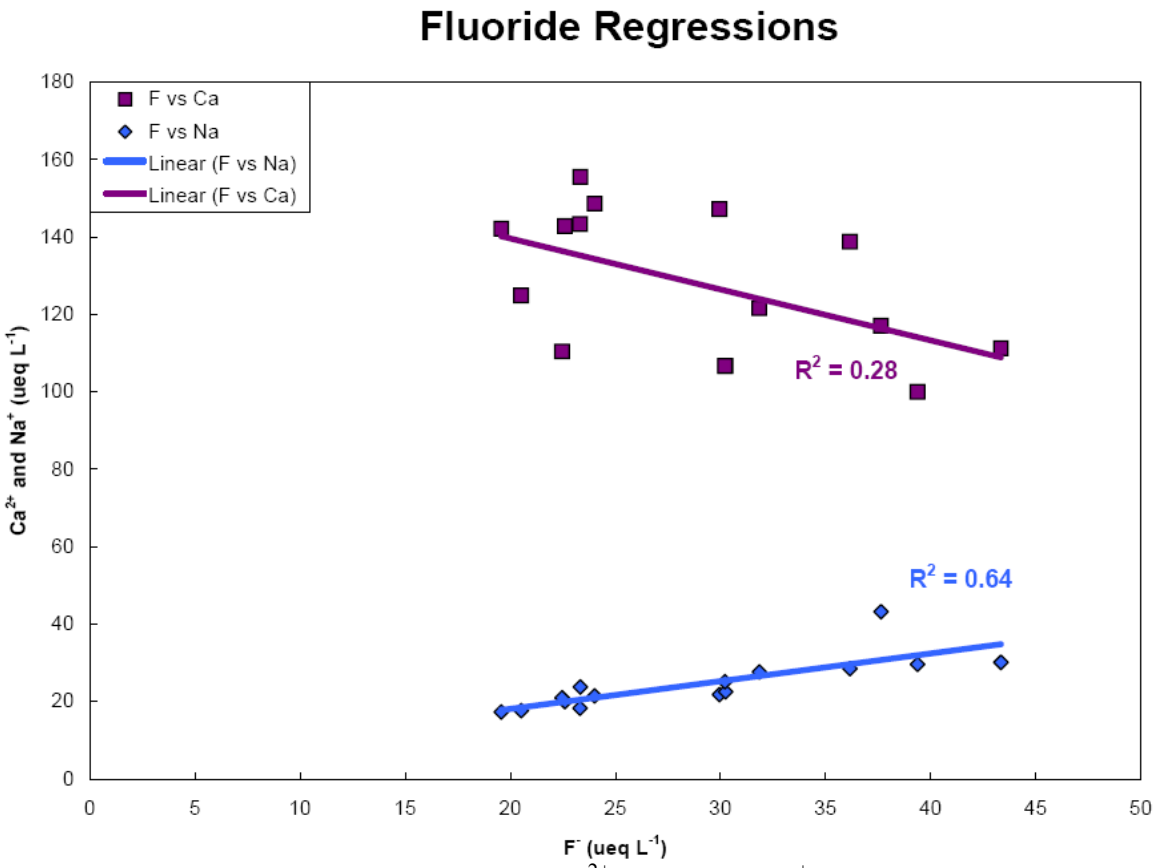


Figure A.6: Regression between dissolved Ca^{2+} and F^- and Na^+ and F^- for the ELS indicates weathering of fluorite or cryolite may be potential sources for high fluoride concentrations in the ELS.

Equations and Assumptions for Tracer Calculations

Salt Tracer Calculations and Assumptions

10 kg NaCl was added to the lake (assuming total lake volume was 16,100 m^3 = 16,100,000 kg H_2O, based on bathymetric map – Figure 3.4B)
Na^+ molecular weight = 22.99 g mol^{-1}
Cl^- molecular weight = 35.4 g mol^{-1}
NaCl molecular weight = 58.44 g mol^{-1}

Mole fraction of Na^+ = 22.99/58.44 = 0.393 g Na^+ mol $NaCl^{-1}$
Mole fraction of Cl^- = 35.4/58.44 = 0.607 g Cl^- mol $NaCl^{-1}$

Mole fraction * 10,000 g NaCl salt slug added to the lake = 3930 g Na^+ and 6070 g Cl^-, which is equal to 3.93 x 10^6 mg Na^+ and 6.07 x 10^6 mg Cl^-.

Assuming full mixing with lake water, the electrical conductivity rise should be reflected by:

3.93×10^6 mg Na^+/16,100,000 kg H_2O = 0.244 ppm Na^+
0.244 ppm Na^+ * 1000/22.99 = 10.6 μeq L^{-1}

And likewise, for Cl^-:
6,070,000 mg Cl^-/16,100,000 kg H_2O – 0.377 ppm Cl^-
0.377 ppm Cl^- * 1000/35.4 = 10.6 μeq L^{-1}

Rhodamine Tracer Calculations and Assumptions

The Turner Designs fluorometer output for rhodamine concentration in each sample was provided in ppm. The output was multiplied by the instantaneous discharge measurement (from the TruTrack probes) for each sampling time point to determine the amount of rhodamine leaving the system; calculations were multiplied by the number of seconds between sampling points to determine g of rhodamine export through time, so it was assumed these discharges were relatively constant between sampling time points. Concentrations of rhodamine leaving the lake between the 14 August 22:00 and 16 August 10:00 and after 16 August 10:00 were extrapolated using an exponential decay curve that was fit to the time fractions and rhodamine concentrations from samples 12-20. The equation was $y = 0.0134e^{-0.4582x}$, where y was the instantaneous rhodamine concentration and x was the time fraction; the curve fit samples 12-20 with an R^2 of 0.89 and extrapolated values are shown in parallel with measured values in the Excel sheet below to demonstrate the goodness of fit the curve provided. Also, since discharge was not recorded after the 20th sample, it was assumed that it was similar to the previous day and thus the previous day's discharges were repeated for each time point after the

TruTrack probe was taken down on 16 August. The Excel sheet with these calculations is provided below:

Sample #	Time	Time fraction since injection (min)	Q (L/s)	Avg (ppb)	Avg (ppm) or mg/L	Extrapolated ppm or mg/L	mg/s	blank subtracted mg/s	mg	g	Sum of rhodamine that left the lake (g)	% of rhodamine that left the lake
1	8/14/06 8:35	0	68	0.08	0.0001		0.01	0.00	0.00	0.00	0.00	0%
2	8/14/06 9:30	0.04	71	0.08	0.0001		0.01	0.00	0.41	0.00	0.00	0%
3	8/14/06 10:00	0.06	73	0.08	0.0001		0.01	0.00	1.01	0.00	0.00	0%
4	8/14/06 10:45	0.09	87	0.10	0.0001		0.01	0.00	8.55	0.01	0.01	0%
5	8/14/06 11:30	0.12	115	0.13	0.0001		0.01	0.01	25.97	0.03	0.04	0%
6	8/14/06 12:15	0.15	160	0.09	0.0001		0.01	0.01	23.17	0.02	0.06	0%
7	8/14/06 13:00	0.18	231	0.26	0.0003		0.06	0.05	145.27	0.15	0.20	0%
8	8/14/06 13:45	0.22	293	2.38	0.0024		0.70	0.69	1869.05	1.87	2.07	0%
9	8/14/06 14:30	0.25	342	7.45	0.0075		2.55	2.54	6865.56	6.87	8.94	2%
10	8/14/06 15:15	0.28	388	8.85	0.0088		3.43	3.43	9252.25	9.25	18.19	4%
11	8/14/06 16:00	0.31	393	13.05	0.0131		5.13	5.12	13833.59	13.83	32.02	6%
12	8/14/06 16:45	0.34	347	13.65	0.0137	0.0115	4.74	4.73	12774.92	12.77	44.80	9%
13	8/14/06 17:30	0.37	299	12.10	0.0121	0.0113	3.62	3.61	9754.56	9.75	54.55	11%
14	8/14/06 18:15	0.40	262	11.25	0.0113	0.0111	2.95	2.94	7944.48	7.94	62.50	12%
15	8/14/06 19:00	0.43	233	10.55	0.0106	0.0110	2.46	2.45	6623.24	6.62	69.12	14%
16	8/14/06 19:45	0.47	196	10.70	0.0107	0.0108	2.10	2.09	5648.67	5.65	74.77	15%
17	8/14/06 20:30	0.50	159	10.00	0.0100	0.0107	1.59	1.58	4279.23	4.28	79.05	16%
18	8/14/06 21:15	0.53	137	8.98	0.0090	0.0105	1.23	1.22	3306.08	3.31	82.36	16%
19	8/14/06 22:00	0.56	96	8.80	0.0088	0.0104	0.84	0.84	2267.19	2.27	84.62	17%
	8/14/06 22:45	0.59	70			0.0102	0.72	0.71	1918.67	1.92	86.54	17%
	8/14/06 23:30	0.62	80			0.0101	0.81	0.80	2163.33	2.16	88.71	18%
	8/15/06 0:15	0.65	70			0.0099	0.70	0.69	1864.11	1.86	90.57	18%
	8/15/06 1:00	0.68	68			0.0098	0.67	0.66	1784.52	1.78	92.35	18%
	8/15/06 1:45	0.72	71			0.0097	0.69	0.68	1837.16	1.84	94.19	19%
	8/15/06 2:30	0.75	73			0.0095	0.69	0.69	1862.25	1.86	96.05	19%
	8/15/06 3:15	0.78	70			0.0094	0.66	0.65	1759.58	1.76	97.81	20%
	8/15/06 4:00	0.81	70			0.0092	0.65	0.64	1734.37	1.73	99.55	20%
	8/15/06 4:45	0.84	70			0.0091	0.64	0.63	1709.51	1.71	101.26	20%
	8/15/06 5:30	0.87	70			0.0090	0.63	0.62	1685.01	1.69	102.94	21%
	8/15/06 6:15	0.90	70			0.0089	0.62	0.62	1660.86	1.66	104.60	21%
	8/15/2006 7:00	0.93	70			0.0087	0.61	0.61	1637.05	1.64	106.24	21%
	8/15/06 7:45	0.97	70			0.0086	0.60	0.60	1613.59	1.61	107.85	22%
	8/15/06 8:30	1.00	70			0.0085	0.59	0.59	1590.45	1.59	109.44	22%
	8/15/06 9:15	1.03	70			0.0084	0.59	0.58	1567.64	1.57	111.01	22%
	8/15/2006 10:00	1.06	73			0.0082	0.60	0.60	1611.97	1.61	112.62	23%
	8/15/06 10:45	1.09	87			0.0081	0.71	0.70	1896.21	1.90	114.52	23%
	8/15/06 11:30	1.12	115			0.0080	0.92	0.92	2475.03	2.48	116.99	23%
	8/15/06 12:15	1.15	160			0.0079	1.26	1.26	3399.68	3.40	120.39	24%
	8/15/2006 13:00	1.18	231			0.0078	1.80	1.79	4844.33	4.84	125.24	25%
	8/15/06 13:45	1.22	293			0.0077	2.25	2.24	6060.63	6.06	131.30	26%
	8/15/06 14:30	1.25	342			0.0076	2.59	2.58	6975.69	6.98	138.27	28%
	8/15/06 15:15	1.28	388			0.0075	2.90	2.89	7803.06	7.80	146.08	29%
	8/15/2006 16:00	1.31	393			0.0074	2.89	2.89	7791.23	7.79	153.87	31%
	8/15/2006 16:45	1.34	347			0.0073	2.52	2.51	6779.69	6.78	160.65	32%
	8/15/06 17:30	1.37	299			0.0071	2.14	2.13	5756.74	5.76	166.41	33%
	8/15/06 18:15	1.40	262			0.0070	1.85	1.84	4970.78	4.97	171.38	34%
	8/15/2006 19:00	1.43	233			0.0069	1.62	1.61	4356.03	4.36	175.73	35%
	8/15/2006 19:45	1.47	196			0.0068	1.34	1.34	3609.86	3.61	179.34	36%
	8/15/06 20:30	1.50	159			0.0068	1.07	1.07	2884.01	2.88	182.23	36%
	8/15/06 21:15	1.53	137			0.0067	0.91	0.91	2447.57	2.45	184.67	37%
	8/15/2006 22:00	1.56	96			0.0066	0.63	0.62	1686.44	1.69	186.36	37%
	8/15/2006 22:45	1.59	70			0.0065	0.45	0.45	1208.34	1.21	187.57	38%
	8/15/06 23:30	1.62	80			0.0064	0.51	0.50	1363.07	1.36	188.93	38%
	8/16/06 0:15	1.65	70			0.0063	0.44	0.43	1173.84	1.17	190.11	38%
	8/16/2006 1:00	1.68	68			0.0062	0.42	0.42	1123.51	1.12	191.23	38%
	8/16/06 1:45	1.72	68			0.0061	0.42	0.41	1107.34	1.11	192.34	38%
	8/16/2006 2:30	1.75	68			0.0060	0.41	0.40	1091.40	1.09	193.43	39%
	8/16/06 3:15	1.78	68			0.0059	0.40	0.40	1075.69	1.08	194.50	39%
	8/16/2006 4:00	1.81	68			0.0058	0.40	0.39	1060.20	1.06	195.56	39%
	8/16/2006 4:45	1.84	68			0.0058	0.39	0.39	1044.93	1.04	196.61	39%
	8/16/06 5:30	1.87	68			0.0057	0.39	0.38	1029.88	1.03	197.64	40%
	8/16/2006 6:15	1.90	68			0.0056	0.38	0.38	1015.04	1.02	198.65	40%
	8/16/06 7:00	1.93	68			0.0055	0.38	0.37	1000.42	1.00	199.65	40%
	8/16/2006 7:45	1.97	68			0.0054	0.37	0.37	986.00	0.99	200.64	40%
	8/16/2006 8:30	2.00	68			0.0054	0.37	0.36	971.79	0.97	201.61	40%
	8/16/06 9:15	2.03	68			0.0053	0.36	0.35	957.77	0.96	202.57	41%
20	8/16/2006 10:00	2.06	73	4.88	0.0049	0.0052	0.38	0.38	1014.38	1.01	203.58	41%
	8/16/06 10:45	2.09	87			0.0051	0.45	0.44	1194.14	1.19	204.78	41%
	8/16/2006 11:30	2.12	115			0.0051	0.58	0.58	1560.20	1.56	206.34	41%
	8/16/2006 12:15	2.15	160			0.0050	0.80	0.79	2144.96	2.14	208.48	42%
	8/16/06 13:00	2.18	231			0.0049	1.14	1.13	3058.59	3.06	211.54	42%
	8/16/2006 13:45	2.22	293			0.0049	1.42	1.42	3827.81	3.83	215.37	43%
	8/16/06 14:30	2.25	342			0.0048	1.64	1.63	4406.51	4.41	219.78	44%
	8/16/2006 15:15	2.28	388			0.0047	1.83	1.83	4929.76	4.93	224.71	45%
	8/16/2006 16:00	2.31	393			0.0047	1.83	1.82	4922.27	4.92	229.63	46%
	8/16/06 16:45	2.34	347			0.0046	1.59	1.59	4282.56	4.28	233.91	47%
	8/16/2006 17:30	2.37	299			0.0045	1.35	1.35	3635.62	3.64	237.55	48%
	8/16/2006 18:15	2.40	262			0.0045	1.17	1.16	3138.56	3.14	240.68	48%
	8/16/06 19:00	2.43	233			0.0044	1.02	1.02	2749.79	2.75	243.43	49%
	8/16/2006 19:45	2.47	196			0.0043	0.85	0.84	2277.89	2.28	245.71	49%
	8/16/2006 20:30	2.50	159			0.0043	0.68	0.67	1818.85	1.82	247.53	50%

Salt Tracer Movement via
Groundwater Calculation and Assumptions

Assuming full mixing of the salt tracer with the lake water and its subsequent transport to groundwater, it is assumed that the groundwater Cl^- concentration was at least 10.6 μeq L^{-1} (see Salt Tracer Calculations and Assumptions above) and that there were no additional sources or sinks for Cl^- (thus, the Cl^- changes in the samples were attributed only to the salt tracer).

The following mixing model equation was used to determine percent contributions of groundwater to the overall discharge in each stream:

$$\%Q_{GW} = (C_t - C_o) / (C_n - C_o) * 100\%$$

where $\%Q_{Gw}$ is the percent contribution of groundwater to overall stream discharge measured with the salt tracer, C_t is the total concentration of Cl^- in the discrete sample from each stream on 7, 10, and 13 August measured on the ion chromatograph, C_o is the background concentration of Cl^- in each stream (determined by subtracting the 4 August $[Cl^-]$ from the 7, 10, and 13 August $[Cl^-]$; the 4 August sample was used because it was the last sample taken from all three streams prior to the salt slug addition), and C_n is the groundwater contribution, which was assumed to be 10.6 μeq L^{-1} from the salt tracer mixing fully with the lake water, as stated above.

For example, the UWLS 7 August groundwater contribution was calculated by the following:
C_t = 5.7 μeq L^{-1} Cl^-, C_o = 0.5 μeq L^{-1} Cl^-, C_n = 10.6 μeq L^{-1} Cl^-

$$\%Q_{GW} = (5.7 - 0.5) / (10.6 - 0.5) = 51\%$$

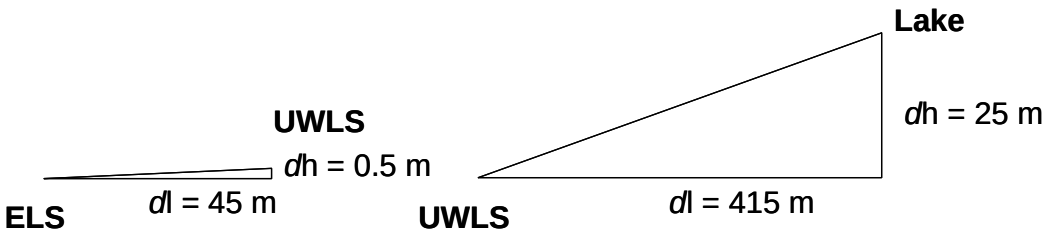
However, the assumption for full mixing of the salt tracer with the lake water to yield a groundwater EC of 10.6 μeq L^{-1} does not appear to be reasonable since, from the calculation above we see that more of the salt tracer appears to have exited via groundwater to the UWLS than exited via the LOS where one would assume most of the tracer would exit assuming full mixing. Thus, it is assumed that the salt tracer did not fully mix with the lake water and instead moved as a plume with an EC of 106 μeq L^{-1} (~10x it would have been assuming full mixing). Given this, we evaluate the above equation:

$$\% Q_{GW} = (5.7 - 0.5) / (106 - 0.5) = 4.9\%$$

Table A.6 displays $\% Q_{GW}$ contribution to each stream assuming full mixing, or 100% dilution efficiency, in addition to a 50% dilution efficiency, and 10% dilution efficiency.

The velocity of the salt tracer was calculated between the lake and UWLS (v_1) and the ELS (v_2) using the equation v = distance traveled/time it took for salt to appear in each respective stream. The distance the salt slug traveled was based on straight line distance between the lake and UWLS and ELS determined using the 1995 aerial photograph and the time it took for the salt slug to reach each stream was assumed to be 1 day which was reflected by an increase in [Cl^-] in each stream on 7 August (a day after the salt slug release).

Two hydraulic conductivities were measured to account for the drastic decrease in slope between the UWLS and ELS. The hydraulic conductivity k was calculated between the lake and UWLS (k_1) using the equation $k_1 = v_1 / (dh/dl)$. The hydraulic conductivity between the lake and ELS (k_2) was measured using the equation $k_2 = (0.9)(k_1) + (0.1)(45$ m / (0.5 m / 45 m), where 0.9 and 0.1 represent the fractions of the total (lake to ELS) distance between the lake and UWLS and the UWLS and ELS.



$v_1 = 415$ m d^{-1}
$v_2 = 463$ m d^{-1}

$k_1 = 415$ m d^{-1} / (25 m / 4 m) = 6889 m d^{-1} = 8 cm s^{-1}
$k_2 = 0.9 * 6889$ m $d^{-1} + 0.1 *$ (45 m d^{-1} / (0.5 m / 45 m)) = 6605 m d^{-1} = 7.6 cm s^{-1}